3-D Frequency Selective Structures

A thesis submitted in fulfilment of the requirements for the degree of Doctor of Philosophy

Saidatul Norlyana Azemi

School of Electrical and Computer Engineering

College of Science Engineering and Health

RMIT University

February 2015

Declaration

I certify that except where due acknowledgement has been made, the work is that of the author alone; the work has not been submitted previously, in whole or in part, to qualify for any other academic award; the content of the thesis/project is the result of work which has been carried out since the official commencement date of the approved research program; any editorial work, paid or unpaid, carried out by a third party is acknowledged; and, ethics procedures and guidelines have been followed.

Saidatul Norlyana Azemi

February 2015

Acknowledgements

First and foremost, I would like to express my gratitude and appreciation to my supervisor, Assoc Prof Dr Wayne Rowe, for his patient guidance, encouragement, precious advice and suggestions through the whole project. I would also like to thank my second supervisor, Professor Kamran Ghorbani, for his valuable and constructive suggestions during the planning and development of this research.

I would also like to extend my sincere thanks to all colleagues in communication group especially Ms. Harita Jamil, Dr. Farid Abdul Khalid, Dr. Thomas Baum, Dr. Amir Galehdar, Dr. Sahan Fernando, Mr. Soumitra Niyogi, Dr. Alexe Bojovschi, Mr. Toby Seidel, Dr. Ali Daliri, Dr. Brendan Pell, Mr. Kelvin Nicholson. Ms. Negin and other, who gave comprehensive knowledge and assisted me with measurement facilities during the past four academic years. Really appreciated my friendships at RMIT University.

I am particularly indebted to Mr. David Welch (Dave) of the School of Electrical and Computer Engineering for his outstanding technical skills and advice. He has spent much time with many practical elements of the work, from the fabrication of the FSSs, to teaching microwave measurement and calibration techniques to make sure all the FSS is working properly.

I wish to acknowledge the support of UniMAP (University Malaysia Perlis) by awarding me the Bumiputera Academic Training Scheme Scholarship. I am able to concentrate on what is important for me, education. Other financial support towards my higher education from Department of High Education is also much appreciated. Your financial generosity has allowed me to be one step closer to my goal.

Finally, I wish to thank my beloved family for their loving consideration and continuous support. For my soul mate, Wan Mohd Ridzuan, thank you for everything especially for your endless love, support and sacrifices. I can face anything because you are by my side. Throughout study period, I have been blessed with two sons, Afiq Daniel Ridzuan, Aidan Fariz Ridzuan. You guys have taught me so much, to be patient, be strong and learn never give up in everything.

I want to extend a heart-felt thank you to my lovely and only big sister. Thank you for being my greatest inspiration and my best friend. My deepest gratitude to my parents and my in laws family for their constant love, patience, support and prayers. It would be impossible for me to work on this thesis completely without the encouragement from my family. Therefore, I am greatly appreciated for both physically and mentally supports they gave me.

Last but not the least I would like to thank everybody who were involved directly or indirectly in successful completion of the present work. Thank you so much!!.

Abstract

Frequency Selective Surfaces (FSSs) are planar periodic structures of identical cells that behave like filters to electromagnetic energy. FSSs are widely used for shielding of non-ionizing radiation. They have been employed to improve wireless networks, radar system, and scientific research infrastructures. However, most of the research into FSSs has been in two dimensional periodic arrays of resonant structures, where a single layer FSS is known to suffer from poor selectivity and narrow bandwidth.

For some practical applications with restricted or conformal transmission area, it is desirable to realize a FSS with miniaturized elements and a stable frequency response for different polarizations and incident angles. A large number of structures and modelling techniques have been proposed, but these features are difficult to obtain through traditional designs. An innovative concept of a three-dimensional (3-D) FSS is proposed, and is proving a promising candidate for the realization of compact high-performance FSSs. The 3-D structures also lend themselves to high aspect ratio micro-fabrication techniques for efficient implementation at higher frequencies.

The purpose of this thesis is to investigate novel designs of 3-D FSSs extending the potential functionality of the structure beyond that of its 2D analogue. First, a novel 3-D FSS architecture based on a circular ring unit element is presented. The length of the cylinder is shown to have a significant effect on the frequency characteristics of the FSS, providing tuning and reconfiguration from a band-stop to a band-pass filter response. Dielectric materials can also be introduced in the center of the cylindrical unit cell elements to simultaneously obtain a stop and pass band with a sharp transition. A similar close band response can be obtained using dual cylinder 3-D Frequency Selective Surface (FSS). The length of the cylinder has significant effect on the stop band frequency selective characteristics of the FSS, resulting in a closely spaced band pass and band stop response.

Conventional FSSs require additional bias circuitry to tune the operating frequency or to change its characteristics. A new tuning technique using spring resonator element is also proposed in this thesis. The FSS frequency response can be adjusted by changing the spring height, h, with applied pressure. The functional characteristic of the FSS can also be altered between a band-stop and band-pass filter response.

Frequency responses of FSSs are dependent not only on frequency but also on incident angle of incident electromagnetic waves. It is often required that an FSS provides stable performance for various incidence angles. Hence, 3-D Frequency Selective Surface (FSS) with a response that is essentially independent of incident angle is presented. The FSS is a periodic array of 3-D hollow tapered resonators. The TE and TM angular stable is obtained by tapering the width of a cylinder with a square cross-section from upper opening to the lower opening. Impressive frequency stability and transmission characteristics have been achieved up to 80 degrees for both TE and TM incidence angles. The principles of operation along with guidelines for the design of the proposed FSS structures are presented.

A novel 3-D Frequency Selective Surface (FSS) with horn shaped resonators is also proposed which exhibits a very wide stop band. Simulation results prove that the FSS can realize selectivity of waves with a bandwidth more than 57%, and for different incident angles. The wideband transmission behavior is very stable under oblique TM incidence angles from 0 to 80 degrees.

FSSs with high selectivity and compact size are of increasing demand in wireless and mobile communication systems. Here, a new type of FSS with miniaturized resonator elements is proposed. The FSS structure is shown to have a unit cell dimension that is miniaturized to 0.067 λ_0, achieved by coupling two meandered wire resonators separated by single thin substrate layer. The FSS produces a stable angular response up to 80 degrees for TE and TM incident angles. The meandered wire resonator structure is also utilized to enable transmission through a subwavelength aperture. The structure exhibits effectively 100% transmission at approximately 1.94 GHz through a square aperture of only 0.035 $\lambda_0 \times$ 0.035 λ_0 in size. The extremely high Q resonance presents a transmission greater than -10 dB over a bandwidth of 0.006%. Frequencies away from resonance are effectively blocked, with transmission down around -40 dB.

A complementary subwavelength resonator is also proposed which exhibits a narrow band filter response operating at 1.92 GHz with a fractional bandwidth of 0.04%. Band-stop transmission away from resonance is once again down around -40 dB. The subwavelength structures are sensitive to fabrication tolerances, but are realizable with modern printed circuit fabrication techniques. The 3-D structures also lend themselves to high aspect ratio micro-fabrication techniques for efficient implementation at higher frequencies. The 3-D

FSS exhibits tremendous potential in alleviating the limitations of 2D FSSs, and offering potential functionality beyond the capabilities of its 2D analogue.

Table of Contents

List of Figures

List of Tables

Abbreviations and Acronyms

2-D	2-Dimensional
3-D	3-Dimensional
AAA	Annular Aperture Array
CST	Computer Simulation Technology
DC	Direct Current
EC	Equivalent Circuit
EM	Electromagnetic
EMP	Electromagnetic Pulse
FDA	Food and Drug Administration
FSS	Frequency Selective Surfaces
MEMS	Micro Electro Mechanical Systems
PBC	Periodic Boundary Condition
PEC	Perfect Electric Conductors
RAM	Radar Absorbing Material
RCS	Radar Cross Section
RF	Radio Frequency
$\|S_{11}\|$	Scattering parameters — the response at Port 1 due to an input at Port 1
$\|S_{21}\|$	Scattering parameters — the response at Port 2 due to an input at Port 1
SRR	Split Ring Resonator
TETRA	Terrestrial Trunked Radio
TE	Transverse Electric Mode
TM	Transverse Magnetic Mode

CHAPTER 1

INTRODUCTION

1.1 Introduction

Frequency Selective Surfaces (FSS) are planar periodic structures of identical patches or apertures of conducting elements repeating periodically in either a one or two-dimensional array on a dielectric substrate. Depending on their physical construction, material and geometry, FSS are divided into four categories which are low-pass, high-pass, band-pass and band-stop filters. Because of its frequency-selective properties, FSS is incorporated in a wide variety of applications, such as radar-absorbing structures, the realization of reflector antennas, radome design, polarisers and beam splitters, and wireless communication systems[1-5].

The FSSs were intensively studied since the early 1960s. Early work concentrated on the use of FSS in Cassegainian subreflectors in parabolic dish antennas. Frequency Selective Surface (FSS) have become one of the most commonly known since their application as "Antenna feed system utilizing polarisation independent frequency selective intermediate reflector" in deep space communication, and moon explorations in the 1960's [6]. FSS are now employed in radomes (terrestrial and airborne), radar, missiles, electromagnetic shielding applications, reflector antennas, making polarizers and beam splitters and radar absorbing material (RAM). Implementation of FSS on radar absorbing material (RAM) increases the absorption, and its physical strength, which is more favorable for practical applications [7].

The usage of FSS in wireless communication systems is realized one of the most important components. As in communication systems applications FSS is designed to reflect or transmit electromagnetic (EM) waves with frequency discrimination, and have contributed significantly toward advancing modern communication systems.

FSS also been used in collision avoidance for aeroplane and helicopter. For instance, rescue helicopters have to be versatile for any weather conditions. By flying at low altitude they are facing obstacles that may not be detected by visual flight rules. A lot of work has been done in the past to develop obstacle sensors for collision avoidance, mainly for the expansion of operating conditions in military applications. For instance, a high gain Fresnel zone plate reflector was developed for helicopter collision avoidance radar. In order to increase the overall efficiency and enhance the antenna performance, the primary source of the reflector is consists of a Frequency Selective Surface (FSS). The frequency bandwidth of the primary source is enhanced by the use of double side etched substrate for the FSS [8].

As for practical applications, it is desired to realize a FSS with miniaturized elements and a stable frequency response for different polarizations and incident angles. However these features are difficult to obtain through traditional designs; and a large number of structures and modelling techniques have been proposed such as single-pole and dual-pole MEFSS, Artificial Magnetic Conductor using Jerusalem Cross Frequency Selective Surface, low pass filter using single folded stepped impedance hairpin resonator, and thick hexagon patches FSS [9-14]. Furthermore, complexity in the design of existing frequency-selective surfaces and their required size and sensitivity to the angle of incidence limits their functionality, such as inconsistency frequency response over a wide range of incident angles. Sensitivity to the angle of incidence limits their functionality, causing inconsistency in the frequency response over a wide range of incident angles. The FSS resonant frequency can diverge from the operating frequency of the communication system, rendering it non-functional. As an example, an airborne FSS radome attached to the nose cone the incident angles can be very large, even up to 80 degrees. Consequently, in order to reduce the radar cross section of radar and to ensure normal communication functionality of the airplane, a FSS with stable performance over large incident angles is required [15]. Thus showing the demand for improving their characteristics. Therefore, the purpose of this research is to develop new Frequency Selective Surface (FSS) that can improved functionality and performance over current FSS.

A new type of FSS that is called 3-D Frequency Selective Surfaces is proposed in this research where it is believed have a capability to give a positive impact in microwave area thus improved communication system technology. Research has shown that 3-D Frequency Selective Surface has demonstrated superior performance than conventional FSS. The third dimension of 3-D FSS extends the potential functionality of the structure and

adding extra degrees of freedom in the design. The extra degree dimension offer 3-D FSS an extra freedom into the structure provide additional advantages such as the ability to tune the frequency response without active component which subsequently reduce the total development cost. Not just has high selectivity characteristic, 3-D FSS is low profile stable performance with various incident angle which is more favorable in many microwave communication applications. Moreover, these new type of FSS is believed would be highly beneficial besides can be used for various applications thus improved our communication system technology.

1.2 Objective/Motivation

This study embarks on the following objectives:

- **To investigate** the use of novel 3D cylindrical frequency selective structures that reflect or transmit wireless band signals
- **To study and understand** performance characteristics of 3D cylindrical frequency selective structures and their correlation with design parameters.
- **To design, fabricate and validate** novel 3D frequency selective structures.

1.3 Thesis structure

The thesis comprises six chapters, and details for the contents of each chapter is given below.

Chapter 2: Chapter 2 of this thesis presents a literature review of research on FSSs. The development history of the FSS and its common applications are addressed. Objectives of this chapter include identifying the key factors which govern the FSS performance, and reviewing available techniques for theoretical FSS analyses.

Chapter 3: This chapter discuss both 2-D and 3-D FSSs employing a circular ring shape unit element. The 3-D structure is formed by raising the circular ring height creating a cylindrical element but keeping the same unit cell with planar case. The effect of varying height and dual cylinder are presented. In addition, a study in to the effect of dielectric materials introduced in the center of the 3-D cylindrical FSS unit cell architecture is also presented. Moreover, a new tuning technique using spring resonator is also been discussed. This technique is applied to 3-D FSS design to make it reconfigurable, and/or fine-tune the response. The versatile FSS geometry introduced here is based on a periodic array of spring resonator element structures. The unit cells consist of a thin aluminum wire (w = 1 mm diameter) wound into a helical spring resonator. The effect of varying height of the mechanical spring FSS which is similar to cylindrical structure also presented in this chapter. The operation and performance of the 3-D FSSs elements are described, and validated both numerically and experimentally.

Chapter 4: This chapter focuses on examining techniques which can be used to stabilize the FSS incident angle response. The design procedure of producing the 3-D

FSSs with independent incident angle, is presented, with its origins from a 2-D and 3-D FSS using square loop shape. Once again, the 3-D structures are formed by raising the four side of the square loop. The proposed FSS is a periodic array of 3-D hollow tapered resonators. The proposed 3-D FSS has reduced sensitivity to the angle of incidence of the electromagnetic wave as a result of tapered structure, compared to other 2-D and 3-D FSSs. The TE and TM incident angle independence is obtained by tapering the width of a cylinder with a square cross-section from upper opening to the lower opening. Impressive frequency stability and transmission characteristics have been achieved up to 80 degrees for both TE and TM incidence angles.

Furthermore, a novel 3-D Frequency Selective Surface (FSS) with horn shaped resonators is presented in this chapter which exhibits a very wide stop band. This new horn shaped resonator is a modification from a 3-D FSS consisting of square cylinder unit elements. This feature introduces frequency-selective surfaces with the added advantage of lowering the sensitivity of the FSS frequency response with respect to the incidence angle. The principles of operation along with guidelines for the design of the proposed FSS structures are discussed and comparisons are made in term of resonant frequency, fractional bandwidth, angular stability and reflection phase responses are also made.

Chapter 5: This chapter presents a Miniature FSS with high Q factor which enables significant reduction of the unit cell size, improves angular stability of the array performance and exhibits very selective narrow band response. The mechanisms underlying the distinctive properties of the wire resonators were examined. The Miniature FSS design procedure is based on an equivalent circuit (EC) model, and key parameters that characterize the required FSS frequency response are also examined.

Chapter 6 summarizes the main findings of this thesis and suggests directions for future developments. This research has thrown up many questions in need of further investigation, including multi-functional 3-D FSS design, FSSs with independent incident angle properties, tunable FSSs, alternative analysis and fabrication techniques, and optimized deployment strategies.

1.4 List of Publications

Journals:

J1. S. N. Azemi, K. Ghorbani, and W. S. T. Rowe, "3-D frequency selective surfaces," Progress in Electromagnetics Research C, Vol. 29, 191-203, 2012.

J2. S. N. Azemi, K. Ghorbani, and W. S. T. Rowe, "A Reconfigurable FSS Using a Spring Resonator Element," Antennas and Wireless Propagation Letters, IEEE 12, 781-784, 2013.

J3. S. N. Azemi, T. Baum, K. Ghorbani, and W. S. T. Rowe, "3-D Tapered Resonator Frequency Selective Surface with Incident Angle Independence" IEEE Trans. Microwave Theory Tech, 2013 – UNDER REVIEW

J4. S. N. Azemi, K. Ghorbani, and W. S. T. Rowe, "Angularly Stable Frequency Selective Surface with Miniaturized Unit Cell" IEEE Trans. Microwave and Wireless Component Letter, 2014– UNDER REVIEW

J5. S. N. Azemi, K. Ghorbani, and W. S. T. Rowe, " Miniature Wire Resonator with Enhanced Transmission using sub wavelength Aperture" Optics Express, 2014– UNDER REVIEW

Conferences:

C1. S.N Azemi, K. Ghorbani, W.S.T Rowe "Development and analysis of 3-D frequency selective surfaces" Microwave Conference Proceedings (APMC), 2011 Asia-Pacific, 693-696, 2011

C2. S.N Azemi, K. Ghorbani, W.S.T Rowe, "3-D Frequency Selective Surfaces with close band spacing" Microwave Conference Proceedings (APMC), 2012 Asia-Pacific, 454-456, 2012.

C3. S.N Azemi, K. Ghorbani, W.S.T Rowe, "A Reconfigurable FSS using a Spring Resonator Element" European Microwave Conference (EUMC), 2013

C4. S.N Azemi, K. Ghorbani, W.S.T Rowe, "3-D Frequency Selective Surface with Incident Angle Independence" European Microwave Conference (EUMC), 2013.

C5. S.N Azemi, K. Ghorbani, W.S.T Rowe, “3D Frequency Selective Surfaces with Wideband Response” International Workshop on Antenna Technology (iWAT), 2014.

C6. S.N Azemi, K. Ghorbani, W.S.T Rowe “Miniaturized Resonator Frequency Selective Surface” Australian Microwave Symposium, (AMS), 2014.

1.5 Contributions

The main contributions of this research are the development and demonstration of various novel 3-D Frequency Selective Surfaces. The benefit of 3-D FSSs has been examined and quantified with both theoretical modelling and practical measurements. A summary of the contribution to the body of knowledge is listed below:

- A novel 3-D Cylindrical FSS is proposed (section 3.2), where it shows that the length of the cylinder has significant effect on the stop band frequency selective characteristics of the FSS. (J1, C1)
- Dielectric materials are introduced in the center of the cylindrical unit simultaneously obtain closely spaced band pass and band stop response with a sharp transition (section 3.2.3) extending the flexibility of the 3D cylindrical FSS and potential functionality beyond its 2-D FSS. (J1)
- Adding extra freedom in design of 3-D Cylindrical FSS, 3-D Dual Cylindrical FSS is proposed (section 3.3), where a closer band response (approaching a 1:1 ratio) can be achieved by extrapolating the height of planar dual ring unit cell without need to design a very close gap between two elements. (C2)
- A comprehensive study of 3-D Cylindrical FSS has been done, enabling the creation of a new tuning technique using spring resonator element called 3-D spring FSS structure is presented (section 3.4). This new structure can achieve functional switching between band-stop and band-pass operation without the need for active device integration. (J2, C3)
- A symmetrical 3-D FSS (section 4.2) identifying key structural parameters on the transmission performance (section 4.3), which enable the creation of 3-D tapered FSSs (section 4.4) with a stability response under oblique incidence angles of up to 80^{o} and 3-D wideband FSS (section 4.5) which has a significant improvement of the bandwidth while the angular stability of the frequency response was nearly unchanged. (J3, C4, C5)
- A miniature wire resonator FSS with angular stability (section 5.2). The FSS structure is shown to have a FSS unit cell dimension that is miniaturized to 1/15 λ_0. (J4, C6)
- A planar miniature wire resonator solution to enhance the light passing through subwavelength apertures down to 1/50 λ_0 square. (Section 5.3). (J5)

CHAPTER 2

Literature review

2.1 Introduction

FSSs are usually formed by creating a periodic array of resonating elements that effectively act as filter to electromagnetic waves. Generally, a FSS is a 2-D planar structure that consists of one or more metallic patterns, each backed by a dielectric substrate. The 2-D FSS is arranged in a periodic fashion and the frequency response is determined by the geometry of the structure in one period called a unit cell. There are a wide variety of possible elements that can be used to realise FSS arrays, for example a circle [16, 17], square [5, 18-20], hexagon [21, 22], fractal geometries, cross dipole [5], or convoluted shapes [23-26]. Different element shapes offer FSS with different frequency responses. Depending on their physical construction, material, and geometry, they can be divided into four categories: low-pass, high-pass, band-pass, and band-stop filters, as shown in Figure 2.1.

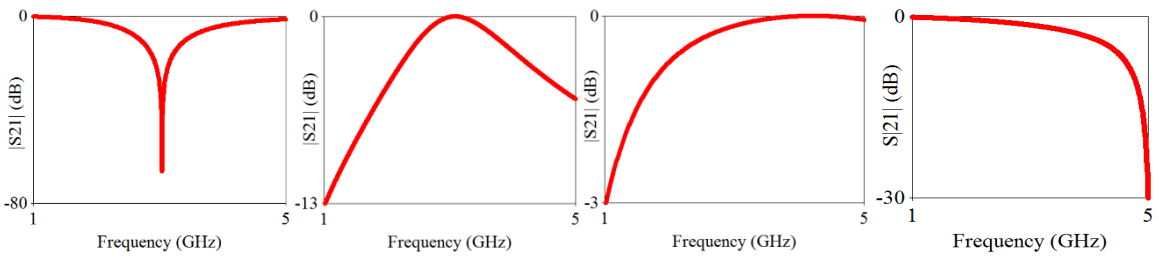

(a) (b) (c) (d)

Figure 2.1: FSSs can be classified into four categories of filter responses: (a) band-stop, (b) band-pass, (c) high-pass, (d) low-pass.

The applications of FSSs are many and varied, ranging over much of the electromagnetic spectrum (refer to Figure 2.2). In communication systems applications, FSSs are designed to reflect or transmit electromagnetic (EM) waves with frequency discrimination, and has contributed significantly towards advancing modern communication systems. The applications of FSS encompass reflecting elements for reflector antennas [27], efficiency and bandwidth augmenters for antenna arrays [28, 29], and EM shielding of indoor environments against interference [30, 31]. FSSs can be applied to radomes to reduce the radar cross section (RCS) of antennas at the out-of-band frequencies. In this situation, the band-pass characteristic of the surface is adopted. In other words, the FSS radome allows the incident signals to pass through at the operating frequency, and reflects the signals outside the operating band to reduce the backscattering radar cross section [32]. More recently, there is an interesting application of FSS in wireless communication systems. In prison cells, public libraries, and theatres, FSSs are printed on the windows and the walls of buildings to block the mobile phone signals and to allow the emergency Terrestrial Trunked Radio (TETRA) services to operate.

Figure 2.2: Some example of Frequency Selective Surface applications [33-35].

Another simple example of an FSS is microwave oven door. The FSS acts as a high-pass filter. The oven door, which blocks the 2.4 GHz microwaves inside the oven, on the other hand, allows visible light to pass through. Hence, the cooking progress can be monitored without any harm. In other words, although the oven door is optically 'transparent', it essentially acts like a closed metal shield to the internal 2.4 GHz microwave transmissions. However, there are very small amounts of radiation leakage through the viewing glass while it is operating due to less sensitivity to the angle of incidence inside the microwave oven. Nevertheless, the Food and Drug Administration (FDA) reports that the amounts of radiation leakage are "insignificant" and "well" below the level known to harm people.

The design complexity of existing FSSs and its required size and sensitivity to the angle of incidence limit its functionality, thus showing the demand for improving their characteristics. Specific characteristics for further research are the ability to tune the frequency response without active components, low dependence of the FSS on the incidence angle of the exciting wave, as well as operability of the surface with small dimensions of the FSS panel compared to the wavelength. In this chapter, an overview of traditional methods in FSS design compared with more recent approaches is provided, demonstrating a requirement for performance superior to that of what is available.

2.2 Key Properties of FSSs

The following chapter will discuss key properties of designing FSS, such as: FSS element shape; FSS configuration; FSS standard responses; unit cell size; as well as angular stability.

2.2.1 FSS element shape

The resonant element geometry (including element shape) is a fundamental aspect in FSS design. The most common FSS element shapes include a simple straight dipole, circular loop, cross dipole, three-legged dipole, square loop, and jerusalem cross, as shown in Figure 2.3. Depending on the physical construction and geometry of the surface, the FSS can efficiently control the transmission and reflection of the incident electromagnetic plane wave and have low pass, high pass, band pass, and band stop behaviours.

The shape of the conducting element which constitutes an FSS is unrestricted. According to Munk [36], element shapes can be generally categorised into four basic groups, namely:

a) Centre connected, such as dipoles, tripoles, Jerusalem crosses, and cross dipoles.
b) Loop types, such as square loops and rings.
c) Solid interior types, usually in the form of patches or apertures. For examples, circular patches and square meshes.
d) Combinations, sophisticated patterns with combinations of any of the centre-connected, loop, or solid interior shapes to overcome FSS performance deficiencies that are associated with simple element shapes.

Some common shapes are illustrated in Figure 2.3. Each shape possesses unique frequency characteristics. Some are possibly more sensitive to incident angles, and some allow a rapid transition between pass and stop bands. Other shapes offer a desirable wide operating bandwidth, but may perform inconsistently between vertical and horizontal signal polarisations. Table 2.1 summarises the performance of some common shapes relative to others, based on a single layer freestanding FSS [37].

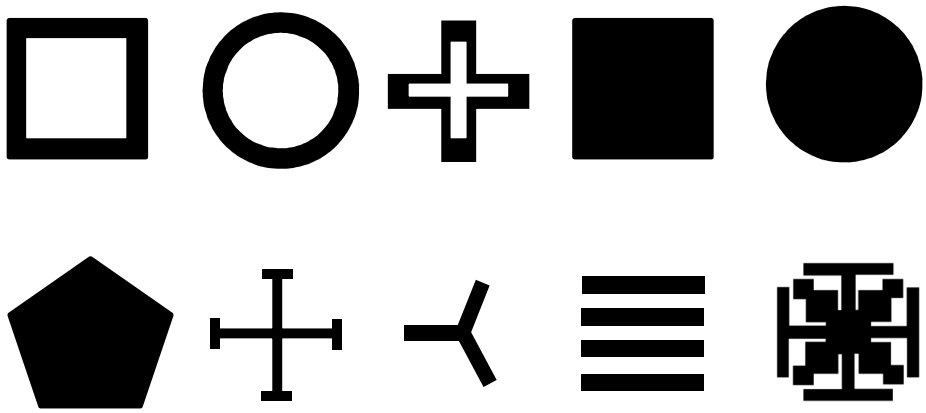

Figure 2.3: Different element shapes offer FSS different frequency responses.

Table 2.1: Performance of FSSs with different element shapes (based on the freestanding FSS performance, reproduced from [37])

Element shapes	Angular stability	Cross-polarization level	Larger bandwidth	Small band separation
Dipole	4	1	4	1
Jurusalem Cross	2	3	2	2
Ring	1	2	1	1
Tripole	3	3	3	2
Cross Dipole	3	3	3	3
Square Loop	1	1	1	1

Ratings: best = 1, second best = 2, third best = 3, least = 4.

Table 2.1 shows that the square loop and ring outperform other types of basic element shapes as they are rated 1 (or 2) in every performance characteristic investigated. A square loop FSS provides the basis for this investigation since it has demonstrated less sensitivity to incident wave angle than other shaped resonator elements. Because of its simple shape and its appropriate frequency characteristics for notching out the transmission, the square loop and ring were chosen as the fundamental FSS element shape for this research.

2.2.2 FSS Configurations

Conventional FSSs consists of a two dimensional (2-D) periodic array of unit-cells either printed on a dielectric layer or cut out of a conductive surface. Two dimensional (2-D) FSSs (or single-layer FSSs) are light in weight and compact in volume, unlike multi-layered FSSs. In some FSS applications, a wide bandwidth is a requirement, and a single layer FSS typically has only one resonant frequency. Conventional single layer FSS are not just restricted on the bandwidth; but are dependent on the polarisation of the incident wave as well [20, 30, 36].

In order to solve to create a wideband FSS, it is necessary to use a very complicated geometry or multilayer structures. Stacking two identical FSS arrays causes a broad bandwidth response. For instance, an FSS can be sandwiched or stacked between thick dielectric materials in order to obtain wideband response. If these two arrays are cascaded, three distinct array interference notches appear at a low, middle, and high frequency [36]. The null at the middle frequency will disappear or become infinitely thin if both layers of the FSS are resonant at the same frequency (middle frequency). In order to make the middle frequency disappears to get a wider bandwidth, the spacing between the arrays is adjusted. Therefore, cascading two identical FSS arrays results in a reflection curve with a much flatter top and a faster roll off compared to a single FSS array [36]. If cascading two identical FSS arrays does not provide sufficient bandwidth, a third FSS layer is added, which is resonant at the upper null. It is also possible to cascade two FSS arrays that are not identical [25]. By varying the separation width or thickness of dielectric, a wideband response is obtained. With a thicker dielectric, effective permittivity increases, and thus the perturbation becomes more distinct as the field is more confined within the dielectric substrate [38, 39].

Multilayer FSSs can be difficult and costly to construct, as several planar FSSs must be manufactured and stacked in some fashion. Such a procedure increases the cost and complexity over a single planar FSS in proportion to the number of stacked FSSs. Secondly, numerical analysis of the structures is vastly complicated due to the coupling effects between the stacked FSSs. As a solution, a single planar FSS with multiple apertures/patches per periodic cell is proposed [40]. Instead of a single perfectly conducting strip, a group of multiple strips constitutes a unit cell. In this case, the group is periodic, not the individual elements. Multiple periodic FSS avoids the cost and complexity of manufacturing several planar FSSs necessary in the stacked design. An added benefit of the multiple periodic element planar design is that it allows for simple rectangular elements to be arranged in a group so as to produce less-polarisation dependent filter designs [41]. Nevertheless, this type of FSS exhibits multiple unwanted resonances features due to the multiple sizes and types of elements per unit cell [42].

2.2.3 FSSs with close band responses

Recently, researchers have shown an increased interest in design of FSS with close band responses [43]. Close band response is needed in some applications such as in military system for their aircraft, missiles, and naval vessel to simultaneously communicate with different communications satellites [44, 45]. FSSs with close band response are also used in reflector antennas for space-borne applications. Multiple operating frequencies are needed in these applications [46]. The challenge is to design an FSS that works for three bands namely S-band (2.2 GHz), Ku-band (14.9 GHz), and Ka-band (25.25 GHz), and two FSSs have been used to isolate the bands that are reflective at S-band, and that are transparent at Ku-band and Ka-band. For each band, the reflection/transmission centre band frequency ratio requirement is approximately 1.48 or less [45]. Typically, in close band FSS design, the band spacing is determined by the clearance between concentric elements. The clearance must be small enough to meet the close band requirement. In practice, a very close clearance cannot be implemented due to the limitations in fabrication. Consequently a strict requirement for fabrication process is needed and some unexpected coupling between the concentric elements occurs.

Gridded square FSSs are proposed to give closer reflection/transmission band ratios, which are 1.3 to 2.1 compared to >2.5 for the single square FSS [18]. This design requires multilayer structure that increases the cost, complexity in fabrication, and difficulty in maintenance. Close band spacing can also be achieved by designing the resonant frequency of the double square units with different loadings by using active components [47-49]. A dual-band loaded FSS design has been introduced to mitigate this issue and to achieve close band spacing. The resonant frequency of the double square unit cells is tailored with different loadings of lumped components. Although this is a very useful solution in order to get a close band response, it requires the addition of a large number of chip capacitors that need to be soldered precisely into each unit cell.

2.2.4 Tunable and Switchable FSSs

Another practical feature of FSS structure design is the ability to electronically tune the frequency response. Tunable FSSs are useful for tunable radomes or adaptive screening of unwanted wireless transmissions [2, 50]. The characteristic of tunable FSS can be seen through conventional methods including loading with active semiconductor device like varactors diodes, PIN diodes, and Schottky diodes in a traditional FSS element design [51-54]. For biasing the active components, DC grid arrays are required in a separate set of circuitry [55, 56]. By adjusting the DC voltage control, the reflectivity and transmitivity of an FSS can be modified. For instance, the transmission characteristics of FSS structures can be switched or varied with different bias states of varactors. However, the large scale biasing grids can limit the performance of FSSs by interfering with the RF signal, resulting in poor selectivity, providing unbalanced biasing, and introducing polarisation dependence. Furthermore, the fabrication cost/complexity and losses associated with the bias grid remain a problem in practical tunable FSS implementations. More recent methods of implementing tunable FSS use micro electro mechanical systems (MEMS) technology to create capacitors or switches to vary the electrical shape of the unit cell [57, 58]. Radio Frequency micro electro mechanical systems (RF-MEMS) switches can provide continuous and smooth transitions between FSS characteristic behaviours. The RF-MEMS devices electrostatically actuate two-state switched capacitors that control the FSS resonant frequency. The switching speed of RF-MEMS is fast, and the DC power consumption is very low. However, these solid state switches suffer from nonlinearity and low isolation. Moreover in FSS applications, a huge number of active elements are required, which again increase cost/complexity and the potential for failure [59, 60].

Mechanical reconfiguration of FSSs claims to deliver the most dramatic FSS parameter variations. Mechanically tunable FSSs can be implemented by shifting one layer of double-layer FSS, hence altering the resonant frequency [61]. The relative shift of one layer with respect to the other changes the coupling capacitance between the layers. Another mechanical reconfiguration technique involves tuning unit cell geometry via pneumatically actuation [62]. It is shown that the pneumatic actuation approach can unite physically separated metallic elements, thus switching the operational frequency of the structure. Pneumatic switching does not require a DC bias supply, and can maintain its switch state

for some time. Moreover, the major advantage of pneumatic actuation is the elimination of metallic biasing wires in the structure, which can interfere with the operation of the structure and could be prone to damage in a harsh environment. Thus, the biasing wires are replaced with RF-transparent air-actuated structures.

2.2.5 Incident angle stability

Once exposed to electromagnetic radiation, a FSS is expected to act like a filter independent on the angle of incidence and polarisation. As in reality signals arrive at various angles, it is desirable to design an FSS that functions consistently over a wide range of incident angles. As electromagnetic waves possibly will strike the FSS from any arbitrary angle and have different polarisations, the transmission and reflection properties of the FSS should have a stable frequency response when the angle of incidence or polarisation changes. However, the spectral response of most FSS depends on the polarisation and the angle of incidence of incoming waves [63]. For an indoor office environment in which an FSS will be applied, signals possibly will very likely undergo multiple reflections between walls or furniture before they reach the receiver. Consequently, signals arrive on the FSS-modified wall at a range of different angles. More specifically, the resonant frequency shifts as the incident angle changes. Therefore, when designing an FSS, or when evaluating its performance, it is very important to take into account the incident angle variation.

The variation in FSS performance due to changing signal incident angles can be somewhat alleviated with a proper FSS design, such as an appropriate choice of element dimensions or the use of multiple FSS layers and dielectric substrates [1, 13, 30, 64]. In an attempt to reduce the angular sensitivity, double-layer configurations have been proposed and investigated [65-69]. For example, Jerusalem Cross FSSs offer stable resonance frequency with respect to the incidence angle of both TE and TM incident plane waves [67, 68]. The frequencies are rather stable up to 50 degrees with only ±1% deviation. By adding an extra layer, the two-layer Jerusalem Cross FSS is obtained and yields smaller cell size and thickness with better angular stability. The separation distance between the two element layers has been identified as a key issue in the design and performance of the FSS. The closer the layers are to one another, the more the angle stability will be improved. However, it has been realised to only increases the stability of the TM incident angle whereas TE incidence performance significantly decreases after 20 degrees [68].

A new method that has independence towards incident angle particularly for TE waves has been proposed in [70, 71]. The design of the FSS is based on the Annular Aperture Array (AAA). A square array of square annular apertures is patterned on a metal film deposited on a glass substrate with a certain value of height. The corresponding transmission position can be tuned by simply modifying the refractive index of the medium placed inside the cavities as well as the height of the metal thickness, which is the length of the annular cavity. The structure is angle-independent up to around 70°; however, additional transmission peaks appear in the case when TM incident angle is increased. Fractal FSSs have shown excellent polarisation and angular stability because of its symmetric fractal configuration [72, 73]. Furthermore, fractal resonators have been proposed as small size scatterers, thus it is able to reduce the angular sensitivity [74, 75]. Split ring resonators (SRR) can also be used as small-sized scatterers for FSS design. However, the transmittance/reflectance of SRRs makes the FSS strongly dependent on the angle of incidence and polarisation. Nevertheless, a stable response can be achieved with proper arrangement of SRRs [76]. A stable SRR is obtained by employing two closely spaced arrays of ring elements with the conductor split at appropriate positions to provide independent control of the resonances for the vertical and horizontal field directions. Therefore, stable responses for TE and TM waves are achieved when the FSS operates at 45° incidence. A suitable isotropic modification of the proper arrangement SRR has been used in the design of a cubic unit element. The results shows that the angles are stable until 50 degrees for TE and TM incidence [77]. The only challenge is to find a suitable arrangement of SRRs that shows an isotropic behaviour for the FSS.

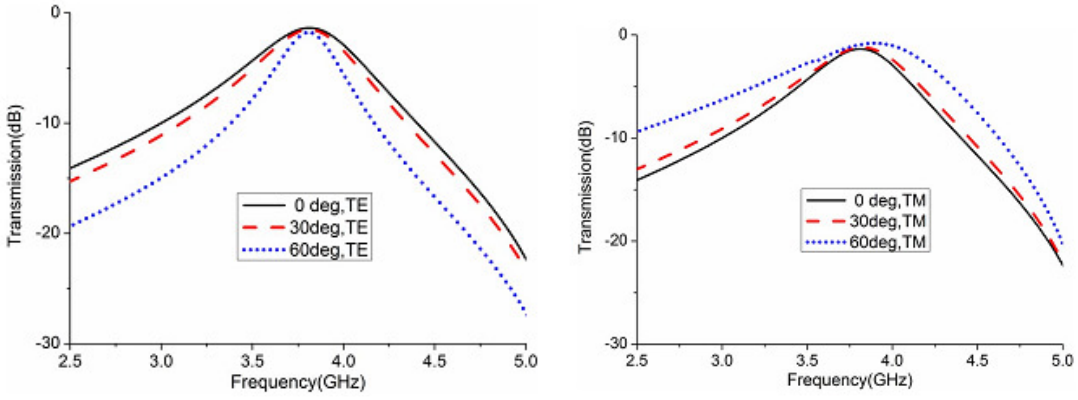

Figure 2. 4: Shows transmittances of the FSS when illuminated by different incident angle. (a) TE polarized wave, (b) TM polarized wave. [69]

2.2.6 FSSs with small unit cell size

Recently, many approaches have been proposed to obtain FSS unit cell dimensions much smaller than a wavelength. Physically, small microstrip arrays exhibit universal application because of its excellent inherent characteristics of simple configuration, light weight, small volume, low cost, and low sensitivity with respect to the incidence angle of the exciting wave. For some applications, FSS of relatively small electrical dimensions that are less sensitive to incidence angle and can operate for non-planar phase fronts are highly desirable. A radome for miniaturised low-frequency antennas and antenna arrays is an example of this category.

In wireless communication systems, small-sized devices are needed to reduce the cost, and thus miniature resonators have been reported as the key components to miniaturise an electronic device [78, 79]. There are few approaches in resonator miniaturisation, among which are the use of lumped element [80-82], loading of the resonator with a helix [83], use of a very high dielectric substrate [84, 85], hair pin resonator, and split ring resonators [86-91]. Another effective way to diminish the size of an FSS unit cell is by integrating a suitable lumped capacitor within two slots, introducing a capacitive gap between two ends of the resonators. The unit cell size diminishes to 0.06 $\lambda_0 \times 0.22\ \lambda_0$ in this case [92]. Specific applications of these types of FSS filters include narrowband astronomy filters and filters for spacecraft instrumentation.

The size reduction of ordinary microstrip line resonators, for example, has been made by using lumped capacitor [82, 91]. The proposed technique achieves 80% smaller in area as compared with its conventional design [90]. This method involves a miniaturisation technique of the hairpin resonator filters using lumped capacitors. The hairpin resonator is designed using a bent open-circuit transmission line with coupled line section for miniaturisation. Further miniaturisation is achieved through the loading of lumped capacitor where the value of C varies the resonant frequency of the resonator accordingly. Lumped-element resonators can be made very small at low frequencies. At high frequencies, however, their extremely small size may result in high insertion loss and possibly low power-handling capacity.

In order to reach a compromise between size and performance, some compact architectures have been proposed. Another form of resonator, which is also a miniature in

size ($1/17\lambda_o$), utilises open loops with inner split rings loading [88]. The structure achieves miniaturisation by first designing the open-loop square resonator at a high frequency, and then through loading method. To further reduce the size, the open-loop structure is modified by introducing a narrow capacitive gap at the open end of the loop. The use of this multiple rings allows a very wide frequency perturbation and eventually allowing significant size reduction as compared to the meander loop resonator or the hairpin resonator [89, 90].

Recently, transmission enhancement from a resonator array of subwavelength apertures has attracted the attention of many researchers. This fascination is mainly due to the recent technological progress in nanofabrication, allowing prospective manufacturing of large periodic structures with high aspect ratios. Furthermore, a narrow and strong peak of transmission is achieved through a small aperture, and the surprising fact is that the diameter of the holes is significantly smaller than the corresponding wavelength. In [93], a multi-split ring resonator is proposed and inserted perpendicular in a hole to enhance the light passing through a subwavelength aperture. By using a proper aperture size, a 98% transmission has been achieved. However, no measured result has been shown to prove the method as this structure is near impossible to fabricate over a broad area.

2.3 Motivations

Traditional FSSs consist of a two-dimensional (2D) planar structure, which is formed by periodic patch elements or slot arrays of simple elements backed by a supporting dielectric layer. These planar FSS structures are easy to fabricate, but have limitations in their performance in terms of susceptibility to changes of polarisation and sensitivity of angle incidence. A wide variety of methods can be found in the literature (section 2.2) for improving the characteristics of traditional 2D FSSs. One trend is to implement a tuning circuit as part of the FSS pattern so that the frequency properties can be varied [56]. When narrow frequency band separation is desirable, a multiband FSS can be constructed using concentric double square elements. However, strict fabrication tolerances are required, and the coupling between the concentric elements difficult to control [43]. Once exposed to electromagnetic radiation an FSS will ideally act like a filter independent of the angle of incidence and polarization, since in reality signals will arrive at arbitrary angles. In an attempt to reduce the angular sensitivity, multi-layer configurations have been proposed to

produce a smaller cell size and thickness with better angular stability [24]. Complexity in the design of existing frequency-selective surfaces and their required size and sensitivity to the angle of incidence limits their functionality, thus showing the demand for improving their characteristics. The pros and the cons of the current FSSs in the literature have been summarised in Table 2.2.

Table 2.2: Summary of the Pros and Cons of Current FSSs.

	Pros	**Cons**
Conventional Single Layer FSS	• A planar	• Incident angle and polarisation-dependent • Narrow bandwidth
Multilayer FSS	• Wide bandwidth • Multiband	• Coupling effect • Difficult and costly to construct
FSS with close band responses	• A very selective Frequency Selective Surface	• strict requirement for fabrication process is needed • unexpected coupling between the concentric elements occurs
Active/Tunable FSS	• Frequency properties can be varied	• Requires huge number of active elements • High cost/complexity • Potential for failure
Small resonator	• Practical to be placed within curved surfaces and limited space • Enhancement of transmission passing through a subwavelength aperture	• High insertion loss and possibly low power-handling capacity • Difficult and costly to construct

The aim of the research in this thesis is to evaluate and validate a novel type of 3-D FSS that is believed to overcome some of the drawbacks identified in conventional FSSs. To add an extra degree of freedom in designing FSSs, the unit cell element was made 3-D by giving it a certain length or height, extending the potential functionality of the structure. The proposed structure consists of two design stages. The first stage is to design the 2-D FSS element and then to map it into a desired 3D shape. The simple ring and the square loop shapes of flat FSS are used. The three dimensional structures are formed by extending the length of the elements creating a cylindrical structure. The characteristics of 2-D and 3-D FSSs are analysed, including the resonant frequency, the fractional bandwidth, and the

stability with different incident angles. Parametric analysis of the 3-D FSS is undertaken using CST electromagnetic software and experimental validation is attained.

2.4 3-D Frequencies Selective Surfaces

Recently, studies have shown that 3-D FSSs have demonstrated superior performance to 2-D FSS. A multimode cavity/resonator 3-D FSS that comprises of a 2-D array of cavities has been proposed [94, 95]. It offers great flexibility in terms of controlling the number and position of desired transmission poles and zeros. For example, to achieve multiple band behaviour, one needs to increase the number of poles and zeros. Its modes and coupling can be controlled in order to obtain a desirable frequency response. As for conventional designs, an increase in the number of poles and zeros translates to having a multilayer FSS. Nevertheless, it has been conclusively shown that the number of poles and zeros can be controlled by using 3-D FSS.

Recent evidence also suggests that filtering behaviour is modified by placing 3-D FSS between the two dielectric layers, and resultantly the FSS shows symmetric filtering response with stable angular stability. The 3-D FSS is sandwiched between two dielectric layers, covered by perfect electric conductors (PEC) and walled by periodic boundary conditions (PBC). Stability of filtering response is expected with the placement of a dielectric layer. This is because an incidence from a larger angle will appear from smaller angle due to the refraction through dielectric material [95]. Recently, a 3D-FSS based on a four-legged loop element for band-stop applications has been shown to have a better angular stability for different angles of both TE and TM polarisations up to 50 degrees. This FSS structure was designed with unit cells arranged on a four-layer PCB and it was implemented using via holes and in multilayer printed circuit board [97].

A wide bandwidth 3-D FSS with a stable angular response reported recently consists of a waveguide element with two connected cascaded cross-shaped elements [96]. The elements achieve a flat band pass response with a bandwidth of 66.6%. The angular response of the FSS can be controlled by changing its periodicity, which in turn determines the angle at which the first higher-order Floquet harmonic begins to propagate. Therefore, the beamwidth of the FSS can be controlled by varying the periodicity, thus leading to an

onset higher-order modes at progressively smaller angles, in turn decreasing the angular bandwidth.

A new concept of 3-D FSS, which is different from conventional 2-D FSS, is proposed in [98]. A metallic cube cavity structure without dielectric layer is introduced, which is different from the mentioned 3-D or multilayer 2-D FSS. The resonance frequency is scalable with the geometry dimension characterised with multiple resonances and with broad relative bandwidth. The bandwidth of the structure is determined by the size of the hollow part of the cube. A larger hollow part results in a broader bandwidth, and the centre frequencies shift to a lower frequency band while a contrary result is achieved with smaller hollow part. The 3-D cube with cavity FSS has also been tested for the potential application in shielding electromagnetic pulses (EMP), showing superior protection. It is concluded that the design of this structure is convenient, and some characteristics are better than the conventional FSS.

This thesis proposes new types of 3-D FSS consisting of vertically arranged cylindrical unit elements of a certain length. This extends the potential functionality of the structure and adding extra degrees of freedom in the design. The frequency response can be tuned as well as producing either band pass or band stop operation by varying the length of the 3-D cylindrical elements. Furthermore, a very selective FSS can be achieved without the addition of lumped components by using two cylindrical elements. A 3-D Tapered FSS produces a stable angular response to at least 80^{o} with less than 0.5% deviation without being sandwiched between two dielectric layers. These structures are also much easier to fabricate with additive manufacture techniques and less complicated than existing 3-D FSS. A new simple multi-layer wire resonator which exhibits sub-wavelength operation, high Q, has low incident angle sensitivity is also investigated. Miniaturization of these unit cell elements can be achieved far beyond that of conventional method of realizing multilayer resonators. A comprehensive study on these new types of FSS is presented in Chapters 3, 4 and 5. Parametric studies are carried out using CST Microwave Studio simulation software to confirm the technique, and the manufactured prototypes verify the results experimentally.

CHAPTER 3

3-D Cylindrical FSSs

3.1 Introduction

This chapter outlines the inception and design methodology for 3-D FSSs considered in this research. The fundamental 3-D FSS consists of vertically arranged cylindrical unit elements of a certain length, extending the potential functionality of the structure beyond that of its 2-D analogue, a circular ring FSS. In order to successfully understand 3-D Cylindrical FSS, the following research questions need to be addressed:

- What are advantages of 3-D FSSs over a conventional FSS?
- What is the mechanism that causes performance improvement of 3-D FSSs?
- How can tunability be implemented in 3-D FSSs?

This chapter addresses these research questions and presents the research findings. In addition, a study of the effect of dielectric materials introduced in the center of the 3-D cylindrical FSS unit cell architecture is presented. The addition of the dielectric filling can significantly modify the frequency response, providing greater design flexibility and the ability to achieve an extremely closely spaced stop and pass band [99, 100].

As an alternative to using a high permittivity filling, a dual cylinder 3-D FSS is also proposed and studied in this chapter. The structure enables a very close band response without using any additional lumped components or filler materials. By varying the length of the dual cylinder 3-D FSS, the frequency response is adjusted, and a closer band response operation can be achieved [101].

3-D FSSs are shown to have the ability to set resonant frequency and shift operational filter states with a change in the length of a cylindrical resonator. For this to be achieved dynamically, a 3-D spring FSS structure is proposed. The 3-D spring FSS structure can be tuned by reconfiguring the pitch angle (and hence height) of a helical resonator of constant wire length. The 3-D spring FSS presented and studied in this chapter offers tuning and switching functionality within the same structure without the use of additional DC bias networks [102]. A parametric analysis of the 3-D FSS elements is undertaken using CST electromagnetic software, and is validated both numerically and experimentally.

3.2 3-D Frequency Selective Surface Structure

A 2-D circular ring resonator element provides the basis for this investigation. A conventional 2-D FSS was created by periodically arraying circular ring elements on top of a 10 mm thick foam substrate (used as the structural support). The circular ring resonator was chosen since it has been demonstrated to have less sensitivity to incident wave angle than other shaped elements [103]. A schematic of the FSS is shown in Figure 3.1(a). The diameter of the ring is determined using the basic ring resonator equation: $d \approx \lambda_0/\pi$. The diameter d of the rings and width w (d_{outer} - d_{inner})/2 = (32 - 29.4)/2 = 1.3 mm of the conducting strip primarily determine the resonant frequency, while seperation period p controls the FSS angular performance. These are general rules of thumb for designing an FSS [36, 103]. Studies have shown that a smaller diameter results in a higher frequency and a smaller p ensures frequency stability with varying incident angles.

Figure 3.1(b) shows the circular ring FSS frequency response and equivalent circuit obtained from an electromagnetic simulation in a CST Microwave Studio. The simulation shows that the FSS has the expected band stop characteristic centered at 3.12 GHz.

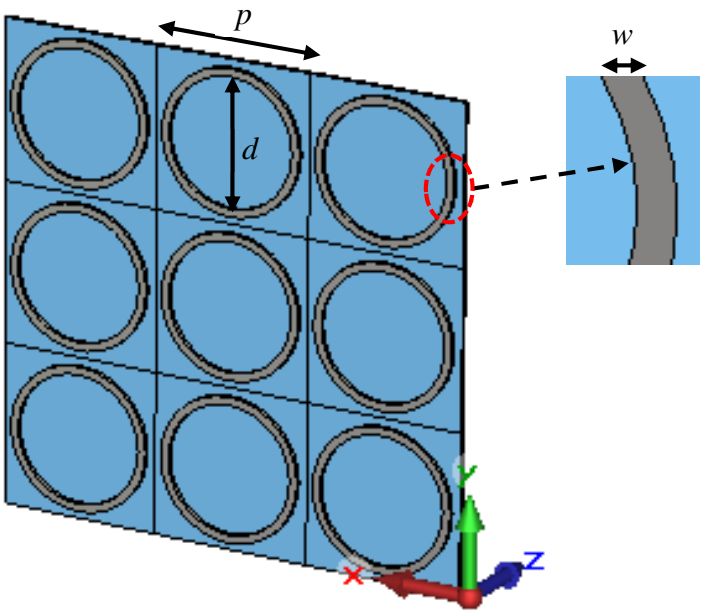

(a)

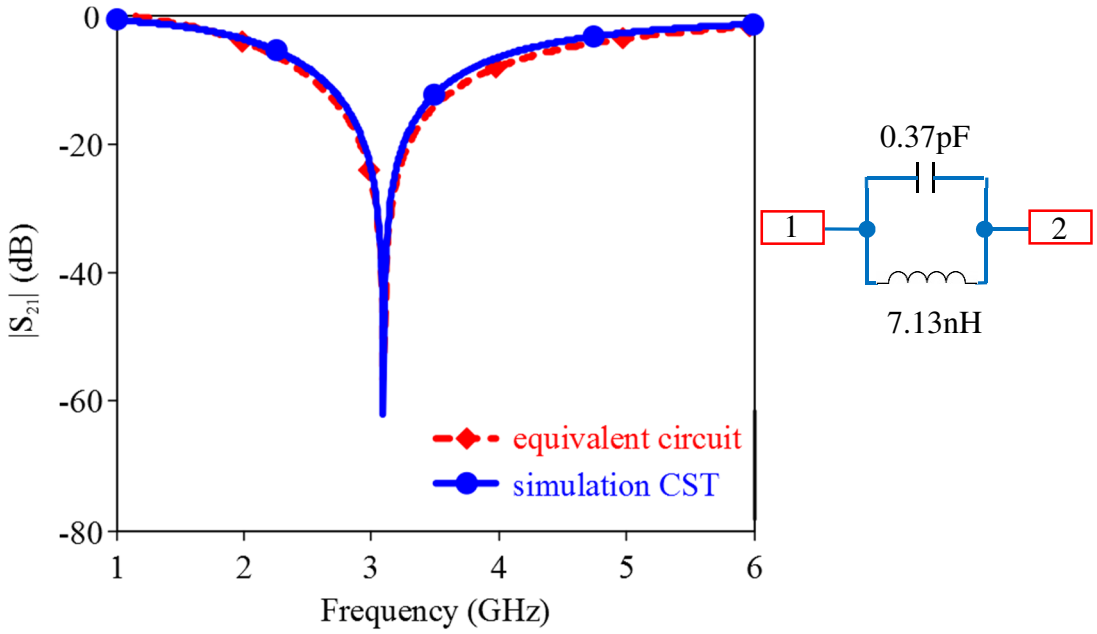

(b)

Figure 3.1: (a) Circular ring FSS – dimensions: p = 34mm, w = 1.3mm, d = 32mm.

(b) Transmission performance and equivalent circuit of the circular ring FSS shown in (a).

The value of inductance (L = 7.13 nH) and capacitance (C = 0.37 pF) is retrieved by using the following equation [104]:

$$L(nH) = 3.937\frac{a^2}{8a + 11c} \times K_g \qquad (3.2.1)$$

$$a = \frac{D_{outer} + D_{inner}}{4}$$

$$c = \frac{D_{outer} - D_{inner}}{2}$$

$$K_g = 0.57 - 0.145\, ln\frac{w}{h} \qquad for\ \frac{w}{h} > 0.05;\ \ where\ h = 0.035\ mm$$

$$C(pF) = \frac{1}{(f.2\pi)^2} \times \frac{1}{L} \qquad (3.2.2)$$

3.2.1 Development of 3-D Cylindrical FSSs

The circular ring FSS was made 3-D by introducing a certain height to the conductors of the unit elements, creating cylinders with a length l (seen in Figure 3.2). The desired operating frequency of this 3-D cylindrical FSS can be obtained by varying the length of the resulting cylinders. Figure 3.3 shows the transmission results of the 3-D cylindrical FSS with different lengths (all other parameters are equivalent to those in Figure 3.2).

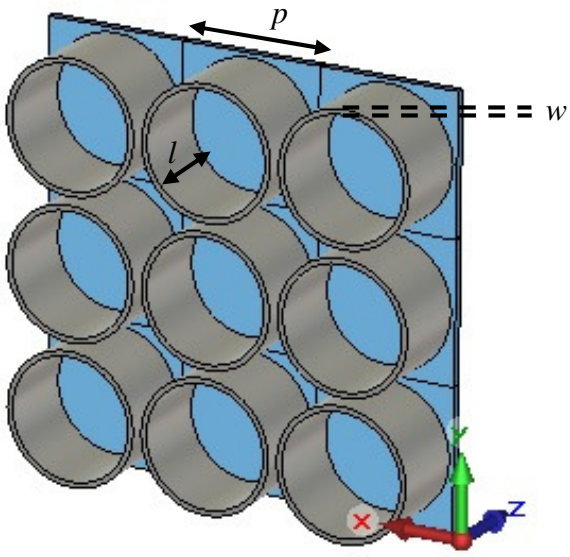

Figure 3.2: 3-D cylindrical FSS - p = 34 mm, w = 1.3 mm, d = 32 mm.

The dependence of the response of frequency selective surfaces on the cylindrical length is studied. An increase of the cylindrical length causes a shift to higher resonant frequencies of the transmission stop band. By changing the length of the cylindrical unit elements to 5 mm, 10 mm, 15 mm and 18 mm as shown in Figure 3.3(a), the center of the band-stop shifted to 3.2 GHz, 3.5 GHz, 4.1 GHz, and 4.7 GHz respectively. This frequency shift initially occurs without substantially affecting the band-stop notch characteristics, although a slight broadening of the bandwidth is observed. The transmission minima and bandwidth obtained from the $|S_{21}|$ curves are reasonably well maintaned until the 18 mm length is reached. Detailed data can be seen in Table 3.1. At this point a significant depth to the structure has been introduced, instigating a transition from a band stop to a band-pass topology for the FSS. As seen in Figure 3.3(b), the FSS creates a band-pass characteristic as the length (l) of the cylinder increases more than 20 mm. Further increasing the length to 24 mm 30 mm and 40 mm, the center of this band-pass decreases in frequency to approximately 5.4 GHz, 4.4 GHz and 3.4 GHz respectively.

The 3-D cylindrical FSS can be seen to cycle between band stop and band-pass performance at a particular frequency as the length is increased. Focusing on 3.12 GHz, the frequency of the circular ring FSS stop band, Figure 3.3(c) shows the 3-D cylindrical FSS becomes band-pass at lengths of 44.5 mm and 92 mm, whilst at an intermediate length of 68.5 mm returns to being band stop (albeit with a less significant transmission notch). Futhermore at 92 mm length, multiple pass bands can be seen between 1 and 5 GHz. For very long lengths, the sequential pass or stop bands create a higher quality factor, thus the bandwidth is reduced. Accordingly, the characteristic response for a particular FSS geometery can be changed by varying the length of the resonant cylinder in the 3-D FSS.

Figure 3.4 shows the surface current density of the 3-D cylindrical FSS illustrating an increased number of maximas as the length of the cylinder is increased. Band-pass reponses shows an odd number of maxima and minima in the current density, while band stop responses show an even number. Band-pass responses also correspond roughly to lengths of a half multiple of the free space wavelength, with stop bands being in between.

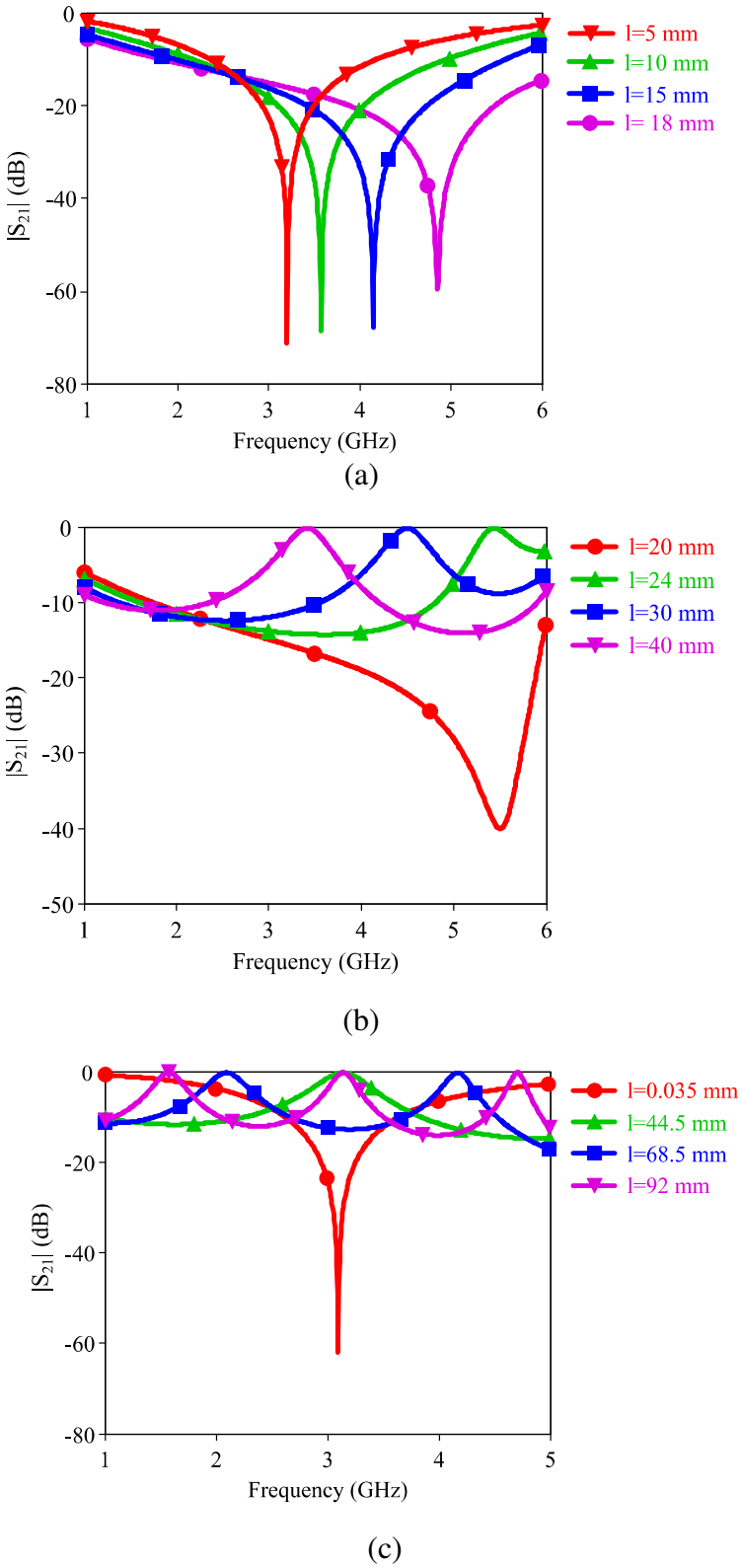

Figure 3.3: 3-D cylindrical FSS transmission ($|S_{21}|$ dB) with varied length *l*. (a) Center of the band-stop is shifted as the length is increased. (b) Transition from a band stop to a band-pass topology after a certain length is reached. (c) 3-D cylindrical FSS can cycle between band-stop and band-pass performance as the length is increased.

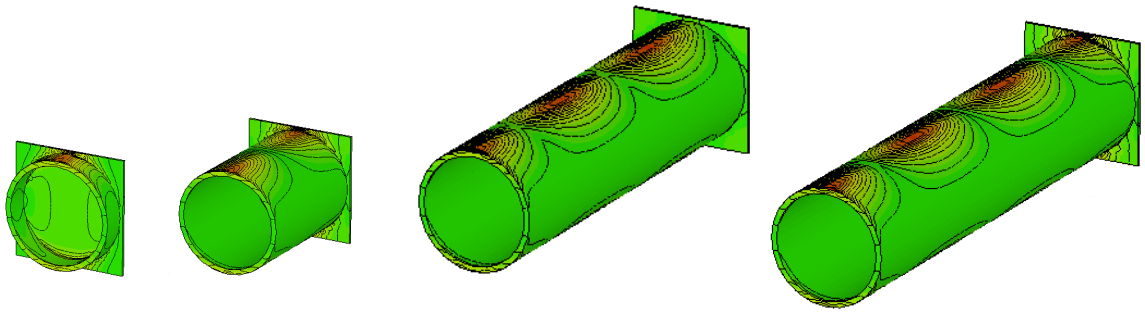

(a) (b) (c) (d)

Figure 3.4: Surface current of cylindrical FSSs of different lengths compared to the wavelength, λ_0.

a) 5 mm, b) 44.5 mm $\cong \lambda_0/2$, c) 68.5 mm $\cong 3\lambda_0/4$, d) 92 mm $\cong \lambda_0$.

Table 3.1: Different length (l) of 3-D Cylindrical FSS

length (mm)	Frequency (GHz)	BW (%)
0.035	3.1	27
5	3.2	54.8
10	3.5	80
15	4.1	83
18	4.7	86

The 3-D FSS composed of metallic cylinders exhibits a resonant behaviour which can be described by the *LC* circuit shown in the inset to Figure 3.5. For cylinders of very short length ($l \approx 0$), the 3-D cylindrical FSS exhibits a band-stop response, resonating at a frequency of $f = 1/(2\pi\sqrt{L_1 C_1})$, where L_1 and C_1 are the equivalent inductance and capacitance of the circular ring geometry. L_1 mainly depends on the diameter d of the ring, and the resonant frequency of the element can be controlled by adjusting d. However in this case, d is fixed. When the value of l is increased, a series inductance L_2 along the cylinder begins to modify the behaviour of the element. The band stop center frequency is tuned to a higher value with increasing l, until eventually L_2 dominates and generates a band-pass resonance. This explains the transformation from band-stop to band-pass for the 3-D cylindrical FSS. Consequently, the equivalent circuit becomes parallel-series when L_2 become dominant.

The equivalent circuit model was validated through comparison to the CST simulations, as depicted in Figure 3.5(b). The value of inductance L_2 can be retrieved by using the following equation [105]:

$$L_2 = \frac{\mu_0}{2\pi}\left(ln\frac{2l}{r} - 1\right), \quad l \gg r \qquad (3)$$

Where r is the radius of the cylinder.

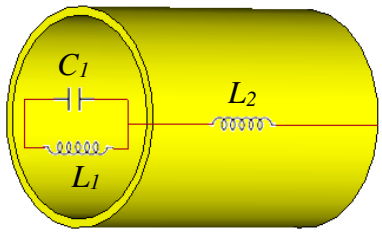

(a)

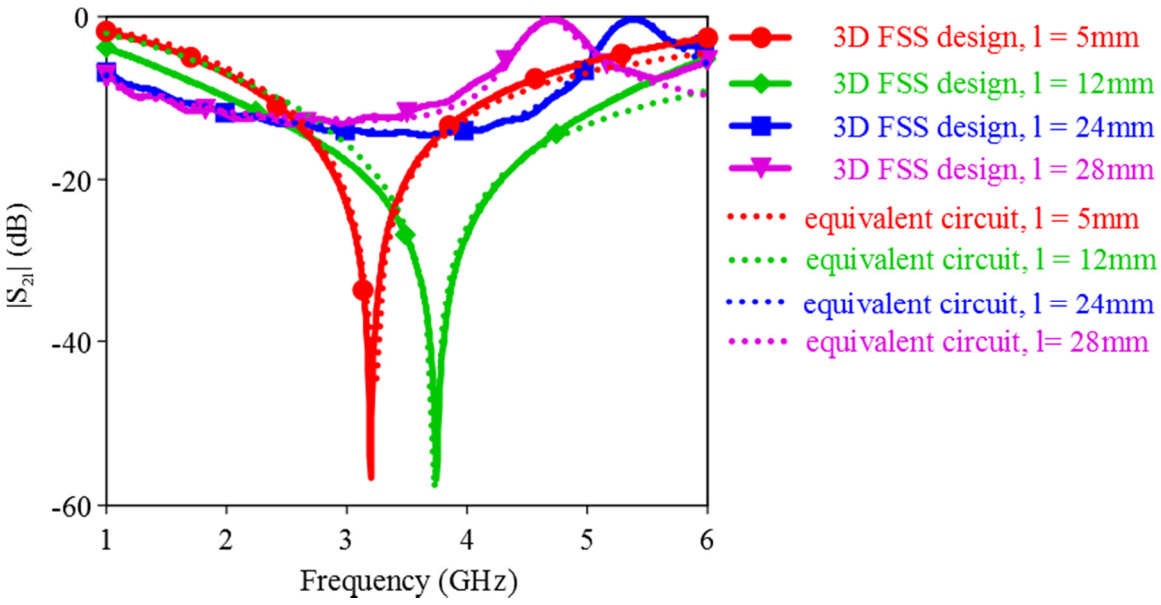

(b)

Figure 3.5: (a) Equivalent circuit model for the 3-D cylindrical FSS. (b) Simulated and equivalent circuit transmission results.

3.2.2 Fabrication and Experimental Results of 3-D Cylindrical FSS

A prototype was fabricated using a cylinder length of 44.5 mm to produce a band-pass response at 3.12 GHz, which is shown in Figure 3.6(a) and (b). The prototype was measured in free space measurement setup as shown in Figure 3.7(a). For the free space measurement, two horn antennas are placed ~ 50 cm from each side of the FSS. The setup is calibrated using a flat metal diffraction plate that is the same size as the prototype. The 3-D cylindrical FSS prototype is then placed in the fixture and the transmission properties are measured. Figure 3.7(b) shows the comparison between the simulated and measured transmission of the 3-D cylindrical FSS. Excellent agreement between simulation and measurement results was achieved, particularly in the vicinity of the band-pass.

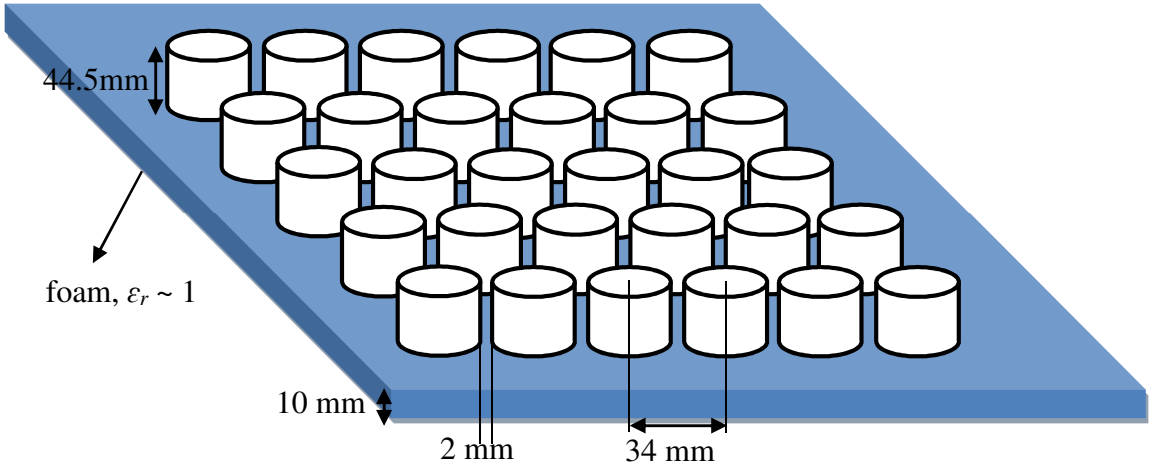

(a)

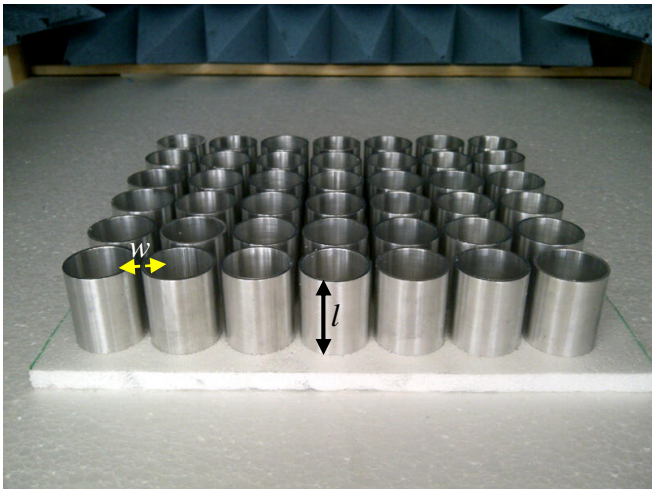

(b)

Figure 3.6: (a) Schematic and (b) Fabricated 3-D Cylindrical FSS - p =34 mm, w = 1.3 mm, l = 44.5 mm.

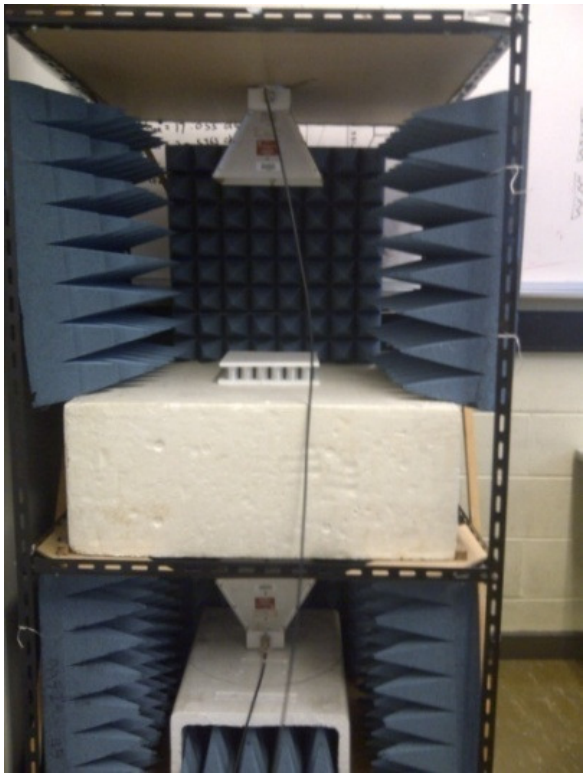

(a) The test setup

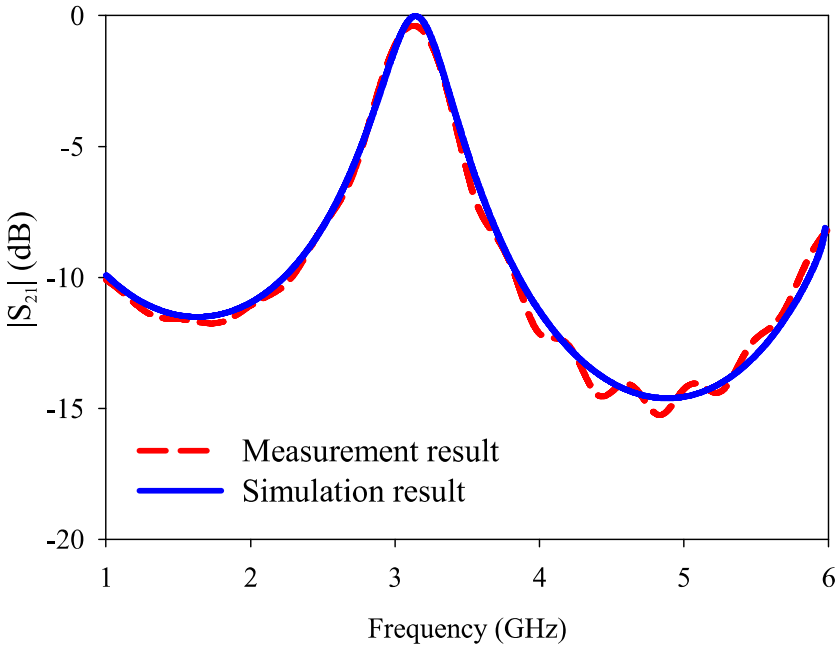

(b)

Figure 3.7: (a) The test setup, (b) 3-D Cylindrical FSS simulated and measured transmission response.

3.2.3 Dielectric Filling of the Cylindrical Unit Elements

To highlight the potential functionality and flexibility of the 3-D cylindrical FSS, a dielectric material was inserted inside the cylindrical FSS unit elements (shown in Figure 3.8). The introduction of the dielectric material enables an almost independent variation of the band-stop and band-pass properties of the FSS, allowing a very closely spaced band-pass and band-stop response for a high permittivity dielectric filled FSS structure. The resonant frequency is also reduced, and with high permittivity filling materials the unit cell becomes much smaller than a free space wavelength, essentially giving it metamaterial properties.

The structure in Figure 3.8 was simulated for different cylinder lengths with a filler material of ε_r=5, and the S-parameter results are provided in Figure 3.9. The dielectric loading shifted the band stop region to a lower frequency (in the range of 2.56 GHz – 2.67 GHz), and a band-pass response (with minimum $|S_{11}|$) is also created below 4 GHz. Similar to the previous study of different length FSS cylinders without dielectric filling in Section 3.2.1, the band stop frequency marginally increases with increasing *l*. However, the band-pass response rapidly shifts lower in frequency for larger values of *l*.

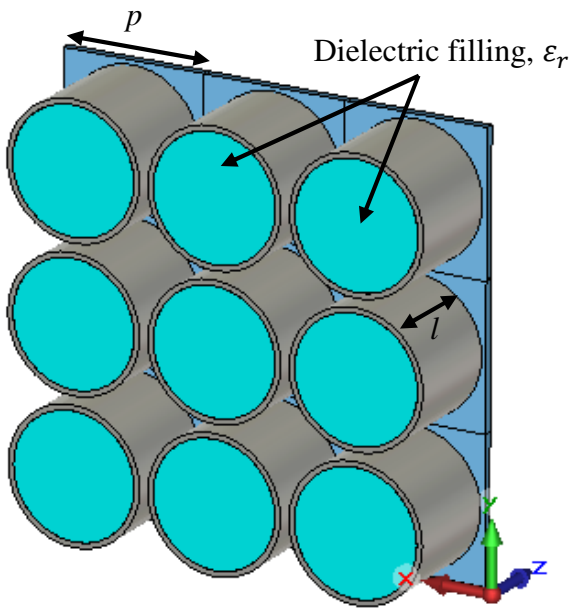

Figure 3.8: 3-D Cylindrical FSS with dielectric filling - *p* = 34 mm, *w* = 1.3 mm, *l*= 18mm.

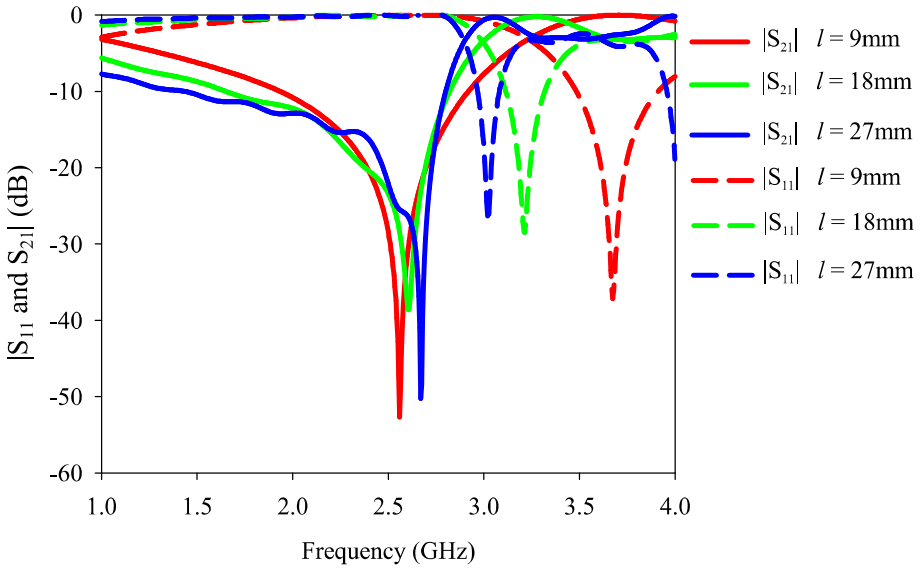

Figure 3.9: S-parameters of the 3-D cylindrical FSS with different length l, using a dielectric filling $\varepsilon_r = 5$.

With the placement of a dielectric filling of ε_r=5 inside each unit cell, the band stop region of the 3-D cylindrical FSS in Figure 3.9Figure 3.8 shifts to a lower frequency of approximately 2.6 GHz (from 4.7 GHz for ε_r=1), as depicted in Figure 3.910. A band-pass response is also seen at 3.2 GHz. Using higher permittivity fillers inside the cylinder such as ε_r=40 and 70 (seen in Figure 3.10) creates sharp band responses that are very closely spaced in frequency.

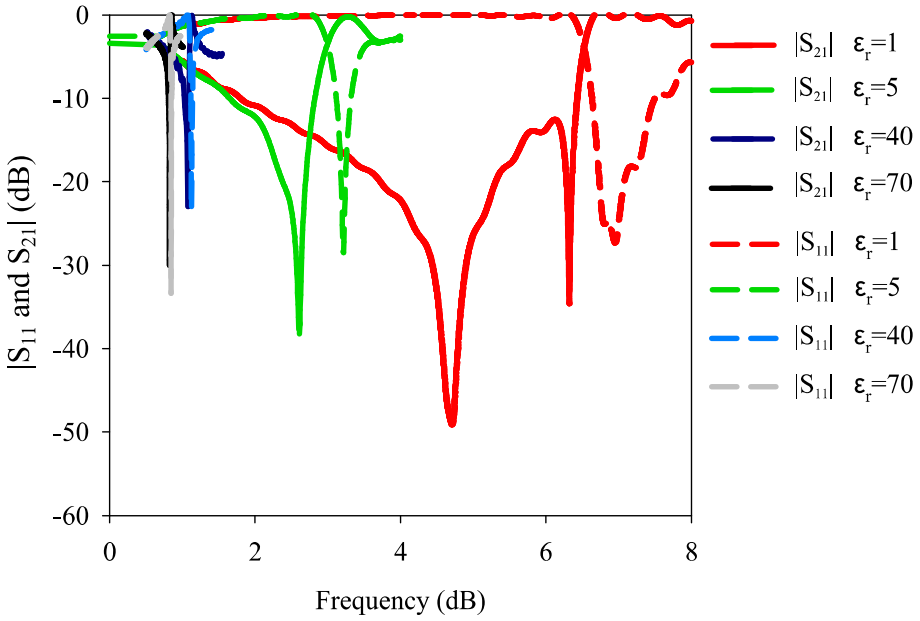

Figure 3.10: 3-D Cylindrical FSS for different dielectric fillings, ε_r

A detailed investigation of the influence of the dielectric filling is shown in Table 3.2, including the band-pass to band stop ratio. Transmission/Reflection band ratios below 1.10 are achieved. These ratios are an impressive result compared to greater than 1.3 for a gridded square FSS and more than 2.5 single square FSS [18]. It should be noted however that as the dielectric value is increased beyond $\varepsilon_r \approx 70$ the s-parameter minima deteriorate.

Table 3.2: 3-D FSS stop and band-pass characteristics for various dielectric fillers, ε_r.

ε_r	Band-stop frequency (GHz)	Band-stop$\|S_{21}\|$(dB)	Band-pass frequency (GHz)	Band-Pass$\|S_{11}\|$(dB)	Frequency Ratio (band-pass/band-stop)
1	4.74	-49.9	7.0	-28.2	1.48
5	2.61	-38.8	3.22	-27.4	1.23
10	1.96	-36.7	2.24	-25.5	1.14
20	1.45	-33.2	1.58	-29.5	1.09
30	1.19	-26.7	1.3	-34.2	1.09
40	1.05	-24.7	1.13	-22.6	1.08
50	0.93	-37.2	1.0	-17.6	1.08
60	0.86	-22.6	0.93	-15.1	1.08
70	0.77	-16.2	0.83	-12.2	1.08
80	0.74	-12.6	0.79	-10.6	1.07
90	0.71	-11.6	0.75	-10.1	1.06
100	0.64	-8.61	0.68	-8.61	1.06
120	0.61	-7.84	0.64	-8.6	1.05

The effective electrical size of the 3-D Cylindrical FSS unit cell becomes a fraction of a free space wavelength (less than $\lambda_0/8$ is used here) for dielectric fillings with $\varepsilon_r > 40$, allowing bulk metamaterial properties to be extracted. Shown in Figure 3.11 are the effective permittivity, permeability and refractive index retrieved from CST simulations of a 3-D cylindrical FSS with a dielectric filling of $\varepsilon_r = 40$. Figure 3.11(a) and (b) show that the real part of the effective permittivity and permeability are negative at approximately 1.08 GHz. Moreover, the refractive index plot in Figure 3.11(c) confirms the negative refractive index band. This negative index is achieved with a single uniform unit cell structure, as compared to the binary unit cells used in [106].

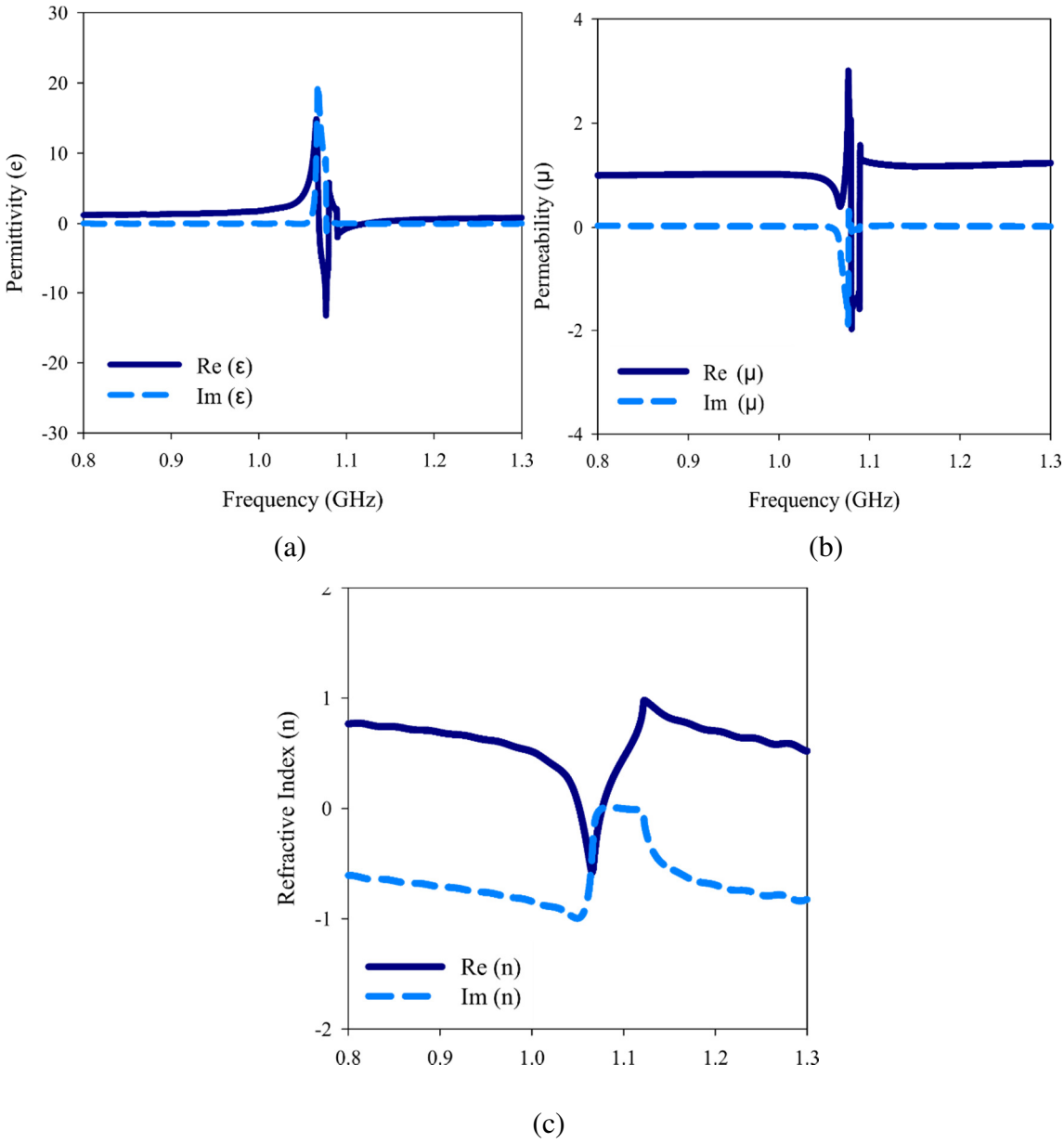

Figure 3.11: (a) Effective permittivity, (b) Effective permeability, (c) Refractive index for a 3-D cylindrical FSS with dielectric filling ε_r= 40.

3.3 Dual Cylinder 3-D Frequency Selective surfaces

Dual cylinder FSS is proposed to design frequency selective surfaces with close band response. For each band, the reflection/transmission centre band frequency ratio requirement is approximately 1.48 or less [45]. In the 3-D FSSs of Section 3.2, the FSS requires a dielectric filling in order to obtain a close band separation. Furthermore, the band separation ratio is dependent on the dielectric permittivity value. A closer band separation is obtained by using higher value of permittivity, and can easily exceed most standard materials which have permittivities less than 10. An equivalent response to a high permittivity material filled 3D FSS can be obtained by designing 3D dual cylinder FSS. Hence, the aim of this study in is to evaluate and validate a 3D dual cylinder FSS with close band response.

The investigation of the dual cylinder 3-D FSS structure begins with the analysis of a planar dual ring unit cell. The periodic cell of the FSS consists of two concentric conducting ring elements. A circuit model is developed to describe the expected frequency behavior of the surface qualitatively. The general geometry and equivalent circuit of the dual ring FSS is presented in Figure 3.12. In this equivalent circuit model, the rings are modelled with two hybrid (parallel – series) resonators consisting of C_{f1}, L_{f1} and C_{f2}, L_{f2} in parallel, placed in series. The diameter of the ring is determined by using a basic ring resonator equation which is $d \approx \chi_0/\pi$. The width w of the rings are (d_{outer} - d_{inner})/2 = 1mm.

The FSS performance was predicted by the CST microwave simulator. The simulations took used the assumption that the FSS is infinite and made of a periodical repetition (unit cell) of an element pattern along the two axes of the FSS plane. For the s-parameter calculation, two Floquet ports are used: one in front and one at the back of the FSS plane. Figure 3.13 shows the circular ring FSS frequency response and equivalent circuit as obtained from an electromagnetic simulation in the CST Microwave Studio. The simulation shows that the FSS has the expected band stop characteristic centered at 3 GHz.

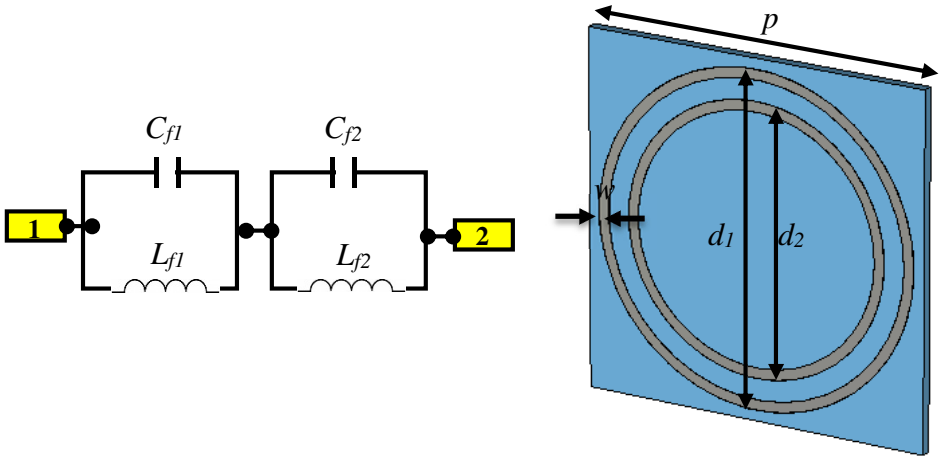

Figure 3.12: Equivalent circuit model of the proposed dual ring FSS. :- p = 36 mm, w = 1 mm, d_1 = 32 mm, d_2 = 28 mm.

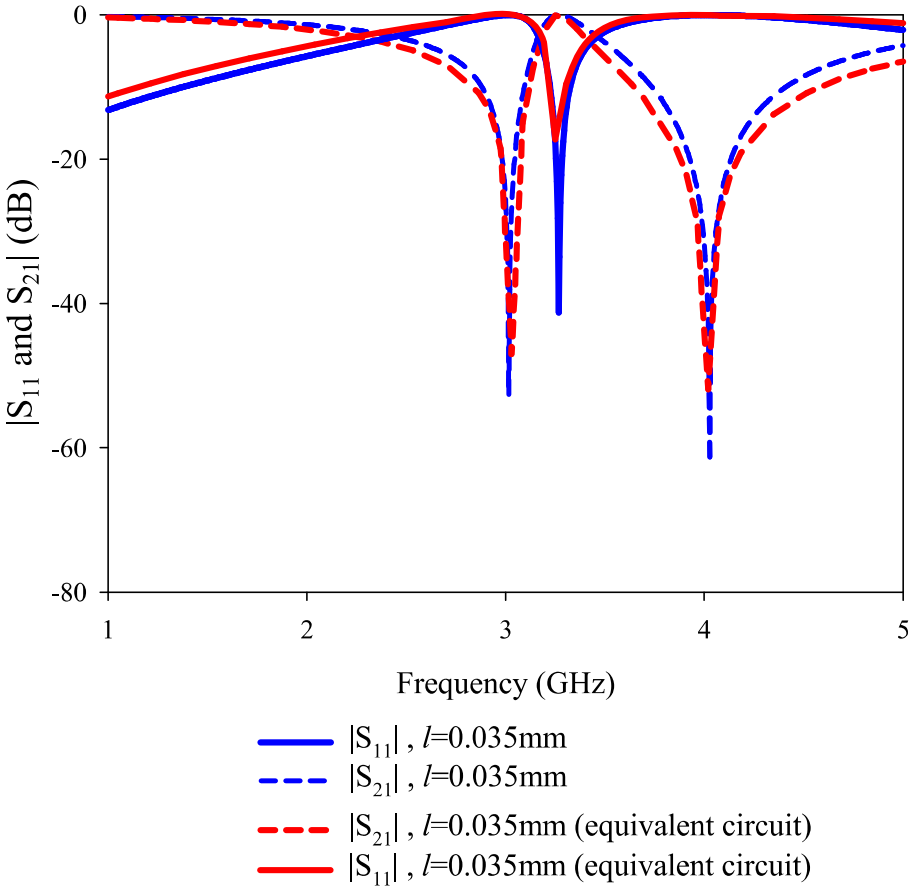

Figure 3.13: Simulated and equivalent circuit reflection and transmission of the circular ring FSS.

The basic equation for calculating capacitance and inductance are given by [36].

$$L(nH) = 3.937\frac{a^2}{8a + 11c}\ x\ K_g \qquad (3.3.1)$$

$$a = \frac{D_{outer} + D_{inner}}{4}$$

$$c = \frac{D_{outer} - D_{inner}}{2}$$

$$K_g = 0.57 - 0.145\ ln\frac{w}{h}\ \ for\ \ \frac{w}{h} > 0.05;\ where\ h = 0.035mm$$

$$C(pF) = \frac{1}{(f.2\pi)^2}x\frac{1}{L} \qquad (3.3.2)$$

For the equivalent circuit given in Figure 3.12, C_{f1}, L_{f1}, C_{f2}, and L_{f2} are calculated as follows [36]:

$$L_{f1} = 2 \times (\frac{L_1 L_2}{L_1 + L_2} \times \frac{d_1}{p}), \quad where\ L_1 = L(p, w_1, \lambda) \qquad (3.3.3)$$

$$L_2 = L(p, w_2, \lambda)$$

$$C_{f1} = C_1 \times \frac{d_1}{p}, \quad where\ C_1 = C(p, w_1, \lambda) \qquad (3.3.4)$$

$$L_{f2} = L_2 \times \frac{d_2}{p}, \qquad (3.3.5)$$

$$C_{f2} = C_2 \times \frac{d_2}{p}, \quad where\ C_2 = C(p, w_2, \lambda) \qquad (3.3.6)$$

3.3.1 Dual cylinder 3-D FSS with Close Band Spacing

As before, the dual ring FSS was made 3-D by introducing a height to the conductors of the unit elements, creating cylinders with a length *l*. The 3-D dual cylinder FSS was created by periodically arraying aluminum cylindrical ring elements (Figure 3.14(a)) on top of a foam substrate 10 mm thick.

The 3-D FSS composed of metallic cylinders exhibits a resonant behaviour which can be described by the *LC* circuit shown in Figure 3.14(b). For cylinders of very short length ($l \approx 0$), the 3-D cylindrical FSS exhibits a band-stop response. However, by introducing the height of cylinder ($l > 0$ mm) the equivalent circuit changes and a series inductor is added as shown in Figure 3.14(b), where the L_a and L_b represent the height of the cylinder. L_a represents the length of the outer cylinder while L_b represents the length of the inner cylinder. The series inductances L_a and L_b along the cylinder begins to modify the behavior of the element, as the value of l is increased, increasing their value of inductance. The detailed geometric parameters of the dual cylinder 3-D FSS (shown in Figure 3.14) are listed in Table 3.3.

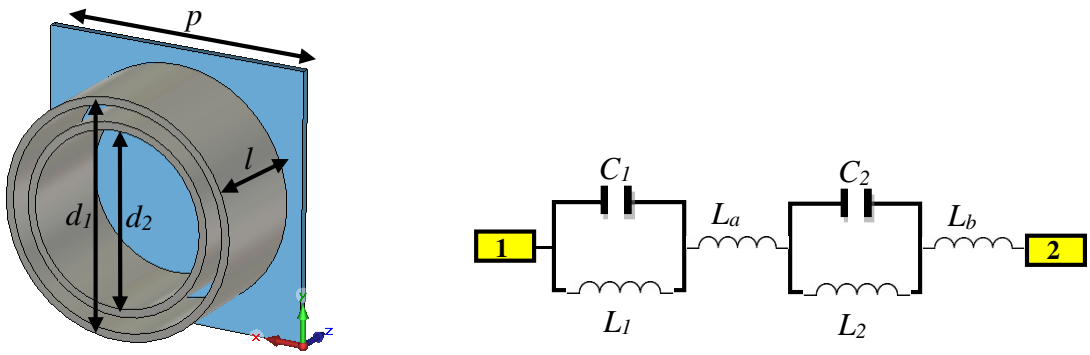

(a) (b)

Figure 3.14: (a) 3-D dual ring FSS (b) equivalent circuit.

Table 3.3: Geometric Parameters of 3-D FSS.

	Dual Ring
***p* (mm)**	36
ring width,w_1 (mm)	1
d_1 (mm)	32
ring width,w_2 (mm)	1
d_2 (mm)	28

The frequency response of the structure as predicted from the equivalent circuit model of Figure 3.14(b) with the values given in Table 3.4 is presented in Figure 3.15. The equivalent circuit values in this table are obtained through an optimization process in CST.

In this optimization procedure the values predicted by equations (1)-(6) were used as initial values while value of L_a and L_b is obtained through optimization. In Figure 3.15, when l = 20mm, the 3-D dual cylinder FSS operates as a band stop at 3.18 GHz, whereas if the length is increased to l = 30mm, the 3-D dual cylinder FSS operates as band-pass at 3.18 GHz. As can be observed, an excellent agreement between the two is achieved.

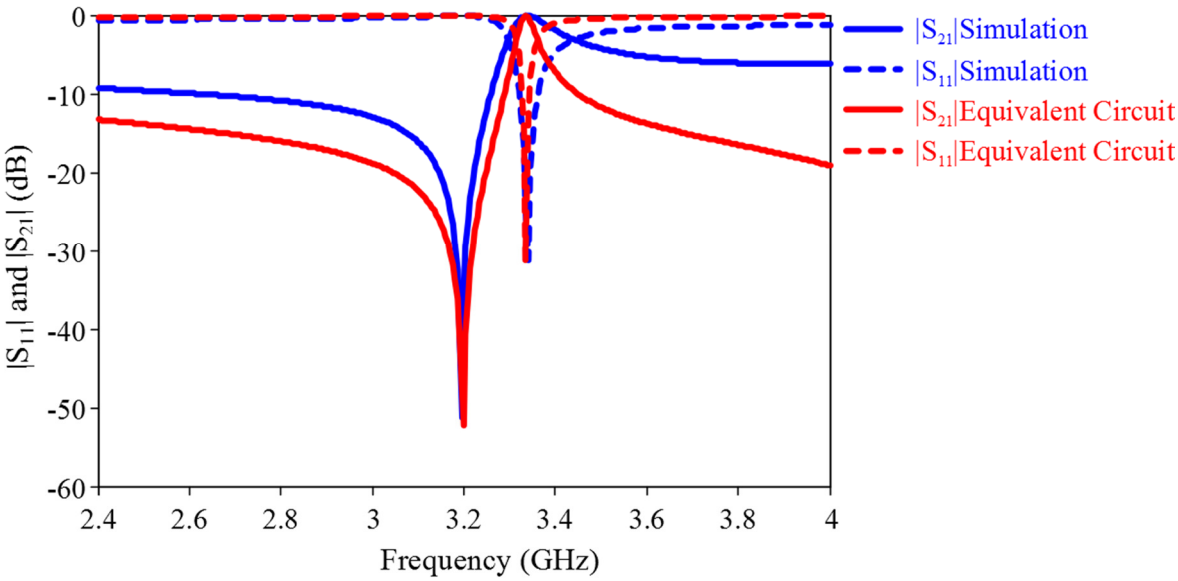

(a)

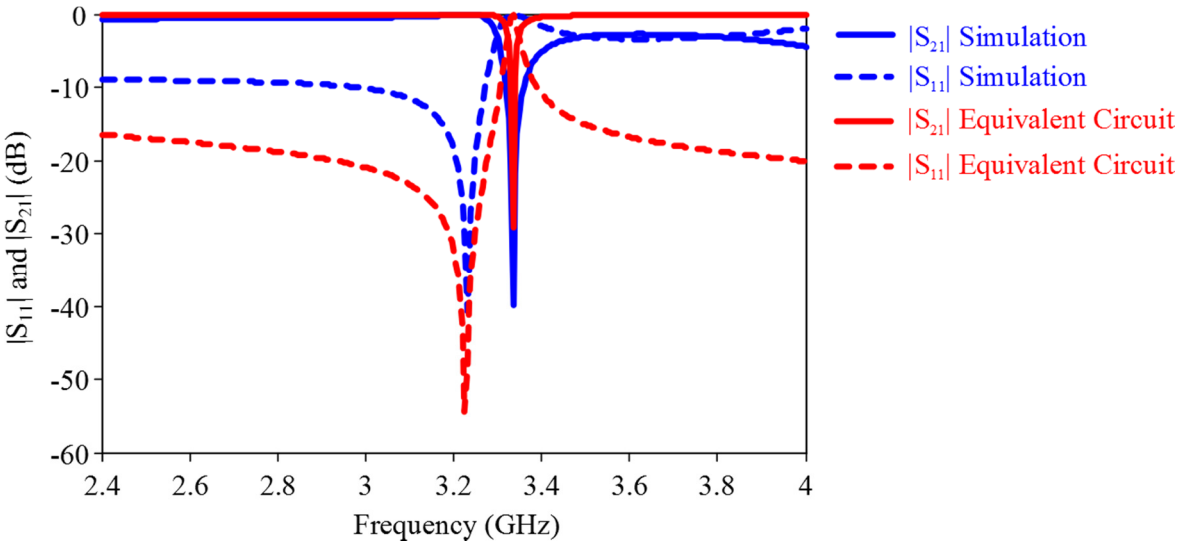

(b)

Figure 3.15: $|S_{11}|$ and $|S_{21}|$ simulated and equivalent circuit results of the 3-D dual ring FSS. (a) Length, l = 20mm.(b) length, l = 30mm.

Table 3.4: Equivalent circuit values of Circuit Model in Figure 3.13(b)

Parameter	C_1 *(pF)*	C_2 *(pF)*	L_1 *(nH)*	L_2*(nH)*	L_a *(nH)*	L_b *(nH)*
(l = 20 mm)	0.8	0.4	2.7	4.5	1.2	1.2
(l = 30 mm)	0.9	0.23	2.7	4.5	10	10

Shown in Figure 3.16 are the transmission and reflection result of the dual cylinder 3-D FSS with different lengths (all other parameters are equivalent to those in Table 3.3). The operating frequency of the dual cylinder 3-D FSS can be adjusted by varying the length of the cylindrical elements. By changing the length of the cylindrical unit elements to 10 mm, 15 mm, 20 mm and 30 mm the center of the band-stop shifted to 3.08GHz, 3.13GHz, 3.20GHz, and 3.32GHz respectively. The band-pass response remains relatively stable lengths of 10 mm, 15 mm and 20 mm at about 3.33 GHz, but jumps down for 30 mm when the stop and band-pass switch sides. Hence, a very close band response is achieved for certain lengths of the cylinders.

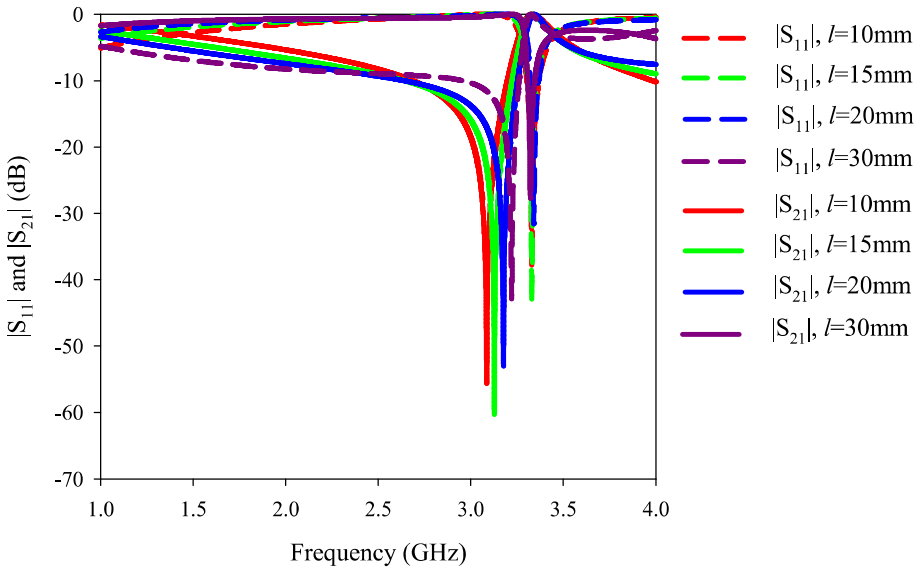

Figure 3.16: 3-D dual cylinder FSS transmission ($|S_{21}|$ dB) with varied length *l*.

The close band spacing refers to how close the first band (band stop) is to the second band (band pass) by calculating the ratio between the bands. If only observing one operating band, the result can be viewed as a sharp roll-off performance. Tabulated in Table 3.5 are the band-pass to band-stop frequency ratios for the lengths investigated. In addition, this dual cylinder FSS can switch from band-stop to band-pass as shown in Figure 3.16. The

dual cylinder 3-D FSS at 10mm length operating at 3.1GHz is band stop; however when the length is increased to 30mm, it becomes band-pass.

Typically in close band FSS design, the band spacing is determined by the clearance between two resonant elements (e.g. the gap between dual ring resonators). The clearance between two elements must be small enough to meet the close band requirement. The close band reflection/transmission centre band frequency ratio achieved in [45] is 1.48. With the 3-D dual cylindrical FSS, a frequency ratio of 1.003 can be achieved. As the length is increased, an inverted frequency ratio (less than 1) is also possible, achieving approximately 0.78 at a length of 30 mm.

As tabulated in Table 3.5, in order to get at least 1.08 reflection/transmission band ratios the gap for a planar dual ring FSS is 0.5 mm. The closer the clearance between the two rings, the closer the band spacing obtained. At 0.25mm and 0.05mm gap, the ratios are 1.03 and 1.006 respectively. In order to get 1.003 frequency ratio for dual ring FSS, the gap between the two concentric elements is 0.025 mm. However, the gap required to obtain 1.003 ratio for 3-D Cylindrical FSS is 1mm gap with length of the cylinder = 28mm. Therefore, with 3-D Cylindrical FSS a closer band response can be achieved by extrapolating the height of planar dual ring unit cell without need to design a very close gap between two elements.

Table 3.5: 3-D dual cylinder FSS Band-stop and Band-pass frequency ratio as the length, *l* was changed.

l (mm)	Band-stop frequency (GHz)	Band-pass frequency (GHz)	Frequency Ratio
0.035	3	3.25	1.08
10	3.08	3.32	1.07
15	3.13	3.33	1.06
20	3.20	3.34	1.04
28	3.30	3.31	1.003
30	3.32	3.25	0.98
45	3.35	2.98	0.89
50	3.20	2.82	0.86
60	3	2.34	0.78

Table 3.6: Planar dual ring FSS Band-stop and Band-pass frequency ratio as the gap between rings is changed.

gap (mm)	Band-stop frequency (GHz)	Band-pass frequency (GHz)	Frequency Ratio
0.5	3.01	3.26	1.08
0.25	2.95	3.03	1.03
0.05	2.91	2.93	1.006
0.025	2.98	2.99	1.003

3.3.2 Fabrication and Experimental Results of 3-D Dual Cylinder FSS

To validate the proposed design procedure, a prototype of the 3-D dual cylinder FSS is fabricated and characterized using a free space measurement system. The 3-D dual cylinder FSS is fabricated on top of 10 mm thick of foam using an l of 20 mm as shown in Fig 3.16(a). The distance and alignment between two cylinders is ensured by cutting a preform into the foam base, and the cylinders are placed accordingly into the predefined slots. For free space measurement, two horn antennas are placed away from each side to ensure that the FSS is excited with plane waves. First, the transmission coefficient is measured by placing a flat metal plate that is the same size as the prototype between the horns. The metal plate is then removed and the reflection of this fixture without the presence of the FSS is measured. This makes up the isolation part and is used for FSS calibration. The 3-D FSS prototype is then placed in the fixture and the transmission coefficient is measured. Figure 3.17(b) shows the comparison between the simulated and measured transmission of the 3-D dual cylinder FSS. The fabricated FSS demonstrates a 20 dB measured insertion loss at the band stop resonance, and a 2 dB measured insertion loss in the band-pass region. The difference insertion loss between simulation and measurement is due to the structure being considered as infinitely array during simulation, however the 3-D dual cylinder FSS is fabricated using only 30 unit cell elements (6 x 5). Consequently, the measured transmission result shows differences although the operating frequency is almost perfectly matched.

(a)

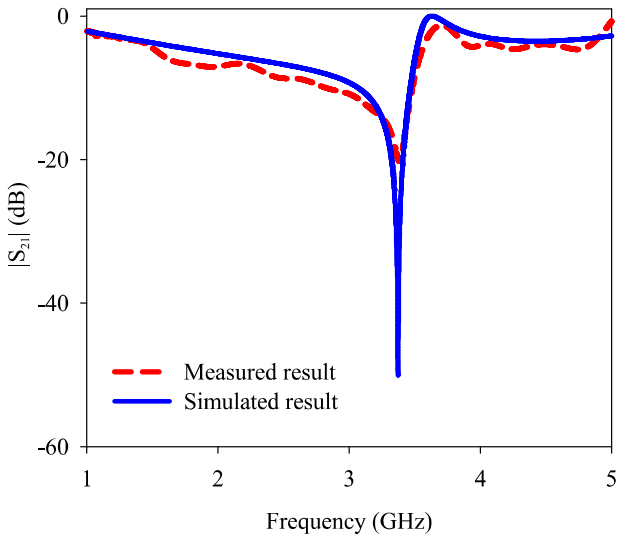

(b)

Figure 3.17: (a) Fabricated 3-D dual cylinder FSS (b) Measured and simulated transmission coefficients of the 3-D dual cylinder FSS.

The sensitivity of the frequency response of the proposed FSS to the angle of incidence of the EM wave for both the transverse electric (TE) and the transverse magnetic (TM) incidence is also studied and examined. Figure 3.18 shows the simulation and measured transmission coefficients of the 3D dual cylinder FSS at various oblique angles for both TE and TM incidence. The frequency response of the structure is shifted less than 3% at 60 degrees incidence. It is observed that for TE incidence, the bandwidth of the 3-D dual cylinder FSS is decreased while the band stop level increases as the incident angle increases. The TE frequency response shifts less for incidence angles up to 60° compared to the TM response, whose transmission bandwidth narrows with increasing incidence angles. Some noise in the transmission measurements was observed for oblique angles of incidence due to the small size of the FSS prototype. Therefore, for large angles of incidence measurements, the small transmission was slightly shadowed by the surrounding absorbers, leading to additional noise in the measured data.

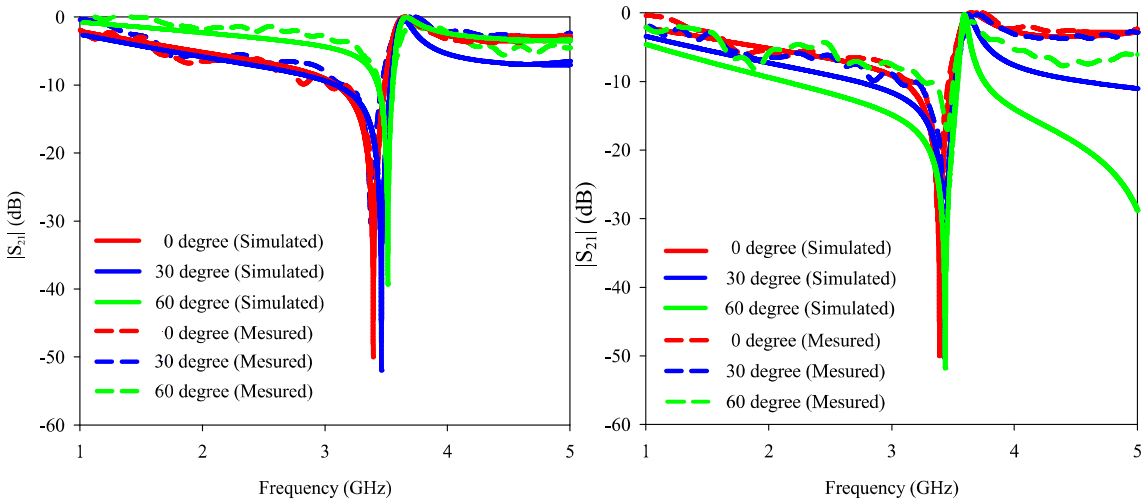

Figure 3.18: Transmission of the 3-D dual cylinder FSS as a function of incidence angle.

(a) TE incidence (b) TM incidence

3.3.3 Comparison with dielectric filled 3-D cylindrical FSS

By inserting dielectric filling, the dimensions of 3-D cylindrical FSS unit cells can be made significantly smaller than a wavelength at the desired frequencies of operation [101]. With the placement of the dielectric filling inside the cylinder, the guided wavelength is reduced and thus the resonant frequency shifts to lower frequency. High dielectric values inserted into the 3-D cylindrical FSS also gives rise to a close band response. The same response can be achieved in the dual cylinder 3-D FSS structure proposed in this section. Their transmission and reflection behavior is depicted in Figure 3.19. Almost identical performance is achieved by the two structures, highlighting the impressive close band performance and fabrication tolerance flexibility of the dual cylinder 3-D FSS structure.

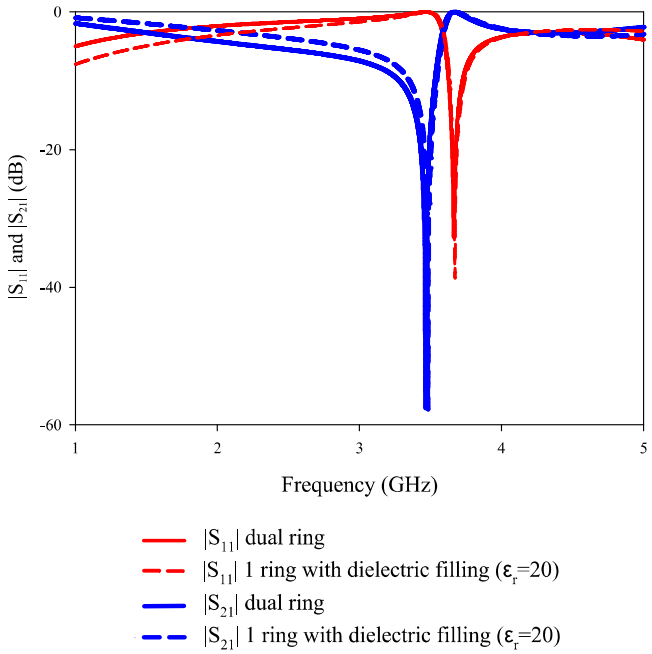

Figure 3.19: Transmission and reflection result of 3-D dual ring FSS and 3-D FSS with dielectric filling.

3.4 Mechanically Tunable and Reconfigurable FSS

3-D FSSs have displayed the ability to set resonant frequencies and shift operational filter states with a change in the length of a cylindrical resonator. Here, a 3-D spring FSS structure tuned by reconfiguring the pitch angle (and hence height) of a helical resonator of constant wire length is presented. Varying the height of the mechanical FSS can tune the frequency of resonance, as well as achieve switching between band-stop and band-pass operation. Mechanical FSSs offer tuning and switching functionality from the same structure without the use of additional DC bias networks.

3.4.1 Mechanically Tunable and Reconfigurable FSS using plastic spring

The FSS geometry introduced here is based on two ring resonator element structures, one of which is placed on the upper side and the other one on the lower side of a plastic spring with number of turns/windings $n = 5$. The unit cell geometry of the proposed tunable spring loaded FSS is shown in Figure 3.20(a) and (b). Figure 3.20(c) depicts the equivalent

circuit representation of the spring loaded FSS unit cell. The parallel capacitance C and inductance L represent the resonance of the circular rings, while C_0 indicates the coupling between the stacked rings. Detailed geometric parameters of the spring loaded FSS are listed in Table 3.6.

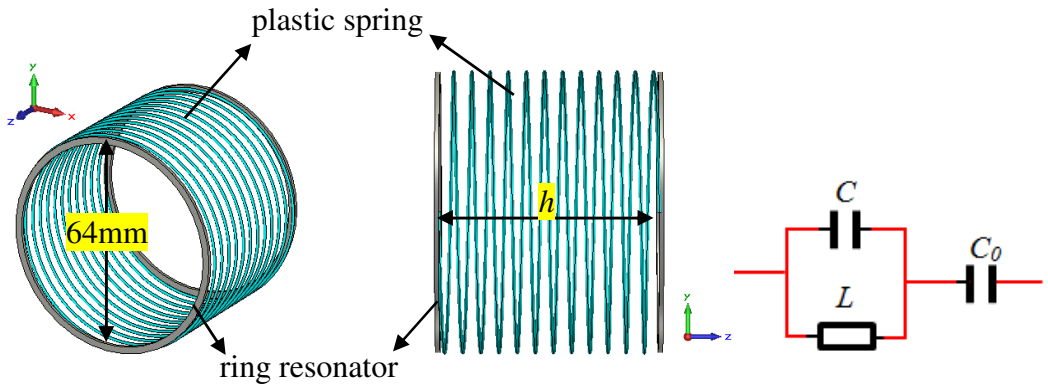

Figure 3.20: Geometry of the spring loaded FSS.

a) Angular view of the unit cell, b) Side view of the unit cell, (c) Equivalent circuit.

Table 3.7: Geometric Parameters of the Tunable FSS

Parameter	**Value**
p (mm)	72
ring width, w_1 (mm)	12
d (mm)	64
n	5
h	10 mm → 90 mm

A spring FSS structure is presented that can tuned by mechanically altering the height of the spring shaped unit cell resonator. The overall height of the spring loaded FSS unit cell can be regarded as a variable, which can then be tuned by applying pressure or tension to the springs using nylon screws at the corners of the FSS. This alters the separation between the ring resonators, adjusting the coupling between them. To predict the performance of the FSS, simulations in CST Microwave studio were utilized.

As seen in Figure 3.21(a), varying the height h of the spring loaded FSS from 10 to 50 mm monotonically increases the center of the FSS band-stop from 1.92 GHz through to 2.45

GHz. By increasing the height of the spring loaded FSS, the capacitance between the rings is varied, thus the frequency is shifted accordingly. When the height h exceeds 50 mm, the spring loaded FSS changes its characteristic performance from band-stop to band-pass, similar to the 3-D cylindrical FSS in [99, 100]. Further extension of the spring creates a band-pass characteristic at approximately 2.60 GHz for h = 60 mm. A highly selective FSS is achieved between h = 60 mm and 70 mm. Further increases in h decreases the center frequency of the band-pass FSS as well as decreasing the quality factor of the FSS, as seen in Figure 3.21(b).

The parallel capacitance C and inductance L of the h = 10 mm spring loaded FSS create a fundamental band-stop resonant frequency at about 1.92 GHz. As the height of the spring is increased the capacitance C_0 value decreases. As seen in Figure 3.21(a), when the height h exceeds 50 mm, the spring loaded FSS changes its characteristic performance from band-stop to band-pass. Further extension of the spring creates a band-pass characteristic which approximately corresponds to the resonance of the series components L and C_0. Thus the transition from band-stop to band-pass when h is increased is a consequence of the diminishing influence of the parallel capacitance C being overtaken by the series C_0.

It is possible to define heights at which band-stop and band-pass can coincide at the same frequency value, as seen in Figure 3.21(c). The heights of 30 and 80 mm produce band-stop and band-pass at 2.18 GHz, while 51 and 65 mm create a highly selective band-stop and band-pass at 2.48 GHz. Hence, mechanically tuning this spring loaded FSS structure between these values can reconfigure the operational characteristic of the FSS. More detailed frequency characteristics are tabulated in Table 3.8.

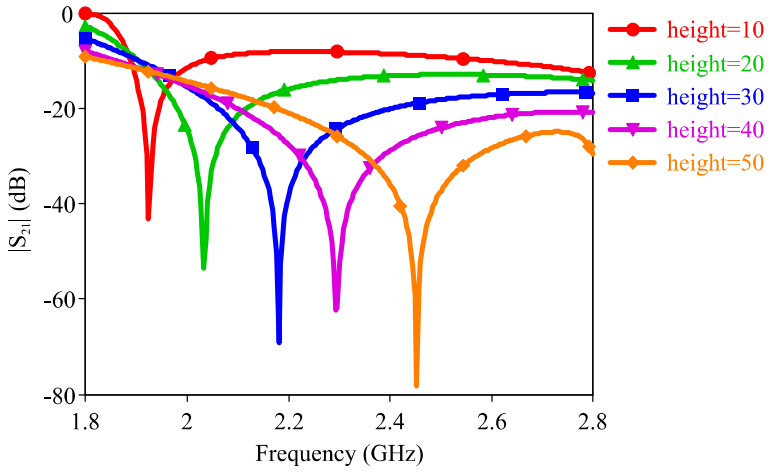

(a)

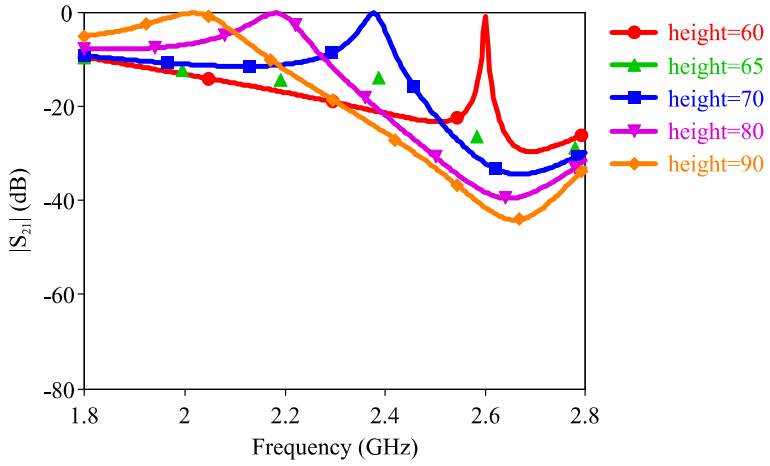

(b)

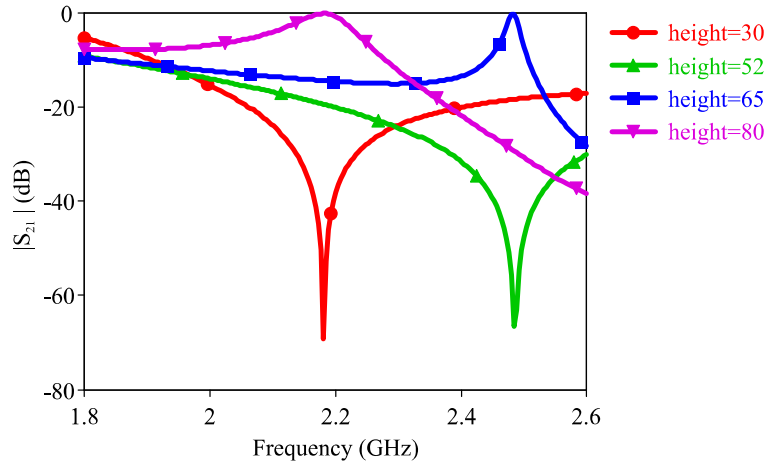

(c)

Figure 3.21: Spring-loaded FSS transmission ($|S_{21}|$ dB) with varied height.(a) Band-stop response (b) Band-pass response (c) Tunable spring-loaded FSS can cycle between band-stop and band-pass performance as the length is increased.

Table 3.8: Detailed Results for the Spring Loaded FSS

Height (mm)	Frequency (GHz) Band-stop	Height (mm)	Frequency (GHz) Band-pass
10	1.92	60	2.60
20	2.03	65	2.48
30	2.18	70	2.37
40	2.29	80	2.18
45	2.37	90	2.02
50	2.45		
51	2.48		

3.4.2 A Reconfigurable FSS using a Spring Resonator Element

A periodic array of spring resonator element structures can also create a tunable and reconfigurable FSS. The unit cells consist of a thin aluminum wire (w = 1 mm diameter) wound into a helical spring resonator. The unit cell geometry of the proposed tunable spring FSS is shown in Figure 3.22, and the parameters are specified as: the helical height h, helical diameter d, helical circumference H, vertical separation between the coils S, number of turns n, and the pitch angle α.

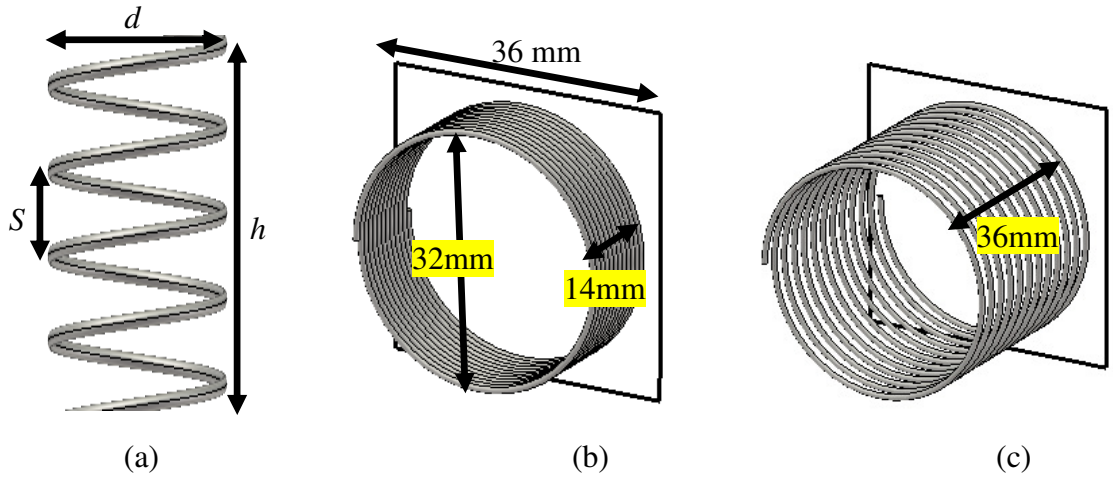

Figure 3.22: Geometry and parameters of the spring FSS unit cell. (a) Spring FSS single element geometry, (b) Spring resonator element with 14 mm height for band-stop response, (c) Spring resonator element with 36 mm height for band pass response.

The geometry of the spring unit cell is described in the following equations [107].

$$\alpha = tan^{-1}\left(\frac{S}{H}\right) \quad (3.4.1)$$

$$h = nS \quad (3.4.2)$$

An equivalent circuit model of the spring resonator is depicted in Figure 3.23. The capacitive and inductive components of the spring can be estimated using the following equations [104, 105, 108, 109]:

$$L(nH) = 3.937\frac{a^2}{8a + 11c} \times K_g \quad (3.4.5)$$

$$a = \frac{D_{outer} + D_{inner}}{4}$$

$$c = \frac{D_{outer} - D_{inner}}{2}$$

$$K_g = 0.57 - 0.145\, ln\frac{w}{h} \qquad for \ \frac{w}{h} > 0.05;$$

$$C(pF) = \frac{1}{(f.2\pi)^2} \times \frac{1}{L} \quad (3.4.6)$$

$$L_0 = \left[\frac{\mu_0}{2\pi r} I_1(r\gamma)K_1(r\gamma)tan^2\emptyset\right] \times h \quad (3.4.7)$$

$$C_0 = \frac{\varepsilon_0 2\pi}{I_0(r\gamma)K_0(r\gamma)} \quad (3.4.8)$$

$$\gamma^2 = \omega^2 C_0 L_0 \quad (3.4.9)$$

Where, $I_{0,1}(r\gamma)$, $K_{0,1}(r\gamma)$ are modified Bessel functions, γ is the transverse constant = 1, $\omega = 2\pi f_0$, r is the cylindrical radius, $\emptyset$ is the angle between windings, and μ_0 and $\varepsilon_0$are the permeability and permittivity of free space.

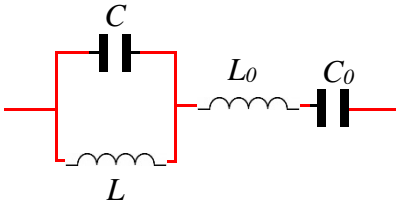

Figure 3.23: Equivalent Circuit.

FSS performance was predicted using the CST microwave simulator assuming that the FSS is an infinite periodical repetition (unit cell) of the spring element pattern along the two axes of the FSS plane. Two Floquet ports are used, one in front and the other behind the FSS plane. In addition, the behavior of the FSS can also be efficiently modeled using the equivalent circuit representation with sufficient levels of accuracy. Figure 3.24 shows the transmission S-parameter results $|S_{21}|$ for a spring FSS obtained from the equivalent circuit model calculations compared to the results obtained by full wave simulation using CST. The simulation/calculation results in Figure 3.24(a) and (b) illustrate very good agreement.

The capacitance and inductance of the windings is varied by changing the height of the spring resonator, as shown in Table 3.9. This technique enables the FSS to be reconfigured or fine tuned in its frequency response. The parallel capacitance C of 0.152 pF and inductance L of 13.87 nH of a h = 14 mm spring FSS create a fundamental band-stop resonant frequency at about 3.43 GHz. As the height of the spring is increased the inductance L value decreases, while L_0 rises with the spring height. The capacitance C initially remains relatively stable. As seen in Figure 3.23(a), varying h between 14, 15 and 16 mm locates the center of the FSS band-stop at 3.43 GHz, 3.53 GHz, and 3.63 GHz respectively.

When the height h exceeds 18 mm, the spring FSS changes its characteristic performance from band-stop to band-pass. Further extension of the spring creates a band-pass characteristic at approximately 3.76 GHz for h = 26 mm, which approximately corresponds to the resonance of the series components L_0 = 3.08 nH and C_0 = 0.658 pF. Thus the transition from band-stop to band-pass when h is increased is a consequence of the diminishing influence of the parallel inductance and capacitance L and C being overtaken by the series L_0 and C_0 resonance. The FSS band-stop center frequency is tuned to a higher value with increasing h, until eventually the series inductance and capacitance (L_0 and C_0) dominates and generates a band pass resonance. Further increases in h decreases the center frequency of the band-pass FSS as shown in Figure 3.24(b).

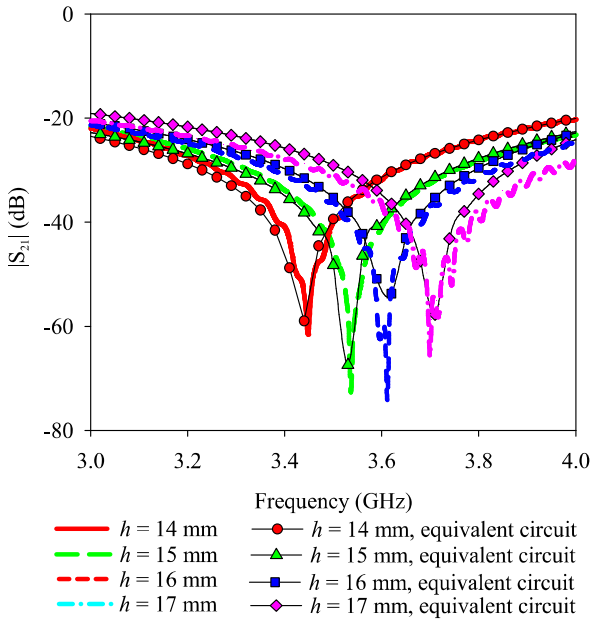

(a)

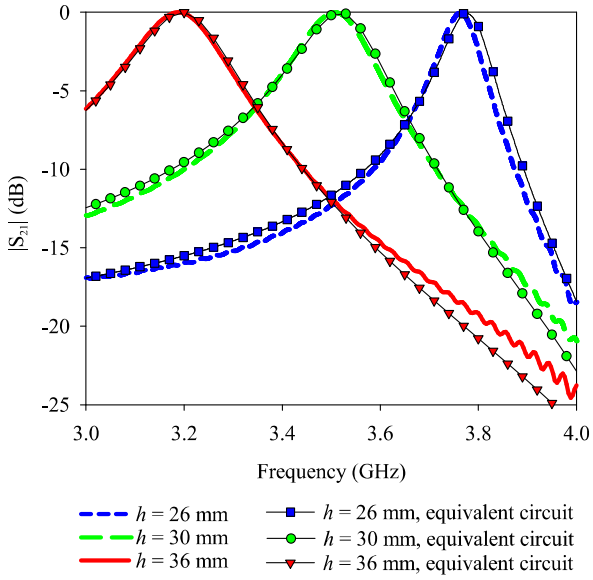

(b)

Figure 3.24: Spring FSS transmission ($|S_{21}|$ dB) with varied height (a) Band-stop response, (b) Band-pass response.

Table 3.9: Capacitance and inductance equivalent circuit values for various spring heights.

***h*(mm)**	***L*(nH)**	***C* (pF)**	***L*$_0$(nH)**	***C*$_0$(pF)**
14	13.87	0.152	0.49	4.096
15	13.12	0.153	0.58	3.452
16	12.46	0.154	1.85	1.099
26	7.26	0.280	3.08	0.658
30	5.71	0.314	4.87	0.417
36	3.70	0.548	8.50	0.239

3.4.3 Fabrication and Experimental Results

A prototype of the spring FSS was manufactured and measured in a free space measurement system, as seen in Figure 3.25. A 6 x 6 array of hand-wound spring unit cell elements are placed between two wideband horn antennas which are connected to the two ports of a vector network analyzer. Electromagnetic radiation from the transmitting horn illuminates the FSS and the transmitted wave is received by the other horn antenna to measure the transmission response. The spring FSS is sandwiched between two 10 mm thickness foam substrates for structural support, and has an uncompressed h of 36 mm.

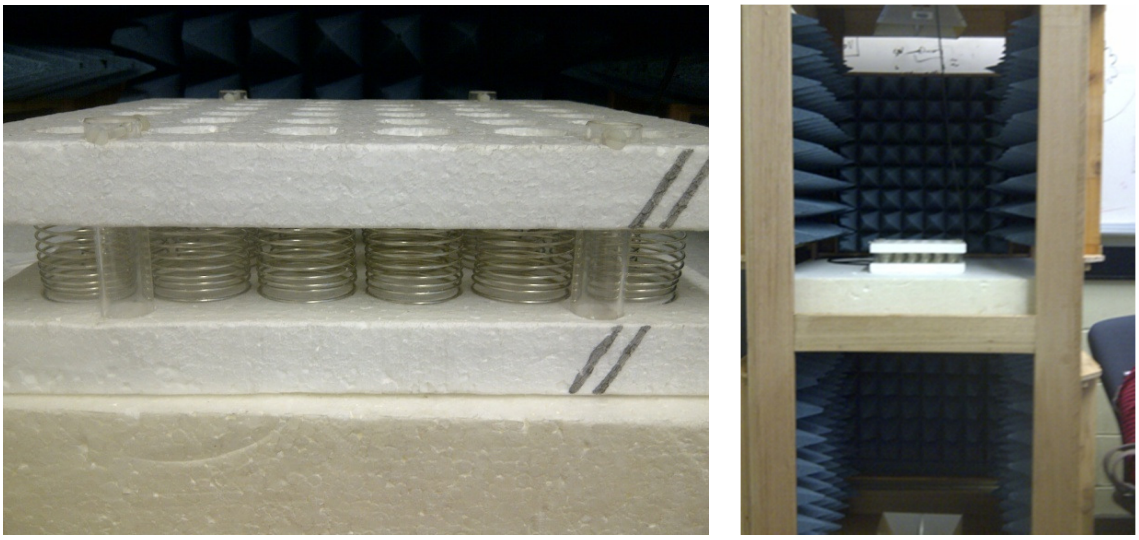

Figure 3.25: Fabricated spring FSS and the test setup.

The simulated and measured $|S_{21}|$ of the prototype spring FSS is presented in Figure 3.26, exhibiting good agreement between the results. The measured transmission band-stop response at 3.43 GHz for the spring FSS compressed to h = 14 mm is slightly shallower (-47 dB as compared to -63 dB) and narrower in bandwidth than was predicted by the simulation. Whilst for the h = 30mm FSS the pass-band response is almost identical, displaying negligible insertion loss and only a marginally narrower measured bandwidth. The slightly non-uniform hand winding of the springs and potentially uneven compression across the FSS degrade the clarity of the measurement results, consequently resulting in the minor differences. These effects are more significant for a lower h as more compression is applied to reach these values. However, the trend of the measured response curves correlate well with the simulated response.

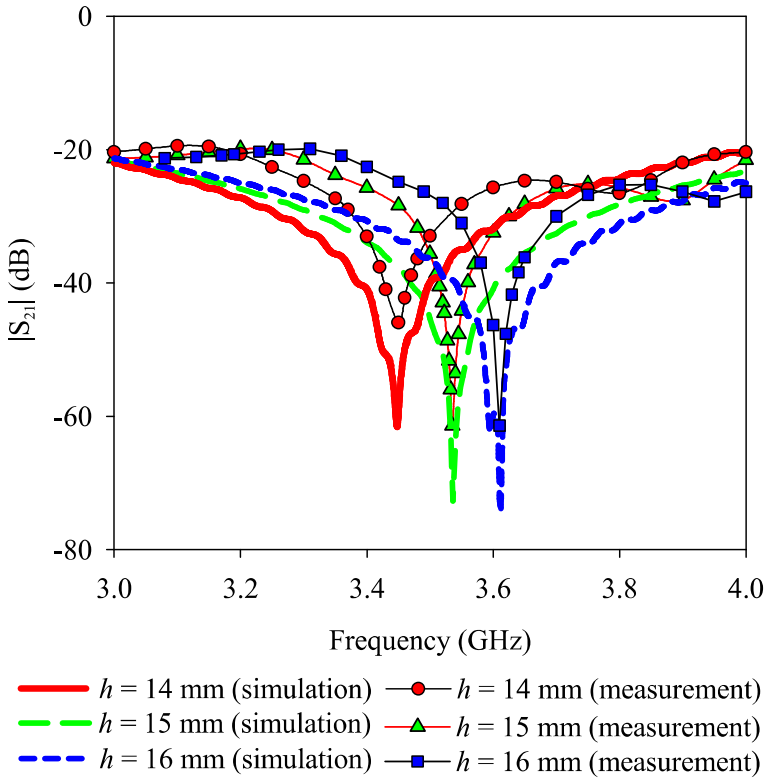

(a)

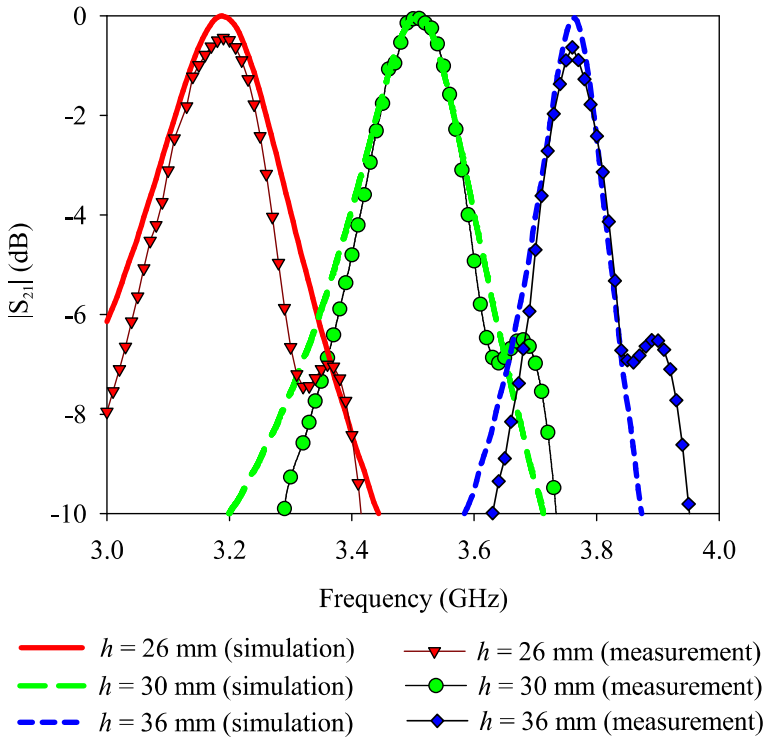

(b)

Figure 3.26: Simulated and measured transmission response of the spring FSS. (a) Band-stop response (b) Band-pass response.

3.5 Summary

This chapter has demonstrated that as height is added to the conducting elements of a circular ring FSS (length of cylinders), the band-stop response is shifted to a higher frequency. The transmission minima and bandwidth are reasonably well maintaned. At certain lengths for a particular operating frequency, the FSS changes from band-stop to band-pass, and continues to cycle between these responses with increased length. The simulated FSS properties were validated through an equivalent circuit model as well as experimental results, both of which showed very good agreement.

A close transmission/reflection band separation can be obtained through inserting a dielectric filling inside the cylindrical unit cell structure of the 3-D FSS. For a dielectric filling with ε_r>40 the effective electrical size of the unit cell was sufficiently reduced to enable the analysis of the bulk metamaterial properties, which exhibited a negative refractive index band.

A very close pass and band-stop response (approaching a 1:1 ratio) can also be achieved without the addition of lumped components or dielectric filling by using dual cylinder 3-D FSS. This structure was formed by extrapolating the height of planar dual ring unit cell. This transforms the rings into cylindrical elements of a certain length. Alteration to the length adjusts the frequency characteristics of the FSS, enabling a close band response to be achieved. At a certain length, the pass and band-stop responses flip in frequency. Furthermore, dual cylinder 3-D FSSs offer a closer band response that cannot be achieved by 2-D dual ring FSS, where a very close gap between two printed ring elements is required.

The frequency response of the 3-D cylindrical FSSs can be fine-tuned by adjusting the cylinder height, and hence a novel 3-D spring FSS structure is proposed that can be tuned by mechanically altering the height of the spring. In addition to this continuous tuning of the FSS resonance, this new structure can also achieve functional switching between band-stop and band-pass operations without the need for active device integration. This avoids complications in the integration of DC bias networks in the FSS structure to obtain tuning/switching and eradicates any influence on the RF performance from the active circuit. The tunable spring-loaded FSS could also be implemented in a sealed structure with pneumatic actuation to control the frequency characteristics. Very good agreement in

frequency performance was observed between equivalent circuit calculations, numerical modelling and experimental testing for the spring FSS. Table 3.10 shows a comparison between the 2D and 3D FSSs developed in this Chapter.

Table 3.10: Comparison between 2-D and 3-D FSSs

	2D FSS	**3-D FSS**
Close Band FSS	• Minimum frequency band ratio: 1.48 [45]	Minimum frequency band ratio: 1.003
Tunable FSS	• Frequency properties can be switched or varied using varactors diodes, PIN diodes, and Schottky diodes. [51-54]	FSS can switched and varied by extrapolating the height of the cylindrical resonator. • Height < 30 mm (band stop) • Height > 30 mm (band pass)
Mechanical FSS	Frequency can varied by shifting one layer of double-layer FSS [61] • tune by shift Δx at (10 to 11 GHz as band pass) • tune by shift Δy at (10 to 15 GHz as band pass)	Frequency can switched and varied using height of 3-D spring resonator (1.8 GHz to 2.5 GHz) • 10mm – 50mm (band stop) • 60mm – 90mm (band pass)

CHAPTER 4

3-D Tapered Frequency Selective Surfaces (FSS)

4.1 Introduction

In the previous chapter, 3-D Frequency Selective Surfaces (FSS) have demonstrated superior flexibility in performance than their 2-D FSS counterparts. 3-D FSSs offer greater flexibility in terms of controlling the frequency response without the use of active components. The frequency response can be tuned, as well as selecting either band pass or band stop operation, by varying the length of the 3-D cylindrical FSS unit elements. However, an in-depth study regarding the incident angle of the incoming electromagnetic wave to these 3-D FSS structures has yet to be presented.

In order to produce a 3-D Frequency Selective Surface (FSS) with a response that is independent of incident angle, a new type of 3-D FSS is proposed and following research question are addressed:

- How can the performance of a 3-D FSS be improved in terms of incident angle?
- What are the important design parameters for creating an incident angle independent 3-D FSS?

The proposed 3-D Tapered FSS is a periodic array of three-dimensional hollow, tapered resonators. The proposed 3-D FSS has reduced sensitivity to the angle of incidence of the electromagnetic wave as a result of tapered structure, when compared to other 2-D and 3-D FSSs. The Transverse Electric (TE) and Transverse Magnetic (TM) angular stable is obtained by tapering the width of a cylinder with a square cross-section from the upper opening to the lower opening. Impressive frequency stability and transmission characteristics have been achieved up to 80 degrees for both TE and TM incidence angles.

The influence of key design parameters on 3-D Tapered FSS characteristics has been investigated using CST simulation software and will be explained in detail in the next section.

In the following section a novel 3-D tapered Frequency Selective Surface (FSS) with horn-shaped resonators is proposed, which exhibits a very wide stop band. This new horn-shaped resonator is a modified version of a 3-D FSS consisting of square cylinder unit elements. This horn-like feature introduces the added advantage of lowering the sensitivity of the FSS frequency response with respect to the incidence angle. Simulation results prove that the FSS can realize selectivity of waves with the bandwidth more than 57%. The wideband transmission behaviour is shown to be stable under oblique TM incidence angles from 0 to 80 degrees.

4.2 3-D Tapered FSS Concept

In order to stabilize the angular transmission response of the 3-D FSS, the structure is studied for two circumstances: TE and TM incident angles. The design simulations took place under the assumption that the FSS is an infinite periodical repetition (unit cell) of an element pattern along the two axes of the FSS plane. For the s-parameter calculation, two Floquet ports are used; one in front and one at the rear of the FSS plane. A 2-D square ring FSS provided the initial basis for this investigation. The square ring resonator was chosen as a foundation element since it has demonstrated less sensitivity to incident wave angle than other shaped resonator elements [110]. It is well known that a symmetric structure can realize dual-polarized operation. However, symmetric structures are not necessarily be insensitive to waves coming from different incident angles, particularly up to and beyond a 60º incident angle [20, 74].

By choosing unit cell size (p) appropriately, very low sensitivity with respect to the incidence angle of the wave can be achieved [111], with a smaller inter-element spacing usually preferred. Therefore, a FSS was created by periodically arraying PEC square ring elements (in free space) in a square unit cell (see Figure 4.1(a)). The dimensions of the square ring are determined using a basic square ring resonator design equation, $a \approx \lambda_0/4$. The dimensions of the square ring and width, s (0.5mm) of the conducting strip primarily

determine the location of the resonant frequency, which in this case is 2.45 GHz. The 2-D elements were then extruded into 3-D cylindrical structures with a square cross section. The 3-D square FSS structure of Figure 4.1(b) performs similarly to the cylindrical structures of [99, 100]. Alteration to the length/height of the cylinders adjusts the frequency characteristics of the FSS. The 2-D square ring FSS ($h \approx 0$) exhibits a band-stop response resonating at a frequency of $f = 1/(2\pi\sqrt{L_1 C_1})$, where L_1 and C_1 are the equivalent parallel inductance and capacitance of the square ring geometry as shown in Figure 4.2. L_1 mainly depends on the diameter a of the square ring, and the resonant frequency of the element can be controlled by adjusting a. However in transition process to a 3-D square cross-section cylinder FSS, a is fixed. When the value of h is increased, a series inductance L_2 along the cylinder length increases and hence modifies the behavior of the element [100]. Consequently, the band stop center frequency is tuned to a higher value with increasing h from 2.45 GHz for 2-D square ring ($h \approx 0$) to 3.0 GHz for 3D square cross-section cylinder FSS with h = 14 mm.

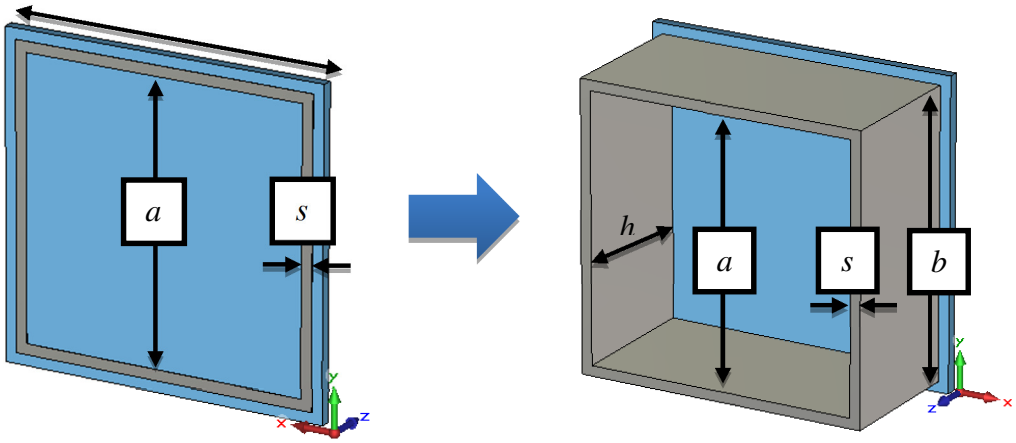

(a) (b)

Figure 4.1: Transition process to a 3-D Tapered FSS: (a) 2-D square ring FSS, (b) 3-D square cross-section cylinder FSS.

Parameters: p = 35 mm, h = 14 mm, a = 28 mm, b = 14 mm, s = 0.5 mm

(a) (b)

Figure 4.2: Equivalent circuit of (a) 2-D square ring FSS, (b) 3-D square FSS.

4.2.1 Control of the TM incident angle response

Figure 4.3 shows that the symmetric 2-D square FSS structure is not independent of the incident angle for TM incidence. The frequency of resonance achieves independence from incident angle for TE incidence only, as shown in Figure 4.3 (a). This is because in the TE incidence scenario, the E-field is always parallel to the metallic strip and excites the full length regardless of incident angle. However, in the TM incidence scenario, the E-Field arrives obliquely to the broadside of the strip, resulting in a shorter projected strip length as the incident angle increases. The resonant frequency shift for TM incident angles seen in Figure 4.3 (b) was 13% for 0 to 80 degrees, and matched the calculation using the equations in [31].

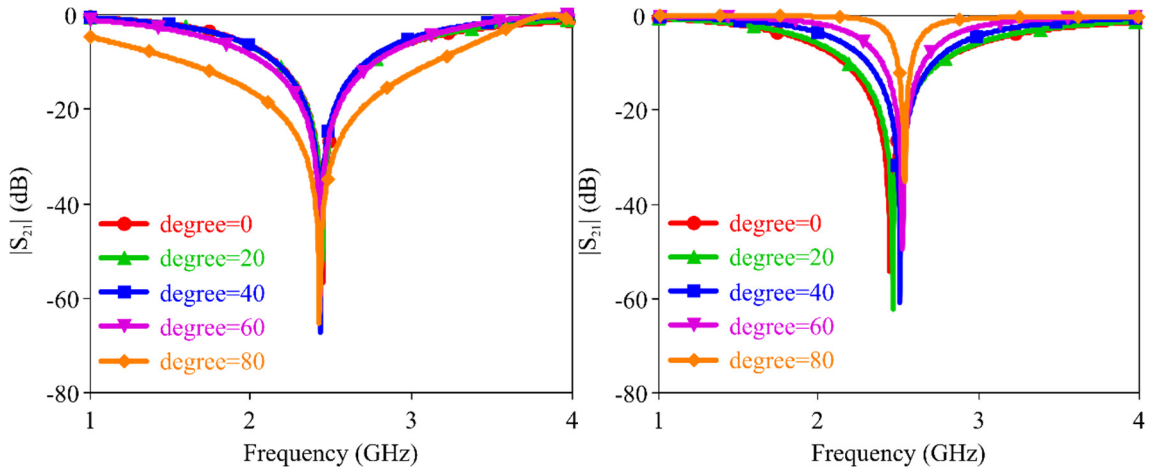

(a) (b)

Figure 4.3: $|S_{21}|$ results for a 2-D Square Ring FSS as incident angle is varied:

(a) TE incidence, (b) TM incidence.

The TM incidence variation of the 2-D square ring FSS can be alleviated by transitioning to the 3-D square cross-section cylinder FSS of Figure 4.1 (b). The 3-D square cross-section cylinder FSS was created by periodically arraying 2-D square ring elements with unit cell size of 35 x 35 mm, and adding significant height to the conductor to create the third dimension.

The resonant response of the 3-D square cross-section cylinder FSS is shown to be independent from TM incident angles (Figure 4.4(a)). However, the resonant frequency at around 3 GHz now varies by 5.1% for TE incidence up to 80 degrees, as observed in Figure 4.4(b). The characteristics of a one- or two- dimensional resonant-length based FSSs usually depend on the way the surface is exposed to the electromagnetic wave. This dependence includes the effective aperture size of the FSS and the incidence angle of the wave. However, by introducing height to 2-D FSS geometry, the resonance characteristics do not solely rely on surface mode but also on a cavity mode, whose resonant frequency is angle-independent [71, 112]. Although the 3-D square cross-section cylinder FSS is angle-independent for TM incidence, the TE incidence response is still governed by a surface (square ring) mode. For the TE incidence response of the 3-D square cross-section cylinder FSS seen in Figure 4.4 (a), a second resonance at around 5.3 GHz remains stable for angles from 0 to 80 degrees. Listed in Table 4.1 is the frequency deviation for TE and TM incident angles of the 3-D square cross-section cylinder FSS from center frequency (at normal incidence).

The aforementioned 3-D square cross-section cylinder FSS exhibits a frequency response that is independent of both TM and TE (2^{nd} resonance) incident angles, albeit at different frequencies. In order to stabilize FSS response for both TE and TM incidence at the same frequency, a modification to the 3-D square cross-section cylinder FSS is proposed which tapers the cross-sectional size of the cylindrical element. This feature enables the FSS to utilize higher frequency cavity resonances that have very low sensitivity to the incidence angle.

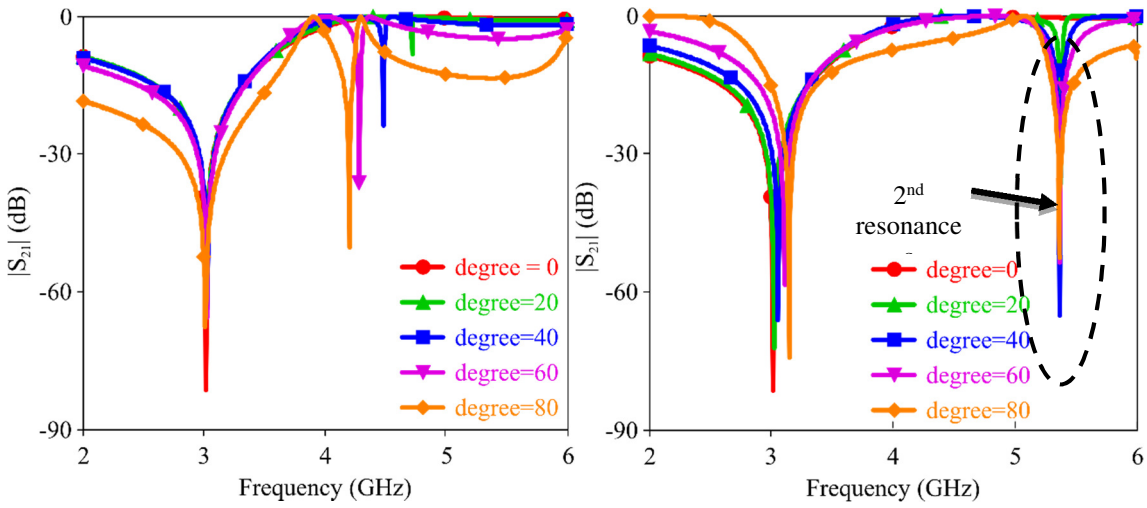

Figure 4.4: $|S_{21}|$ for the 3-D square cross-section cylinder FSS as incident angle is varied for TE and TM incidence. (a) $|S_{21}|$ for 3-D TM incidence, (b) $|S_{21}|$ for TE incidence, indicating the 2nd resonance shows a stable resonance.

Table 4.1: Values of the Center Frequencies – 3-D square cross section cylinder FSS

Degree	**Frequency (TE incidence)**	**deviation %**	**Frequency (TM incidence)**	**Deviation %**
0	3.002 GHz	0	3.002 GHz	0
10	3.002 GHz	0	3.002 GHz	0
20	3.009 GHz	0.23	3.009 GHz	0.23
30	3.037 GHz	1.16	3.009 GHz	0.23
40	3.058 GHz	1.87	3.009 GHz	0.23
50	3.072 GHz	2.33	3.011 GHz	0.29
60	3.114 GHz	3.6	3.009 GHz	0.23
70	3.126 GHz	4.13	3.002 GHz	0
80	3.156 GHz	5.13	3.002 GHz	0

Here, different values of the lower aperture dimension *b* (as per Figure 4.5) are studied in order to obtain an independent frequency response for both TE and TM incidence. The simulated transmission coefficient at 0 and 60 degree incident angles for different *b* values are shown in Figure 4.6 with fixed values of h = 14 mm and a = 28 mm.

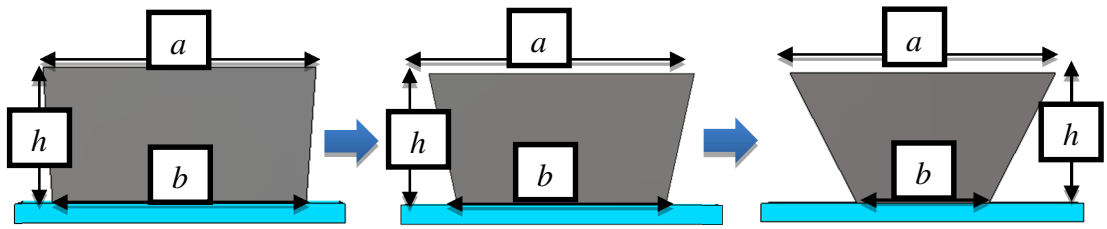

Figure 4.5: Transition process of 3-D square cross-section cylinder FSS with different values of the lower aperture dimension *b*.

As can be seen in Figure 4.6, a reduction in b maintains TM incident angle independence with an increased resonant frequency. At b = 14 mm, the center frequency of the band-stop reaches 5.256 GHz, whilst the second resonance for TE incidence at 60 degree matches the 0 degree case at 5.256 GHz. However, as b is increased from 22 mm to 30 mm, the center frequency reduces and begins to vary when the incident angle changes. For the larger values of b, congruence between the 0 and 60 degree cases is lower, especially for TE incidence. Therefore, in order to maintain FSS response for both TE and TM, it is found a reduction in b to 14 mm maintains the TM incident angle independence with an increased resonant frequency, whilst improving the TE incident angle response.

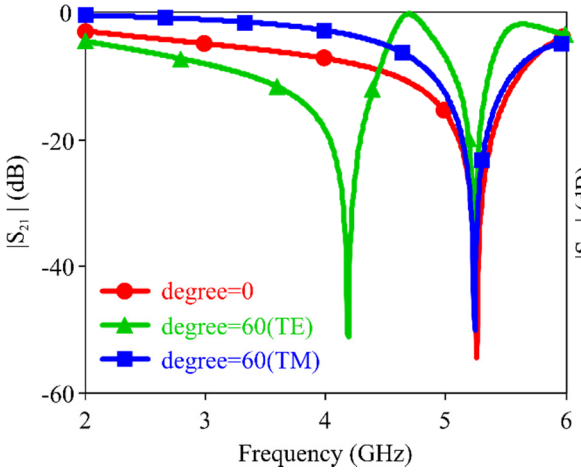

(a) b = 14 mm

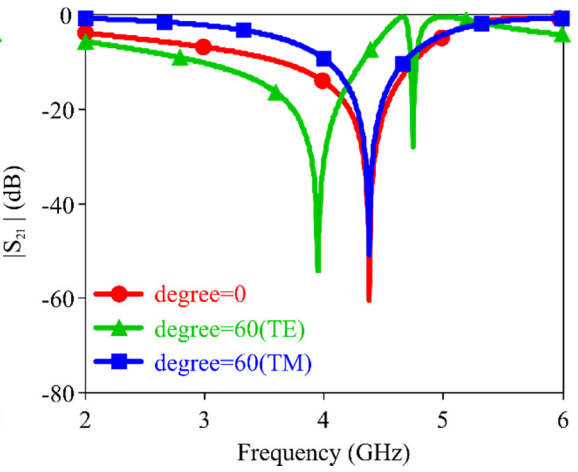

(b) b = 18 mm

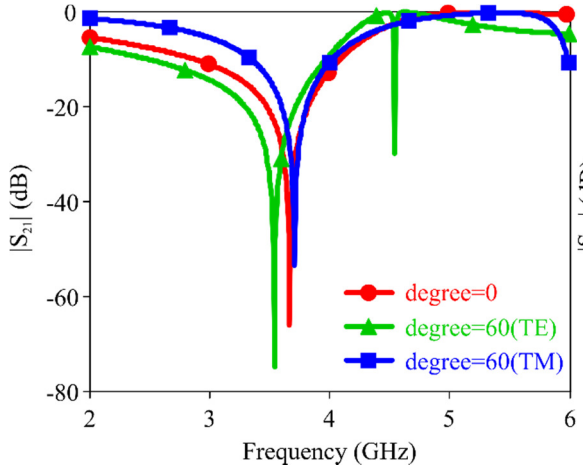

(c) b = 22 mm

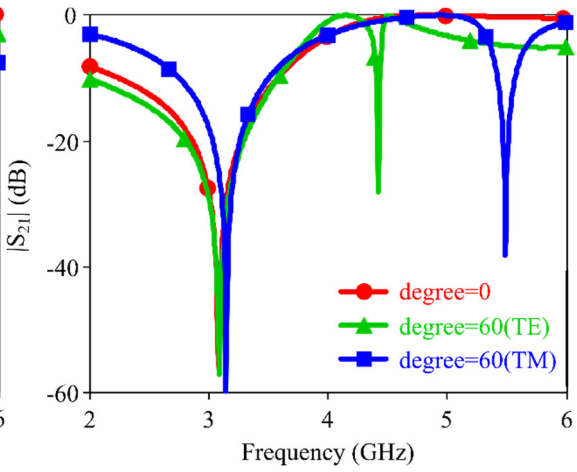

(d) b = 26 mm

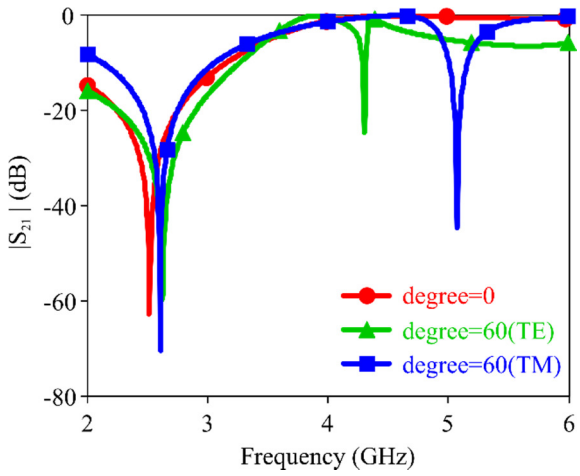

(e) b = 30 mm

Figure 4.6: TM and TE incidence for different values of b at 0 and 60 degrees.

(a) when b = 14 mm, (b) 18 mm, (c) 22 mm, (d) 26 mm, and (e) 30 mm.

Different heights, h of 3-D Tapered FSS are also studied in order to obtain a stable performance of the FSS resonant frequency verses the angle of the incident plane wave. The dimensions of the unit cell, a and b, are kept at 28 mm and 14 mm respectively; only the height parameter is changed. The height of the 3-D Tapered FSS is set to h = 12 mm, 18 mm, 22 mm and 26 mm, respectively. When the height of the structure is increased, the length of the tapered section is also increased, which would cause the resonant frequency to decrease in theory [36].

Figure 4.7 shows the transmission response 3-D Tapered FSS with varying height. The comparison of the resonant frequency, the fractional bandwidth and the angular dependence of the structures are presented in Table 4.2. As predicted, simulation results show the resonant frequency decreased as the height is raised at the same incident angle. The frequency offset at TE angular incidence is again larger than that of the TM incident angle. Thus, the height of the 3-D tapered FSS can also play a role in stabilizing the TE incident angle response. From this study, it is found that the best angular stability occurs when the height, h is between 12 mm and 18 mm. From Figure 4.6, the optimal value was shown to be 14 mm, or when $h = b$. There is a change of the fractional bandwidth at -10dB as the height is increased. The bandwidth of the 3-D Tapered FSS with h = 12 mm is slightly wider than for larger values of h.

Table 4.2: 3-D Tapered FSS with different height, *h*

		TE Incident	TM Incident	Bandwidth (%)
Incidence angle	**0º**	**60º**	**60 º**	
h =12 mm	5.30	5.32	5.30	8.61
h =18 mm	5.26	5.11	5.263	6.73
h =22 mm	5.22	5.00	5.17	5.77
h =26 mm	5.12	5.20	5.03	4.85

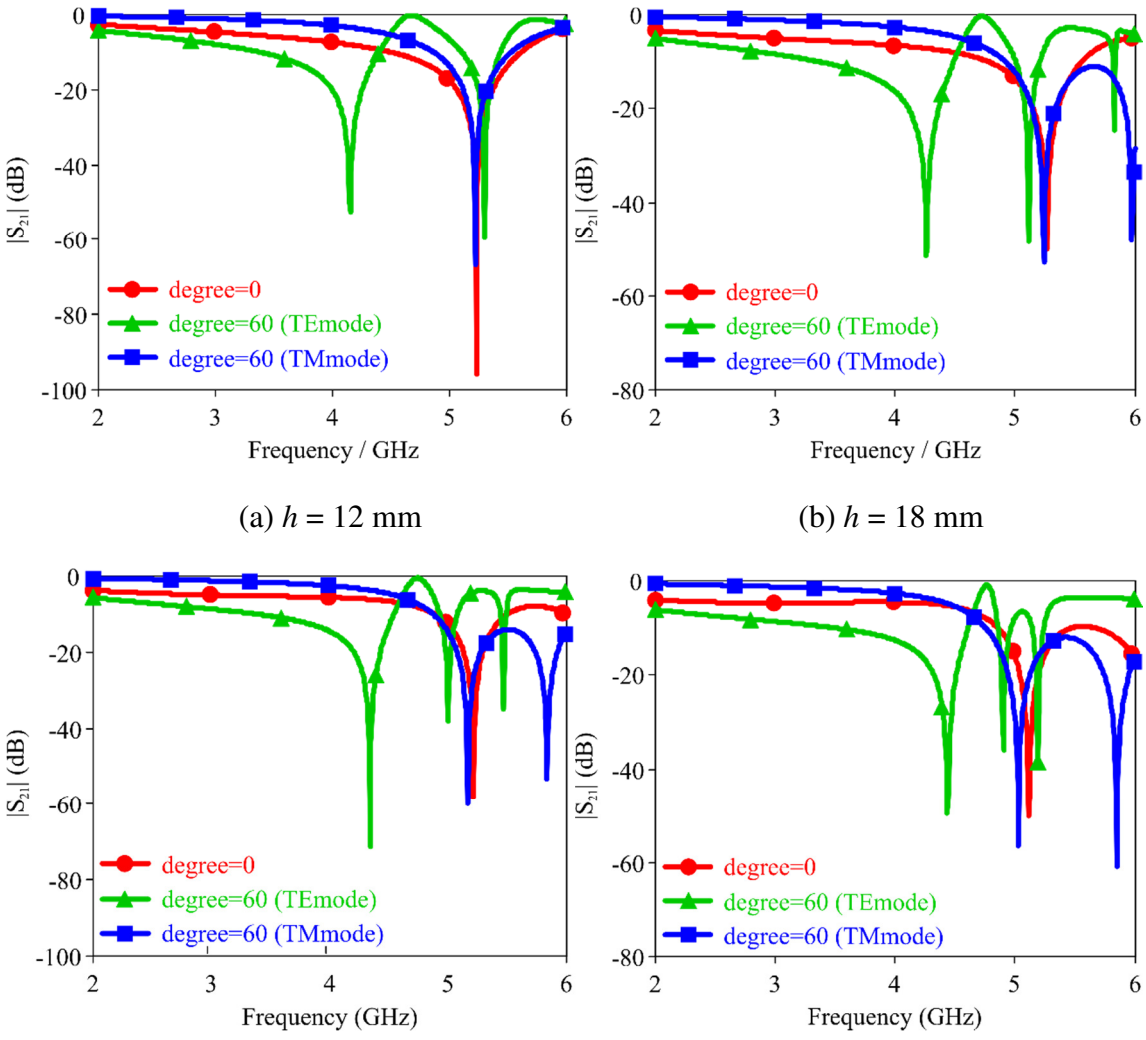

(a) *h* = 12 mm (b) *h* = 18 mm

(c) *h* = 22 mm (d) *h* = 26 mm

Figure 4.7: Transmission response of 3-D Tapered FSSs with varying height, *h,* at different incident angles. (a) *h* = 12 mm, (b) *h* = 18 mm, (c) *h* = 22 mm, (d) *h* = 26 mm.

4.3 Design of 3-D Tapered FSSs with Angular Stabe

The aforementioned 3-D square cross-section cylinder FSS exhibits a frequency response that is independent of both TM and TE (2^{nd} resonance) incident angles, albeit at different frequencies. In order to stabilize the FSS response for both TE and TM incidence at the same frequency, the cross-sectional dimension of the 3D square FSS element is tapered. This feature enables the FSS to utilize higher frequency cavity resonances that have very low sensitivity to the incidence angle. Furthermore, the simulation software CST Microwave Studio was used to investigate the design parameters of the 3D FSSs and confirm the angular stability.

In the previous section (4.2.1), tapered dimensions of the 3-D FSS introduced an additional design parameter that enables enhanced control of TE and TM incidence responses separately. Using these concepts, a 3-D Frequency Selective Surface (FSS) with a response that is independent of incident angle for both TE and TM incidence can be generated.

The proposed 3-D FSS has reduced sensitivity to the angle of incidence of the electromagnetic wave compared to other 2-D and 3-D FSSs as a result of the tapered structure. The TE and TM angular stability is obtained by tapering the width of a cylinder with a square cross-section from upper opening to the lower opening. Impressive frequency stability and transmission characteristics are shown to be achieved up to 80 degrees for both TE and TM incidence angles. The influence of key design parameters on the 3-D Tapered FSS characteristics has been investigated using CST simulation software and will be explained in detail in this section.

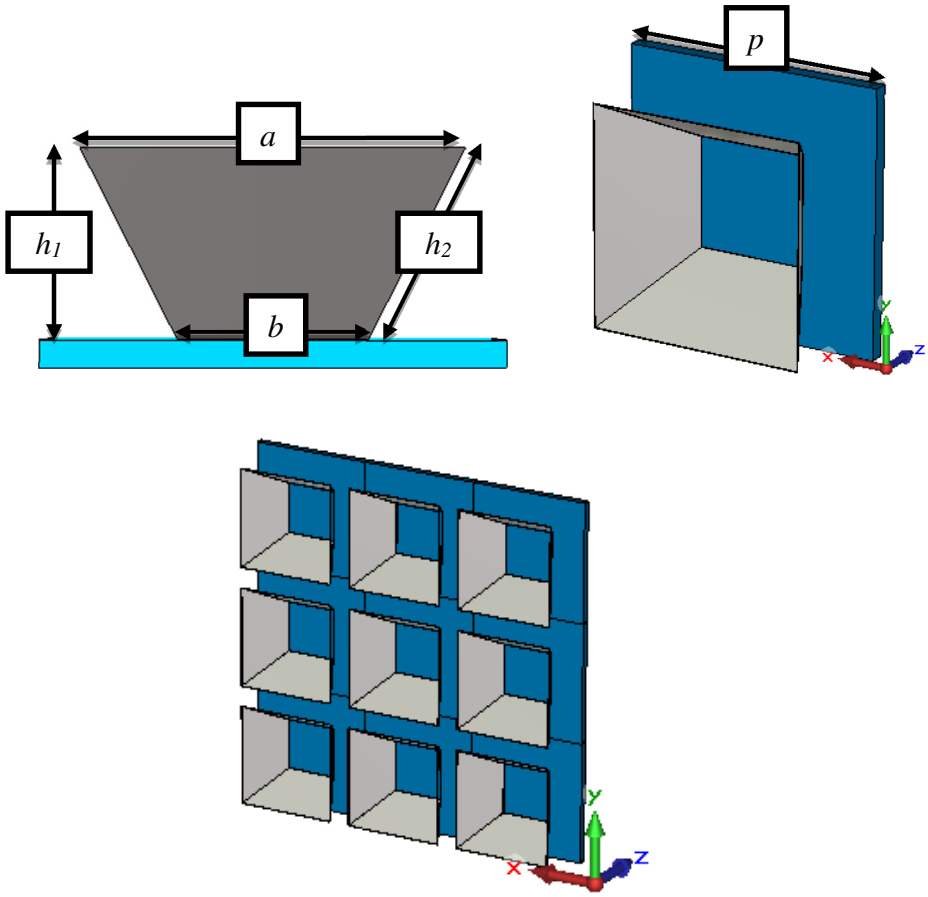

Figure 4.8: Geometry 3-D Tapered FSS :- h = 14 mm, a = 28mm, b = 14mm, p = 35 mm.

The 3-D tapered FSS consists of a three-dimensional periodic array of horn shape resonators as seen in Figure 4.8 with h = 14 mm, a = 28 mm, b = 14 mm. By tapering to $b = \lambda_0/4$ at the desired frequency, a cavity mode whose resonant frequency is angle independent is accessed. The dimensional requirements of the 3-D tapered elements for frequency stability up to 80 degrees are as follows: $b = a/2$ and $h \approx b$. The lattice spacing (p) is chosen to avoid grating lobes for all scan angles; for a square lattice this corresponds to $\lambda_0\sqrt{3}$, which is 35 mm at 5.2 GHz [104]. The dimensional requirements of the 3-D tapered elements for frequency stability up to 80 degree incidence can be calculated as follows:

$$f = \frac{c}{\lambda} \qquad (4.3.1)$$

$$a = \frac{\lambda}{2} \qquad (4.3.2)$$

$$a = 2b \qquad (4.3.3)$$

$$h_2{}^2 = h_1{}^2 + \left(\frac{a-b}{2}\right)^2 \qquad (4.3.4)$$

Equation (3) is inserted in equation (4), hence;

$$\left(\frac{b}{2}\right)^2 = h_2{}^2 - h_1{}^2 \qquad (4.3.5)$$

Equation (1), (2) and (3) is inserted in equation (4):

$$h_2{}^2 = h_1{}^2 + \left(\frac{\frac{c}{2f} - b}{2}\right)^2 \qquad (4.3.6)$$

$$4(h_2{}^2 - h_1{}^2) = \left(\frac{c}{2f} - b\right)^2$$

$$\sqrt{4(h_2{}^2 - h_1{}^2)} = \left(\frac{c}{2f} - b\right)$$

$$\frac{c}{\sqrt{4(h_2{}^2 - h_1{}^2)} + b} = 2f(GHz)$$

$$f(GHz) = \frac{c}{2\left[\sqrt{4(h_2{}^2 - h_1{}^2)} + b\right]}$$

Replacing $(h_2{}^2 - h_1{}^2)$ with $\left(\frac{b}{2}\right)^2$ (from equation 5) simplifies the equation as:

$$f(GHz) = \frac{c}{2\left[\sqrt{4\left(\frac{b}{2}\right)^2} + b\right]}$$

Where *c* is light velocity, 3×10^8 and all dimensions are in mm.

The equivalent circuit model of 3-D Tapered FSS is shown in Figure 4.9(a), and is used to analyze the structure. L_1 and C_1 are the equivalent inductance and capacitance of the square ring geometry of the larger upper opening of the tapered structure. L_1 mainly depends on the diameter of the ring. A series inductance L_2 related to the height, h_1 of the structure appears in series with the parallel combination of L_1 and C_1. A second parallel combination of $L_1/2$ and C_1 represents the smaller lower opening of the 3-D tapered resonator. In order to validate the *LC* model, the transmission characteristics of the 3-D Tapered FSS of Figure 4.8 have been simulated in CST Microwave Studio and compared to the *LC* model

prediction. The transmission coefficient of the equivalent circuit model is plotted in Figure 4.9, and the resonant frequencies agree well with the simulations.

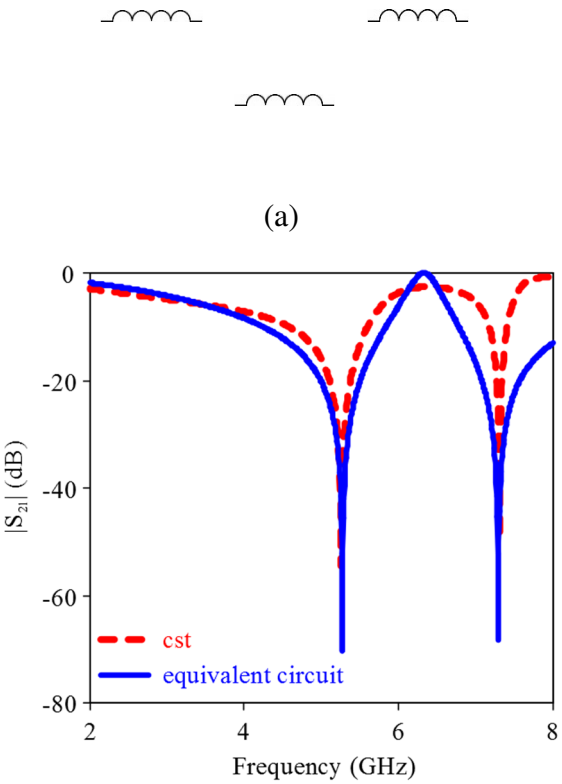

Figure 4.9: (a) Equivalent circuit of the 3-D Tapered FSS shown in Figure 4.8. (b) Simulation result compare with numerical calculation equivalent circuit.

The value of inductance (L_1 = 3.8 nH, L_2 = 0.84 nH) and capacitance (C_1= 0.48 pF) used in the equivalent circuit model can be retrieved from the following equations [104], [113]:

$$L_1(nH) = 3.937\left[\frac{\left(\frac{b+a}{4}\right)^2}{8\left(\frac{b+a}{4}\right)+11\left(\frac{b-a}{2}\right)}\right]\times 0.57$$

$$C_1(pF) = \frac{\left(\frac{1}{f.2\pi}\right)^2}{L_1}$$

$$L_2(nH) = \frac{\mu_o h_1}{4\pi}\left[\frac{2a^2\ln(a) - a^2(2\ln(b)+1)+b^2}{a^2b^2}\right]$$

Where;

a = inner diameter

b = outer diameter

h_1= length

f = frequency

The 3-D Tapered FSS was modeled using CST for TE and TM incident angles from 0 to 80 degrees. The results are shown in Figure 4.10, and values of the center frequencies and their deviation from the 0 degree response are presented in Table 4.3. In Figure 4.10(a) and (b) the transmission results are reported. The transmission band-stop for normal incidence occurs at approximately 5.26 GHz, with minimal frequency variation for all angles up to 80 degrees. A corresponding resonant phase transition is also observed in Figure 4.10(c) and (d). Although the frequency response is stable for TE incident angles, a resonance appears below 5.26 GHz for 40, 60 and 80 degrees. This is due to the incident angle exciting a surface resonant mode on the upper square opening of 3-D Tapered FSS. This finding is supported by the distribution of the electric field that will be discussed further in this section. Table 4.3 confirms the angular stability, with a maximum deviation of the resonant frequency of 0.4% for both TE and TM incidence up to 80 degrees. The -10 dB fractional bandwidth is approximately equal to 21%. A slight decrease in the bandwidth with elevated angles to 60 degree is evident, particularly for TE incidence, and increases again when approaching grazing angles.

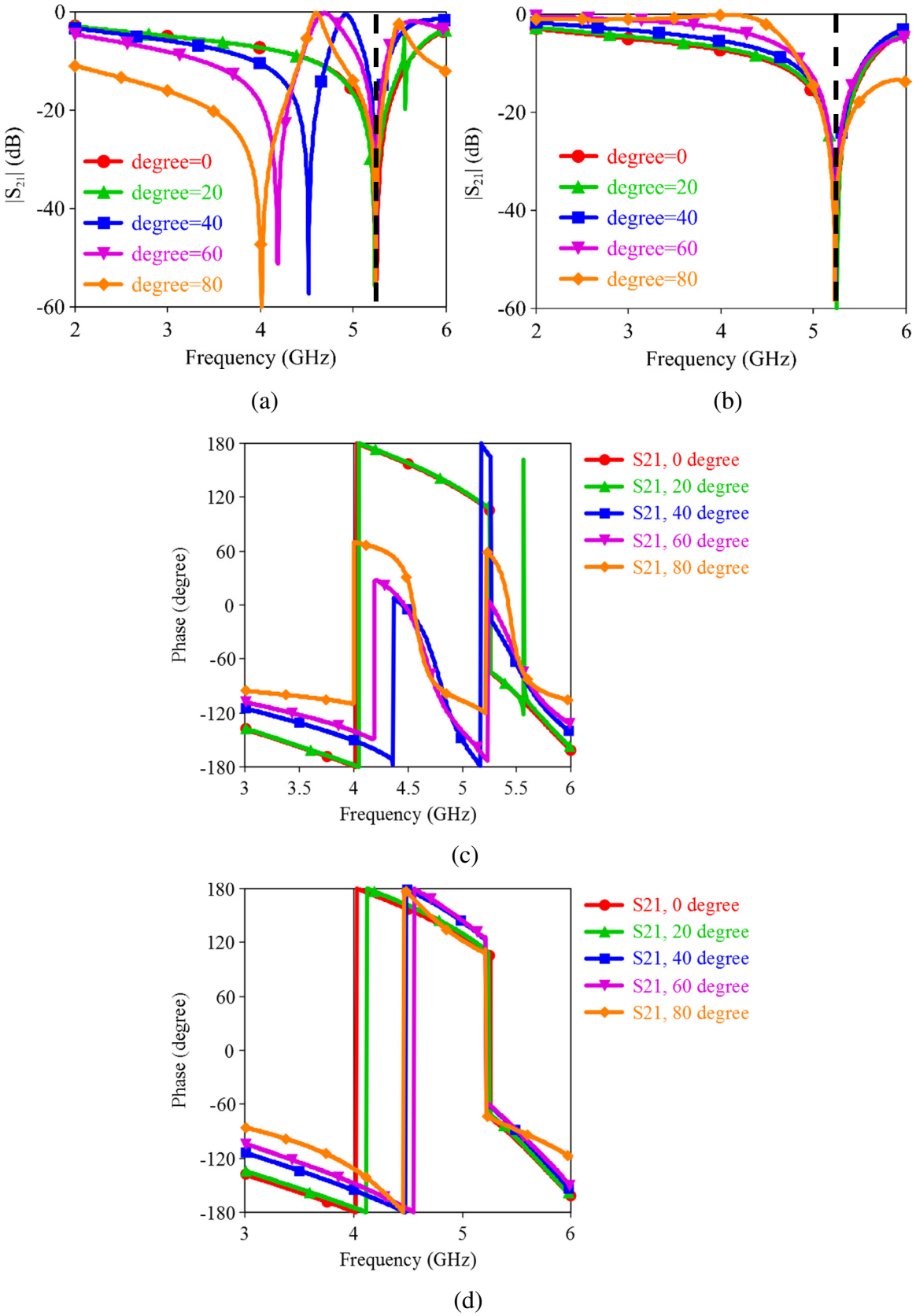

Figure 4.10: Simulated $|S_{21}|$ for the 3-D Tapered FSS: (a) TE incidence, (b) TM incidence, (c) $|S_{21}|$ Phase versus Frequency - TE incidence, (d) $|S_{21}|$ Phase versus Frequency - TM incidence.

Table 4.3: Center Frequency Values – 3-D Tapered FSS

Degree (°)	**Frequency (TE incidence)**	**Deviation %**	**Frequency (TM incidence)**	**Deviation %**
0	5.256 GHz	0	5.256 GHz	0
10	5.256 GHz	0	5.256 GHz	0
20	5.256 GHz	0	5.256 GHz	0
30	5.256 GHz	0	5.256 GHz	0
40	5.255 GHz	0.02	5.255 GHz	0.02
50	5.250 GHz	0.11	5.250 GHz	0.11
60	5.250 GHz	0.11	5.247 GHz	0.17
70	5.248 GHz	0.15	5.240 GHz	0.30
80	5.245 GHz	0.21	5.235 GHz	0.40

A comparison of the electric field distributions at the respective centre frequencies for the 3-D Tapered FSS and the 3-D square cross-section cylinder FSS in both incident planes is shown in Figure 4.11 and Figure 4.12. The cavity modes seen in Figure 4.11 for both structures display a similar shape for all TM incident angles. This reinforces the finding of stable center frequencies for TM incidence. However, the electric field mode is disparate for increasing TE incident angles in the 3-D square cross-section cylinder FSS in Figure 4.12. The tapered design of the 3-D Tapered FSS elements introduces an additional design parameter that controls the scattered field, enabling a relatively stable cavity mode at the same frequency for TE and TM incident angles.

Degree (°)	TM incidence (3-D Tapered FSS)	TM incidence (3-D square cross section cylinder FSS)
0	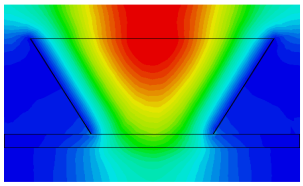	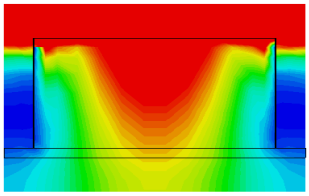
40	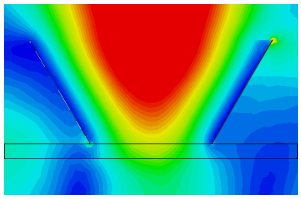	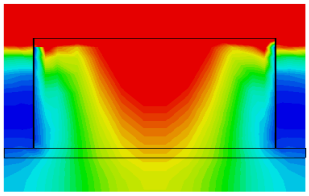
60	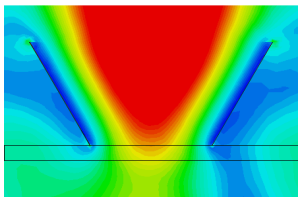	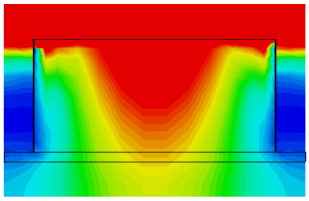
80	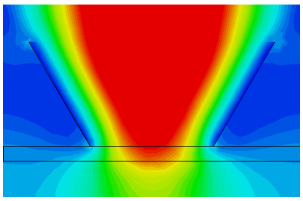	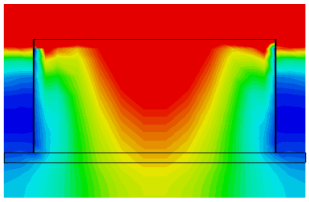

Figure 4.11: Cross-section view of electric field distribution for the 3-D Tapered FSS and 3-D square cross-section cylinder FSS at resonance (5.256 GHz and 3 GHz respectively) in the y-z plane at 0, 40, 60 and 80 degrees (TM incidence).

Degree (°)	TE incidence (3-D Tapered FSS)	TE incidence (3-D square cross section cylinder FSS)
0	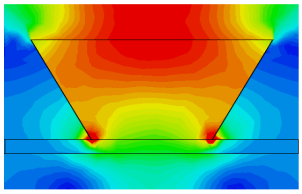	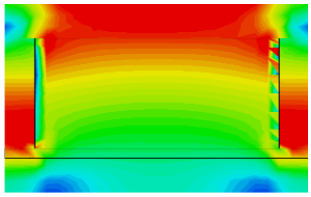
40	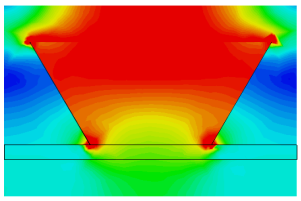	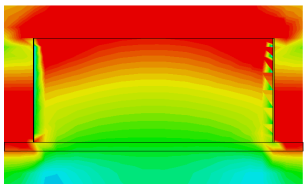
60	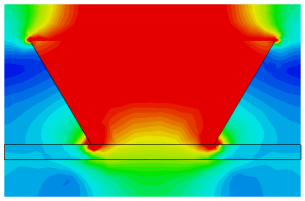	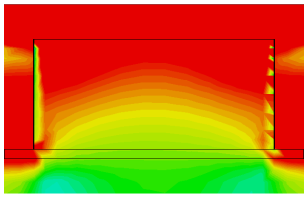
80	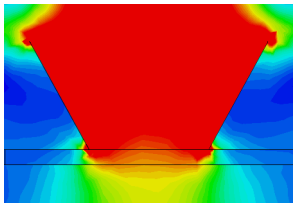	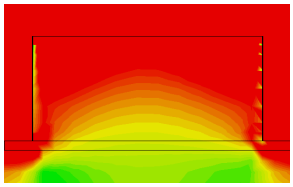

Figure 4.12: Cross-section view of electric field distribution 3-D Tapered FSS and 3-D square cross-section cylinder FSS at resonance (5.256 GHz and 3 GHz respectively) in the x-z plane at 0, 40, 60 and 80 degrees (TE incidence).

4.4 3-D Tapered FSS Prototype

To verify the independent incident angle response of the 3-D Tapered FSS, a prototype was constructed using 3-D printing technology. This additive manufacturing technology enables the realization of complex 3-D shapes and is perfectly suited for these 3-D FSS prototype structures. The downside to this technology is its limitation in material selection, resolution and sometimes cost.

A U-Print Plus SE was used to manufacture the proposed 3-D Tapered FSS structure out of Acrylonitrile Butadiene Styrene (ABS). The process used is called Fuse Deposition Modelling (FDM) and is extremely cheap. The structure is printed layer-by-layer using the ABS polymer. The dielectric properties of this polymer are different to free-space (which was used in previous sections for the 3-D FSSs) hence a redesign of the 3-D tapered FSS was required. The dielectric structure of the FSS also needs to be metalized to realize the tapered resonator elements. A silver spray coating was employed to metalize the required planar surfaces of the tapered resonators, as indicated in Figure 4.13(a). An alternative, more expensive process would be to directly print the metallic structure using the Selective Laser Melting (SLM) method.

To simulate the effects of ABS on the FSS structure, its complex permittivity was measured using a waveguide transmission/reflection method. The resultant relative permittivity (ε_r) was extracted and was found to be 2.12. The low permittivity is attributed to the high porosity of the printed material, and as such the loss tangent was minimal (~0.001). The 3-D Tapered FSS was redesigned using the structure of Figure 4.13(a). The unit cell dimensions are presented in Figure 4.13(b).

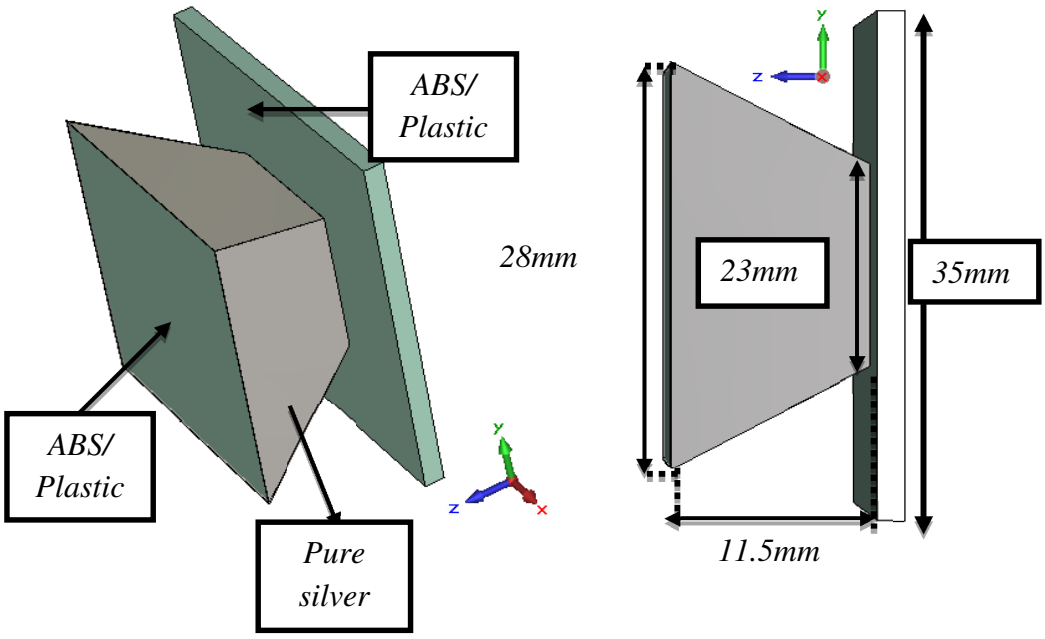

(a) (b)

Figure 4.13: The geometric configuration of the fabricated prototype 3-D Tapered FSS. (a) Unit cell structure of the proposed 3-D FSS showing the dielectric ABS/Plastic and silver materials, (b) Side view of the structure with detailed dimension values.

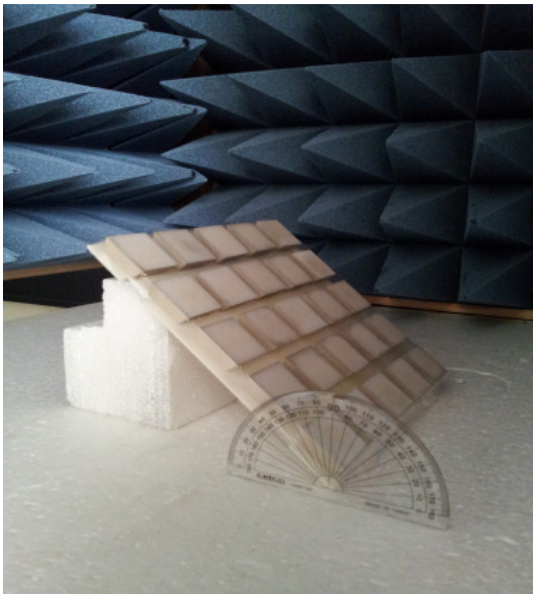

Figure 4.14: Fabricated prototype of the proposed 3-D Tapered FSS.

The FSS comprises of 6 x 6 elements with an overall lateral dimension of 238 x 238 mm^2, as shown in Figure 4.14. An ABS base plate was used to locate the individually printed tapered resonators at the precise unit cell spacing. The 3-D Tapered FSS was tested in a free-space measurement setup as shown in Figure 4.15. This comprised of two double-ridge wideband horn antennas which were placed about 1 meter from each other. The setup was calibrated using a through calibration (with isolation), and the 3-D Tapered FSS prototype was placed in the fixture and the transmission coefficient ($|S_{21}|$) was measured.

Figure 4.15: The measurement setup for 3-D Tapered FSS

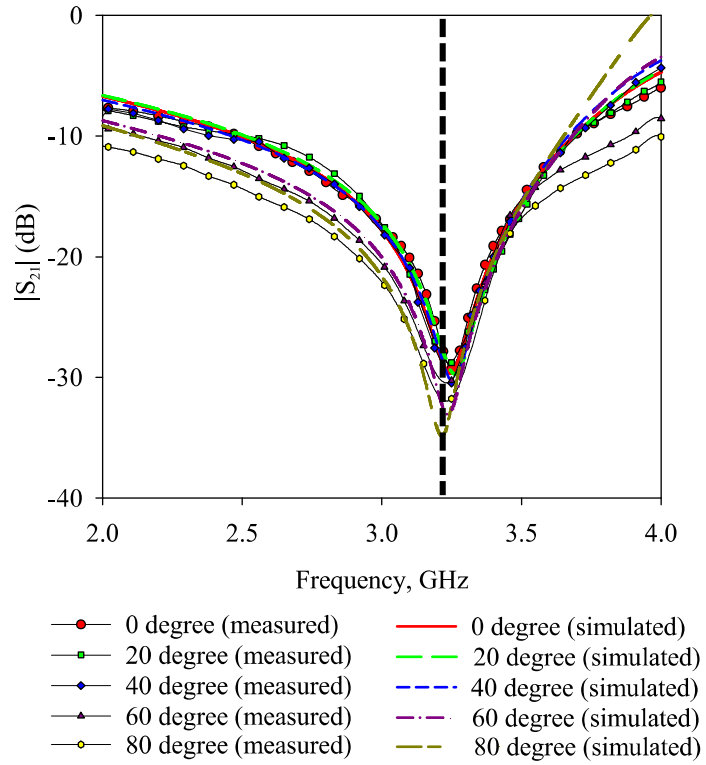

(a) TE incidence

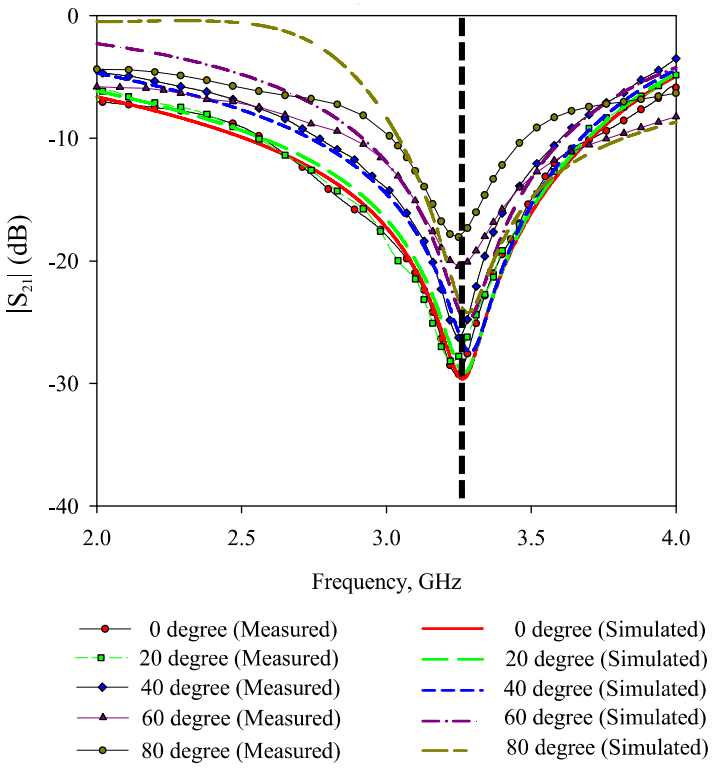

(b) TM incidence

Figure 4.16: Comparison of the simulated measured results for the 3-D Tapered FSS for θ=0° to 80°. (a) TE incidence, (b) TM incidence.

Parameters: p = 35 mm, h = 11.5 mm, a = 28 mm, b = 23 mm.

Figure 4.16 compares the simulated and measured results of the fabricated 3-D Tapered FSS, and no considerable change in the resonant frequencies of the FSS are observed for TE and TM incident angles up to 80 degrees. Figure 4.16(a) shows that the bandwidth becomes narrower for TE when the angle of incidence increases, though in Figure 4.16(b) the bandwidth becomes broader for TM incidence. The measured -10dB bandwidth at normal incidence is about 33%, which displays good similarity to simulated results. Less bandwidth variation is observed in the realized prototype of 3-D tapered FSS due to the dielectric in the cavity as compared to 3-D tapered FSS in Section 4.3. The measured and simulated transmission minima at the center frequency 3.3 GHz are 28 and 30 dB, respectively under normal incidence. The measured results do deviate slightly from simulations for larger oblique angles (60 and 80 degrees) for TE incidence. This is due to the finite size of the FSS presenting an increasingly smaller cross section at higher angles. Nevertheless, a very good level of agreement is seen between simulated and measured results

4.5 3-D Tapered FSS with Wideband Response

This section demonstrates that a widened bandwidth response can be obtained by using a 3-D Frequency Selective Surface. A novel 3-D Frequency Selective Surface (FSS) with horn-shaped resonators is proposed which exhibits a very wide stop band. This new horn-shaped resonator is also a modification from a 3-D FSS consisting of square cylinder unit elements. The proposed structure provides a wide bandwidth response without using any dielectric material. By varying key parameters of the 3-D FSS, the frequency response can be adjusted as well as producing a wider frequency response.

As can be seen in Figure 4.17(a) and (b), one end of a square cylinder unit cell resonator is flared in both lateral dimensions from a intermediate point in the cylinder's height, enlarging the aperture and forming the horn-like shape. The influences of the various geometrical parameters of the 3-D horn-shaped FSS shown in Figure 4.18 were determined and optimized using CST simulation software to widen the stop band. In the designed structure, the two parameters a and l_2 are primarily considered. The values of a and l_2 are changed in isolation, whilst all other parameters remain the same. These two parameters are considered as they have the greatest influence on enhancing the bandwidth of 3-D FSS. In principle, any variation which changes the perturbation of the cavity field leads to a change

in frequency spacing and thus bandwidth [36]. In the l_2 case, smaller values lead to a higher resonance frequency, whilst the contrary will happen in the a situation.

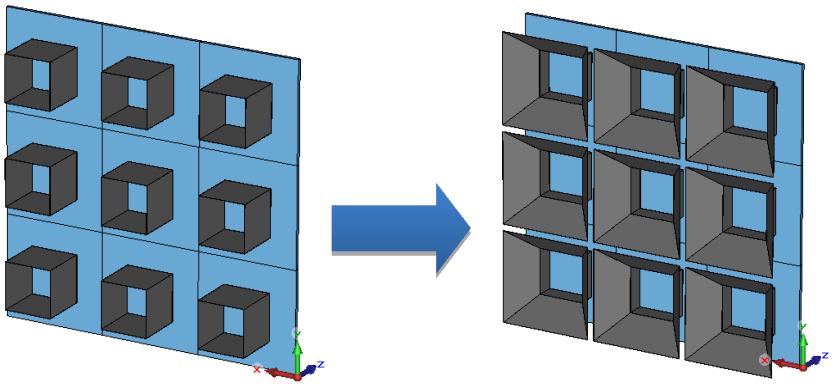

(a) (b)

Figure 4.17: (a) 3-D FSS with square cylinder resonators, (b) 3-D horn-shaped FSS.

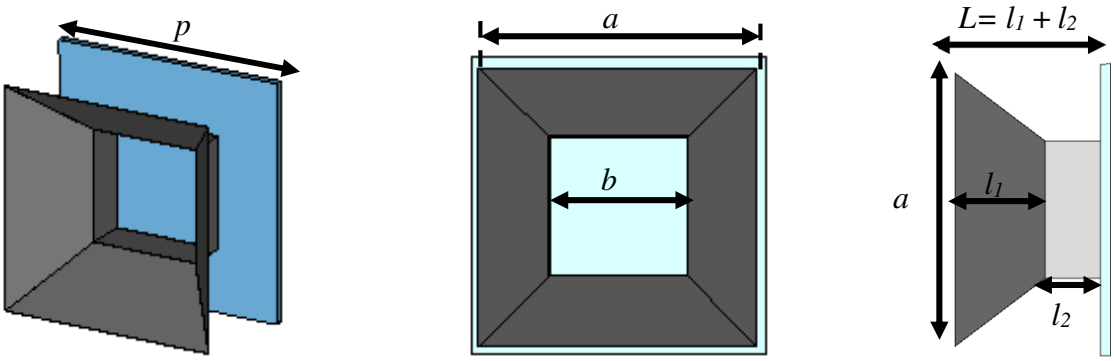

Figure 4.18: Three- and two-dimensional views of 3-D Horn-Shape FSS geometry with:

$a = 56$ mm, $b = 28$ mm, $p = 60$ mm, $l_1 = 18$mm, $l_2 = 11$mm.

A plot for a parametric sweep of these two parameters is shown in Figure 4.19(a) and (b) respectively. When increasing a (the square aperture becomes wider), the center frequency of the band stop region moves to lower values and has enhanced bandwidth. A wide bandwidth response is obtained between 53 mm to 56 mm. Varying the l_2 length leads to an opposite effect. It has been identified that from the parametric study that a narrower bandwidth is obtained as the length of l_2 is increased. Optimizing the two parameters together leads to the proposed design with the dimensions $l_2 = 11$mm and $a = 56$mm, as they provide the desired wide bandwidth response.

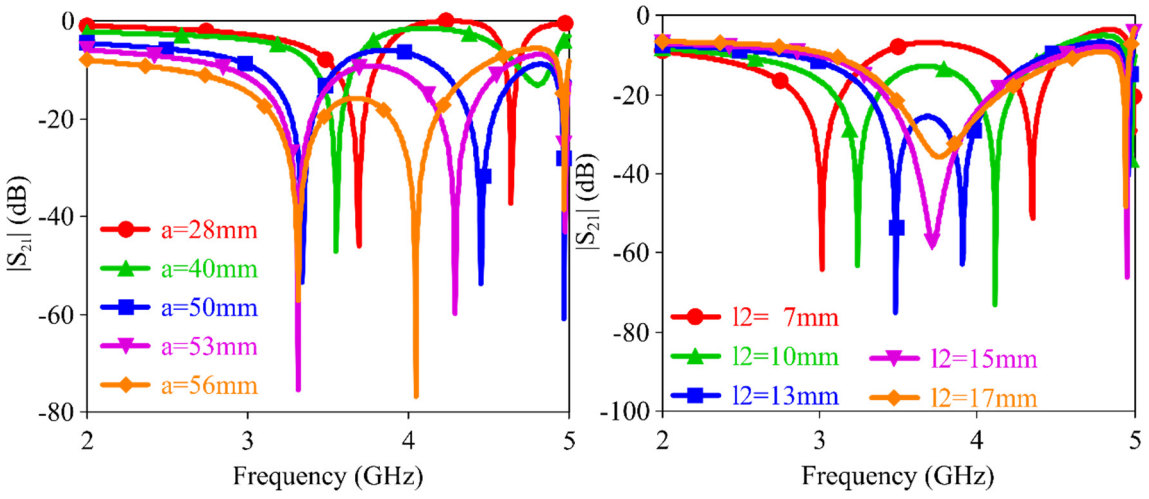

(a) (b)

Figure 4.19: Transmission performances of the FSSs with different radii and lengths when illuminated by normal incident waves.

(a) $|S_{21}|$ result with different a,. (b) $|S_{21}|$ result with different l_2.

The square cylinder resonators (a = 28 mm) produce a band-stop centered at approximately 3.7 GHz with a bandwidth of approximately 6.25%. Flaring the end of the resonator to a horn-like shape significantly broadens the band-stop to more than 57% (for greater than 10 dB transmission loss). A comparison of the resulting frequency responses is given in Figure 4.20(a). This horn-like feature also has the advantage of lowering the sensitivity of the FSS frequency response with respect to the incidence angle of the propagating wave. To investigate the oblique incidence performance, an analysis has been carried out for different incident angles θ, where θ is defined with respect to the normal of surface of the FSS. The wideband transmission behavior seen in Figure 4.20(b) is very stable under oblique TM incidence angles from 0 to 80 degrees. Also, the transmission bandwidth of the FSS increases from 57% to 61% when the angle of incidence is varied from the normal to θ = 80°. Table 4.18 contains the complete bandwidth analysis of the FSS. The extra degrees of freedom in 3-D FSS design have led to a horn-shaped unit cell geometry that enables a very wide band-stop and impressive angular tolerance.

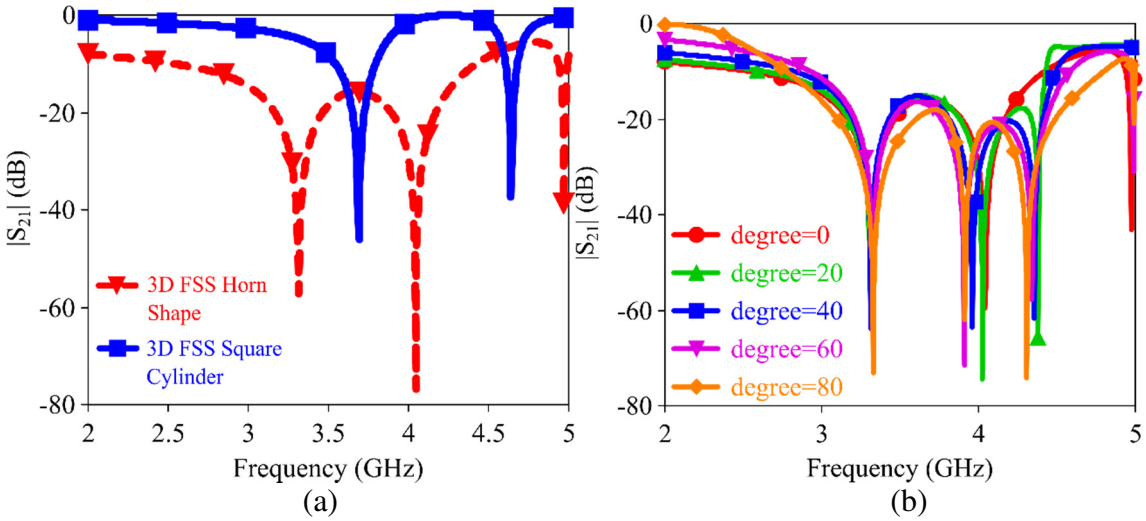

Figure 4.20: (a) Comparison $|S_{21}|$ result between the 3-D FSSs with horn-shaped and square cylinder resonators, (b) Transmission performances of the FSS when irradiated by waves of different TM incident angles

Table 4.4: Oblique Incident Bandwidth Analysis

Degree (°)	f_{lower} **(GHz)**	f_{upper} **(GHz)**	**Bandwidth (%)**
0	2.5	4.5	57
20	2.5	4.5	57
40	2.5	4.6	59
60	2.6	4.8	59
80	2.6	4.9	61

4.6 Summary

A symmetrical 3-D FSS with a resonant frequency independent of incident angle and polarization was presented in this chapter. The 3-D tapered FSS is shown to have significantly improved frequency stability characteristics as the incident angle is steered from normal to 80°. Traditional FSS design techniques using multiple layers or additional dielectric layers to achieve enhanced angular responses (for example, Jerusalem Cross), offer stable resonant frequency with respect to the incidence angle of both TE and TM incident plane waves up to 50 degrees with only ±1% deviation [67, 68]. The 3-D Tapered FSS is shown to have significantly improved resonant frequency stability characteristics from 0 to 80° for both TE and TM incidence.

The effect of key structural parameters on the transmission performance was examined. It was found that the combination of the upper square and lower square opening dimensions of the 3-D unit cell resonator have a great influence on the structures frequency selective angular performance. Parametric analysis of the tapered structure (formed by changing the *b* dimension) enables a stable cavity resonance to be matched at a single frequency for both TE and TM incident angles. The 3-D Tapered FSS was shown via electromagnetic simulation to have a maximum frequency deviation of 0.4% for angles up to 80 degrees from normal incidence. The validity of the proposed 3-D Tapered FSS concept was experimentally demonstrated by fabricating a prototype 6 x 6 element FSS using 3-D printing technology and testing its frequency response using free space measurements. The measurement results correspond very well with the simulation results and demonstrate that the 3-D Tapered FSS structure can achieve frequency performance independent of incident angle.

A 3-D wideband FSS which uses a horn-shaped resonator element has also been presented and discussed. The optimized results show that bandwidth properties of the FSS can be strongly enhanced by enlarging the aperture *a* and reducing the length of l_2. The response has also been shown to be stable under oblique incidence angles of up to 80^o. A 93% improvement of the bandwidth was observed while the angular stability of the frequency response was nearly unchanged.

CHAPTER 5

Frequency Selective Surface with Miniaturized Unit Cell

5.1 Introduction

Recently, many approaches have been proposed to obtain FSS unit cell dimensions much smaller than a wavelength. New geometries such as convoluted ring slots, fractals, multipoles, and patches or their complementary structures have been proposed, where the size of unit cell has been shrunk to around $0.16\lambda_0$ [114, 115]. A miniaturized FSS has been proposed comprising of a periodic array of a dual-concentric square element with reduced size slots printed on one side of a dielectric substrate, and an inductive grid printed on the other side [116]. The combination of the capacitance of the patch array and inductance of the wire mesh results in a parallel *LC* combination, which acts as a first-order band-pass filter at the resonant frequency of the structure. Similarly, a complimentary design can be created to selectively absorb narrow band-pass regions. Another effective way to diminish the size of an FSS unit cell is by integrating a suitable lumped capacitor within two slots, introducing a capacitive gap between two ends of the resonators. The unit cell size diminishes to $0.06\ \lambda_0$ x $0.22\ \lambda_0$ in this case [87]. Specific applications of these types of FSS filters include narrowband astronomy filters, and filters for spacecraft instrumentation.

As a driver for creating a miniature wire resonator FSS, following research question are addressed:

- What are the key performance advantages of creating miniature FSS?
- How can the transmission through a subwavelength aperture be enhanced with the use of a miniature wire resonator?

This chapter presents a novel miniaturized resonator element which can be applied to frequency-selective surfaces, and also as an alternative solution to enhance transmission through a subwavelength aperture. Miniaturization of the FSS unit cell is achieved by coupling two meandered wire resonators separated by single thin substrate layer. The capacitance due to the small separation between the meandered wire elements results in a lowering of the resonant frequency. To demonstrate the validity of the design, the meandered wire resonator FSS was fabricated and tested using a free space measurement facility.

5.2 Angularly Stable Frequency Selective Surface with Miniaturized Unit Cell

In some applications, a low sensitivity with respect to the incidence angle of the incoming wave is required, or in cases where a uniform phase front is difficult to establish, the overall FSS size needs to be small. In such applications with limited space, the concept of miniaturized element FSSs has been proposed using sub-wavelength resonant elements instead of much larger traditional elements [9]. These miniaturized element FSSs can achieve large element numbers in a limited space to act more like an infinite FSS. Therefore miniature FSSs yield less distortion of elements and more consistent performance for FSS structures with significant curvature, such as radomes.

In this chapter a miniature wire resonator has been presented, with application to FSSs and enhanced subwavelength transmission. Common approaches of resonator miniaturisation include integrating lumped capacitors between two slots, consequently introducing a capacitive gap between two ends of the resonator. The unit cell size can be diminished to 0.06 λ_0 × 0.22 λ_0 in this case [92], however an large number of lumped capacitors are required to realise the FSS, increasing cost and complexity. A miniature FSS with angular stability has been demonstrated in this chapter which consists of a printed micro-wire frequency selective unit cell structure that realizes a 0.067 x 0.067λ_0 resonance. The miniaturization of the unit cell reduced the sensitivity of the FSS to variation in incidence angles. This section describes a printed micro-wire frequency selective unit cell structure that realizes a 0.067 x 0.067 λ_0 resonator and produces a stable angular response up to 80^O for TE and TM incidences.

5.2.1 Design Procedure

The micro-wire resonator was inspired by miniaturized 3-D dipole antennas structures constructed on a large conducting ground plane [117]. In [117], a cube was chosen to realise one half of a center fed, symmetrical dipole, mapped to 27 (3 × 3 × 3) grid points. This structure uses a meander line technique where the meander path was found by numerical optimisation, and is illustrated in Figure 5.1.

An analogous printed wire resonator structure in free space was devised and optimized for application as an FSS element shown in Figure 5.2 (a). The micro-wire structure resembles a 2-layer compressed version of the 3D dipoles without vertical interconnecting conducting elements. The increased capacitance between the micro-wire elements due to the small separation results in a lowering of the resonant frequency.

Figure 5.2 shows the geometry of the micro-wire resonator, consisting of meandering printed wires separated by a single substrate layer. The printed wires are chemically etched on the upper and lower surfaces of a 0.127 mm thick Rogers RT/duroid 5880 substrate with a dielectric constant of 2.2 and a loss tangent of 0.0009. The unit cell design parameters are also indicated in Figure 5.2, including the wire trace width w = 0.75 mm, the maximum wire strip length d = 6.0 mm, the substrate thickness t_d = 0.127 mm, and the periodic separation, s = 6.3 mm.

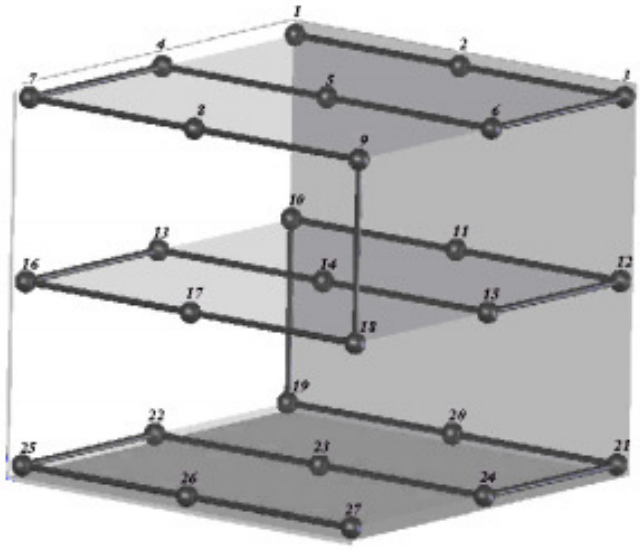

Figure 5.1: An example of cubic meander line [117].

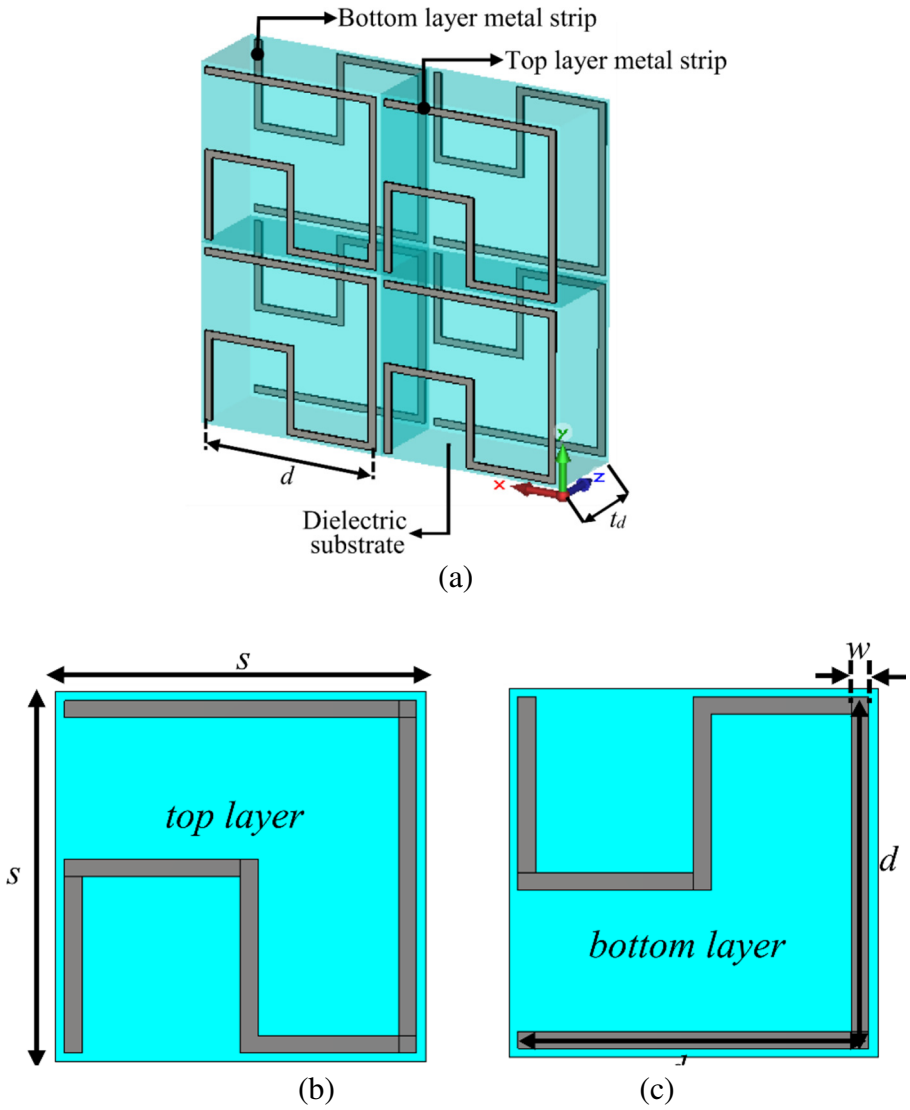

Figure 5.2: Geometry of the proposed micro-wire FSS: (a) 2 x 2 unit cell structure, (b) upper printed layer, and (c) lower printed layer. :- dimensions: s=6.3mm, d=6.0mm, t_d=0.127mm, w=0.75 mm.

Numerical analysis of the micro-wire FSS was performed using CST Microwave Studio using unit cell boundary conditions to provide periodicity along x and y directions. The FSS is excited by an electromagnetic wave with the propagation vector (k) in the z direction, electric field vector (E) in the y direction, and magnetic field intensity vector (H) in the x direction. It is known that thin metallic strips supporting axial electric current excited by an incident wave generate an inductive response, where the total inductance produced depends on the wire width and length.

The equivalent circuit model of the micro-wire resonator is shown in Figure 5.3(a), and is used to analyze the structure. The equivalent circuit is generated by placing Port 1 between the two open ends of the micro-wire on the bottom and top layer of the substrate, whilst Port 2 is placed across the opposing open ends. The lengths of conductor with no opposing conductor on other side of the substrate contribute to equivalent inductances L_1. The capacitances C_1 result from the sections of the unit cell that have broadside coupled conductors on opposing sides of the substrate. From a physical standpoint, a weaker capacitive content (which has been neglected) also arises in the wire resonators due to the edge coupled conductor arms running parallel to the surrounding unit cells when the FSS array is constructed.

The wire resonator inductive responses (L) can be calculated using following equation [118]:

$$L = 0.002 \times l\left[ln\left(\frac{4.0 \times l}{d}\right) - 1 + \frac{d}{2.0 \times l} + \frac{\mu_r T(x)}{4.0}\right](\mu H)$$

$$T(x) \approx \sqrt{\frac{0.873011 + 0.00186128x}{1.0 - 0.278381x + 0.127964x^2}}$$

$$x = 2.0\pi r\sqrt{\frac{2.0\mu f}{\sigma}}$$

Where: d is diameter (cm) of wire (w), l is the length (cm), f is frequency in GHz, r is d/2 (cm), μ is absolute magnetic permeability of conductor,

$$(\mu) = \mu_o \times \mu_r$$

While capacitance (C) value is calculated using the equation for capacitance between two parallel plates:

$$C = k\varepsilon_o \frac{A}{d}$$

Where: k is dielectric constant of the material, A is the overlapping surface area of the plates, d is the distance between the plates, and $\varepsilon_o = 8.854 \times 10^{-12}$.

Using this theoretical calculation, the *L* and *C* parameters for the FSS have the values L_1 = 1.27 nH, and C_1 = 0.33 pF. In order to further validate the *LC* model, the transmission characteristics of the micro-wire resonator with the unit cell of Figure 5.2 have been simulated in CST Microwave Studio and compared to the *LC* model prediction. The transmission coefficient of the equivalent circuit model is plotted in Figure 5.3(b) which agrees well with the simulations. A band-stop center frequency of 3.33 GHz is obtained and the band-stop transmission coefficient less than -10 dB from 3.25 GHz to 3.38 GHz (a bandwidth of ~ 4%). The micro-wire resonator exhibits a superior miniaturization factor and is capable of generating resonance at 0.067 x 0.067 λ_0.

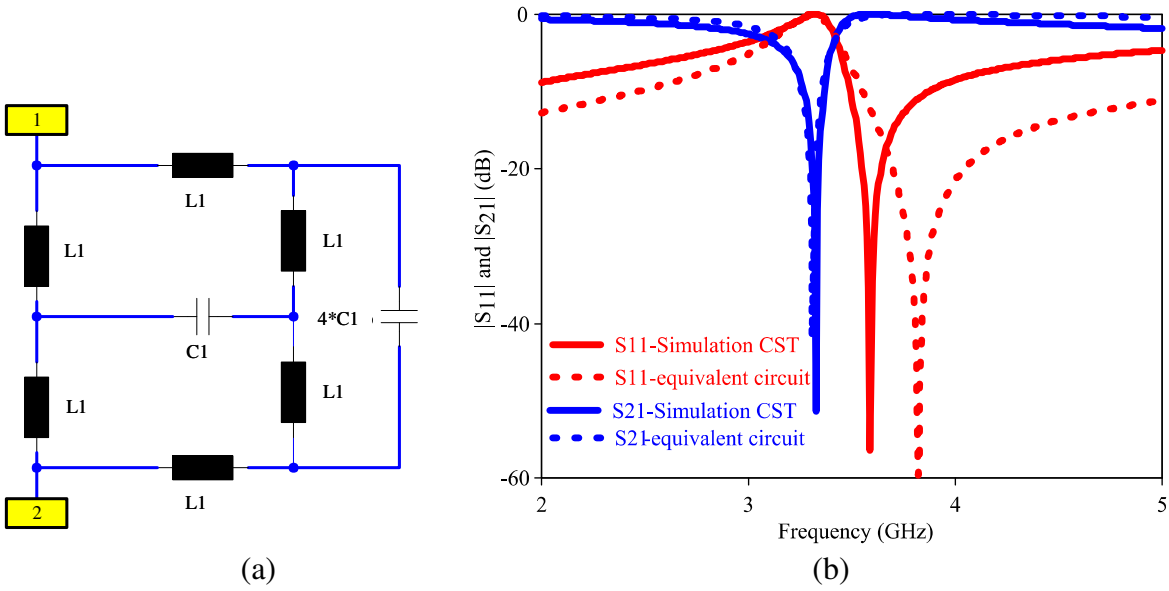

(a) (b)

Figure 5.3: (a) Equivalent circuit model, (b) Transmission and reflection properties of the micro-wire resonator FSS.

Miniaturization of the unit cell reduces the sensitivity towards incidence angles by stabilize the transfer characteristic of the FSS. To demonstrate the resonant stability performance of the FSS, the angular response is shown in Figure 5.4. The FSS has extremely stable resonance with respect to incidence angles up to 80 degrees for both TE and TM incidence, maintaining a band-stop transmission coefficient below -10 dB. The resonant frequency stability performance still holds for incident angles larger than 80 degrees, however transmission rises above -10 dB for TM incidence. Band-stop bandwidth broadens for elevated TE incidence angle, but narrows for TM incidence.

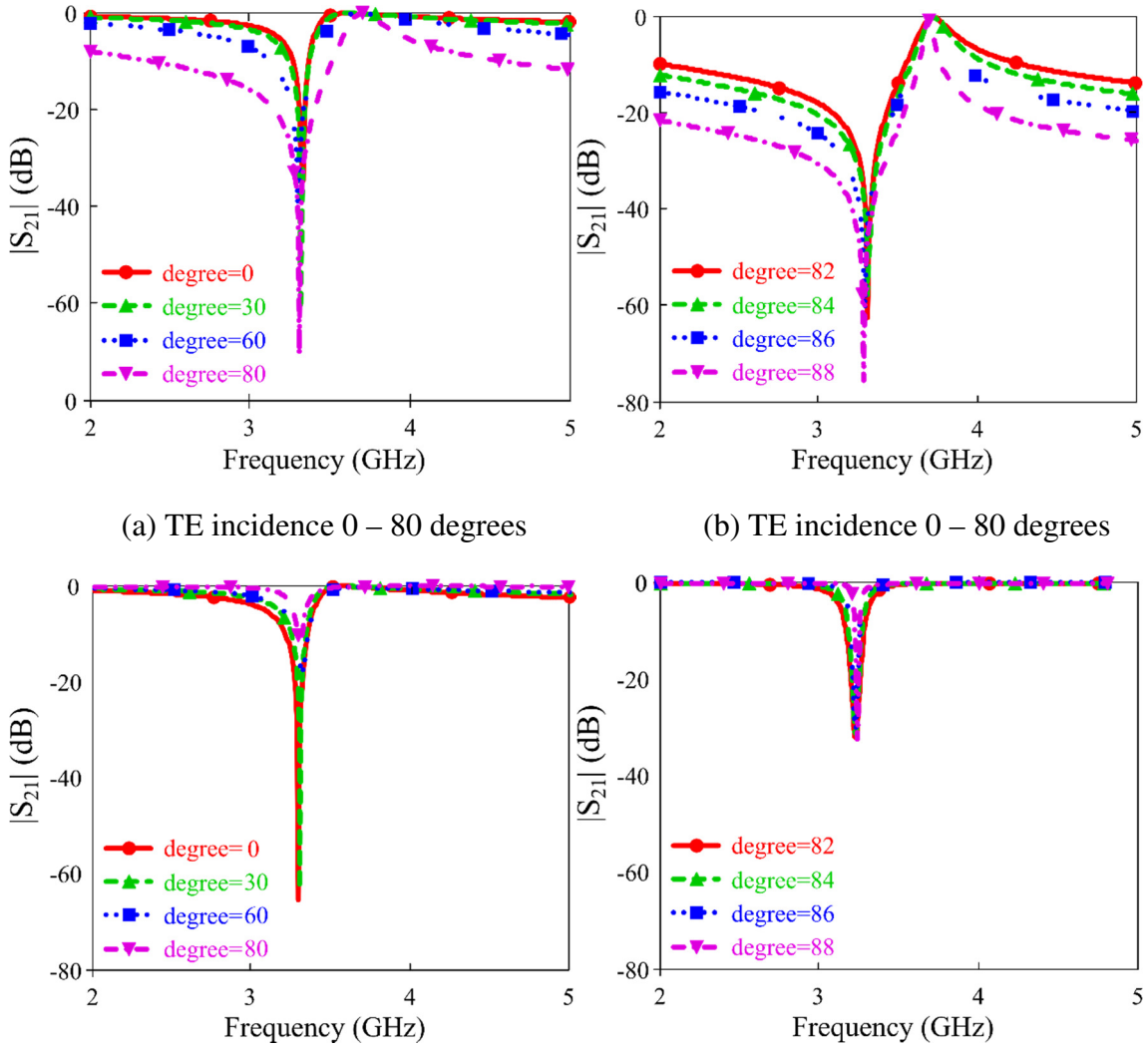

(a) TE incidence 0 – 80 degrees

(b) TE incidence 0 – 80 degrees

(c) TM incidence 0 – 80 degrees

(d) TM incidence 82 – 88 degrees

Figure 5.4: Transmission coefficients results of micro-wire resonator FSS as a function of incident angle for TE and TM incidence from 0 to 88°.

5.2.2 Parametric study

i) Substrate thickness, t_d

A parametric analysis of the center frequency of the band-stop versus the substrate thickness is also studied. The studies indicate that the substrate thickness can strongly influence the band-stop centre frequency, reducing it significantly for thinner substrates. Figure 5.5 shows the center frequency of the band-stop at different thickness of the substrate. As substrate's thickness t_d is decreased from 0.2 mm to 0.02 mm, the resonant frequency of the FSS decreases from 3.8 GHz to 1.5 GHz. A second observation is that the band-stop depth also decreases with decreasing substrate thickness.

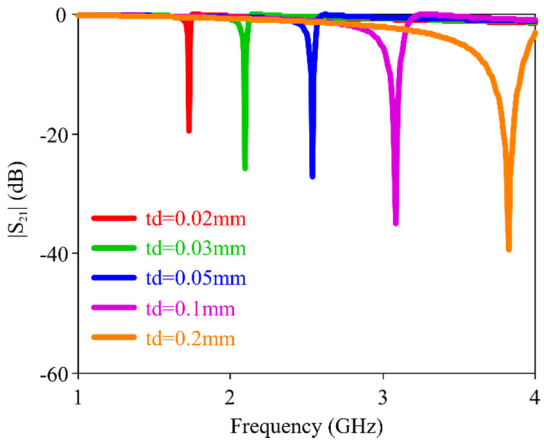

Figure 5.5: Result of wire resonator as difference thickness of substrate is varied.

ii) Resonator line width, w_t

The effect of the variable line width of the wire resonator on resonance frequency, f_r and bandwidth is shown in Figure 5.6. As the printed wire width *wt* increases from 0.2 to 0.8 mm, the bandwidth narrows and the resonant frequency decreases monotonically, leading to a much smaller size. For instance, when w_t = 0.2 mm, the -10 dB band-stop is from 3.48 GHz to 3.66 GHz, with a centre frequency of 3.59 GHz. Therefore the relative bandwidth is 5%, with a resonator size of $0.07\lambda_0$. When the line width increases to *wt* = 0.8 mm, the band-stop if from 3.0 GHz to 3.14 GHz, with the center frequency 3.07 GHz. The relative bandwidth decreases to 4.5%, and dimension of the resonator is even smaller at only $0.06\lambda_0$. However, the only drawback is that the band-stop depth is weaker as the line width is increased. These results are also validated against the equivalent circuit model, with very good agreement.

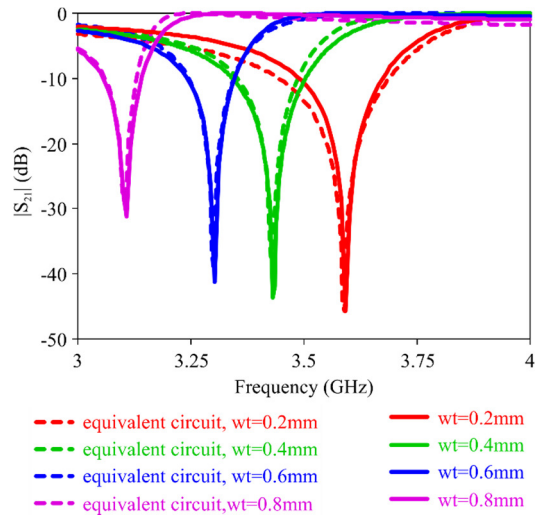

Figure 5.6: $|S_{21}|$ results for different line width compared with equivalent circuit calculation.

iii) Extraction of bulk permeability and permittivity properties

Each wire structure resonates with a dimension much smaller than the wavelength and hence bulk permeability and permittivity properties can be extracted, and may be suitable to construct artificial materials. Figure 5.6 shows a comparison of the real part of the material properties (Eps = ε, Mu = μ) between 4, 8 and 16 layer resonators with the same cell size of 6.3 mm. The 4, 8 and 16 layer resonators have a strong electric resonance. A negative permittivity and negative permeability response appear around the frequency of 2.3 GHz, 1.95 GHz, and 1.68 GHz for 4, 8 and 16 layers respectively as shown in Figure 5.6. This negative refractive index is achieved with a single uniform unit cell structure, as compared to the binary unit cells used in [106]. The electromagnetic properties of the resonator can be controlled conveniently by changing its size and the substrate properties [119, 120].

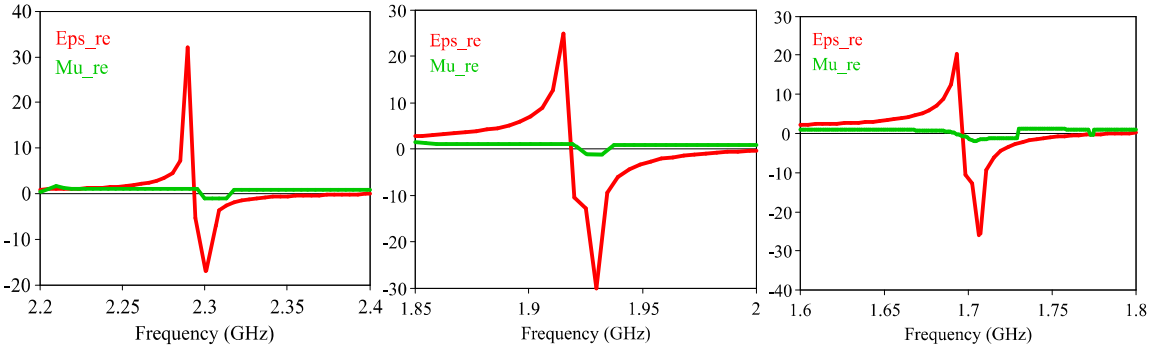

(a) (b) (c)

Figure 5.7: Extracted Permittivity and permeability of: (a) 4 layers, (b) 8 layers, (c) 16 layers.

iv) Wire resonator FSSs with 4, 8 and 16 layers

The miniaturization of the microwire resonator FSS unit cell can be futher reduced by stacking extra meander wire layers on the original structure, as shown in Figure 5.7. Simulation results of wire resonators with 4, 8 and 16 layers when illuminated by at a range of incident angles are shown in Figure 5.8. The wire resonators with 4, 8 and 16 layers simulated at oblique incidence have demonstrated high stability of their response over a broad range of incidence angles. It is observed that the resonance frequencies at normal and up to 80° incidence are practically indistinguishable. Even for oblique waves of 80° incident angle for 4 layers FSS, the band-stop only changes from 2.3 GHz to 2.33GHz, a 1.3% deviation. The angular response in even better as more layers is added, where only 0.8% and 0.68% deviation for 8 and 16 layers respectively.

Strong capacitive coupling between the metallic strips at different layers are introduced in such resonators to significantly reduce the resonator size. As more layers are added, the structures become more angularly stable while the bandwidth decreases. The size reduces from $0.067\lambda_0$ at 2 layers, to $0.046\lambda_0$, $0.039\lambda_0$, and $0.033\lambda_0$ for 4, 8 and 16 layers respectively. The characteristics of the micro-wire resonator arrays at normal and oblique incidence are summarized in Table 5.1.

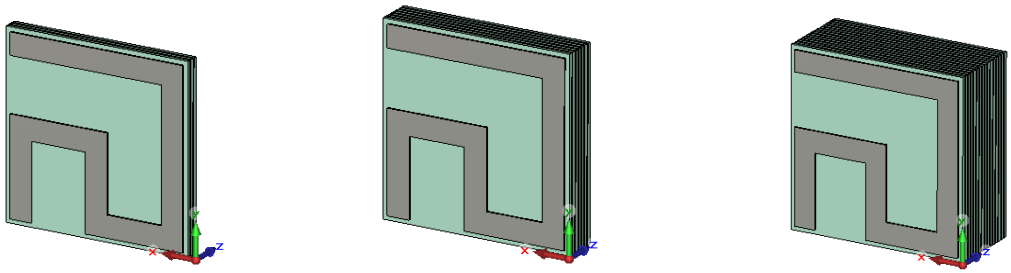

(a) (b) (c)

Figure 5.8: Multilayer wire Resonator. (a) 4 layers, (b) 8 layers, (c) 16 layers.

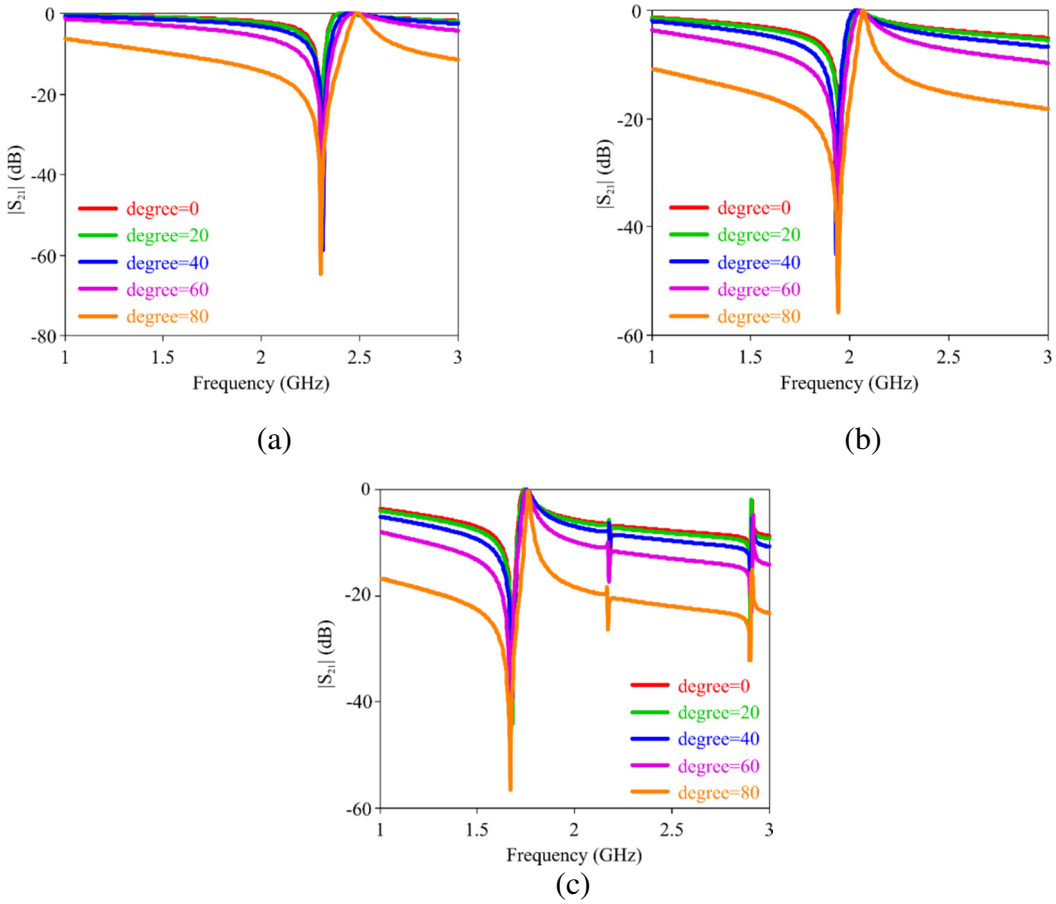

(a) (b)

(c)

Figure 5.9: $|S_{21}|$ result of multilayer wire resonator with different angles. (a) 4 layers, (b) 8 layers, (c) 16 layers.

Table 5.1: Data of the wire resonator arrays at normal and oblique incidence.

Layers	Center Frequency, f_c	Bandwidth (%)	Size ($\lambda_{0)}$
2	3.33	3.9	0.067
4	2.30	3.4	0.046
8	1.95	3.2	0.039
16	1.68	2.9	0.033

5.2.3 Experimental validation

The micro-wire resonators as shown in Figure 5.2 were fabricated on a Rogers RT/duroid 5880 substrate with relative dielectric constant of 2.2, loss tangent of 0.0009 and thickness of 0.127 mm. The fabricated FSS contained 30 x 30 elements on each side of the substrate, and is shown in Figure 5.10. Measurement is performed using two horn antennas in a free space measurement setup. The distance from transmitting to receiving antenna is 1 meters, with the FSS located centrally between the two. The measurement setup is calibrated using a through transmission coefficient (with isolation) where metal diffraction plate the same size as the prototype FSS is used. The micro-wire FSS is placed in exactly the same place as the metal plate used during the calibration and the transmission coefficient was measured.

Figure 5.11 displays a comparison of the measured and simulated frequency selective characteristics of the micro-wire FSS. The measured central frequency of the band stop response is located at 3.3 GHz, in good agreement with the simulation. However, the measured transmission band-stop has a broader response, and is significantly shallower (-18.8 dB as compared to -51.3 dB) than was predicted by the simulation. This is primarily due to the fabricated sample being of finite size (approximately 2 x 2 wavelengths at 3.3 GHz) compared to the infinite simulation, as well as minor fabrication tolerances and flatness variations.

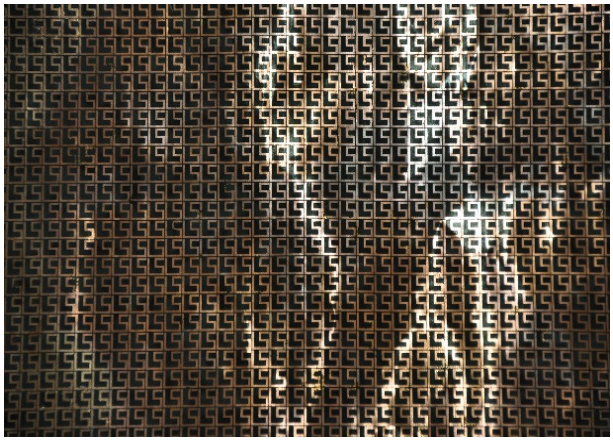

Figure 5.10: Photograph of the fabricated micro-wire resonator FSS.

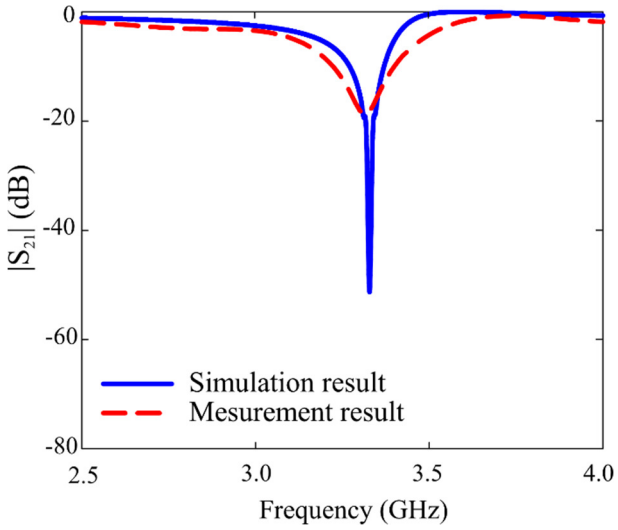

Figure 5.11: Comparison of measured and simulation $|S_{21}|$ results for the micro-wire resonator FSS.

Figure 5.11 shows the measured vs simulated transmission coefficients of the micro-wire FSS prototype for TE and TM incident angle variation. The measured central frequencies and band edges have reasonable congruence with the simulated results. Table 5.2 and Table 5.3 present the detailed data of measurement and simulation results. Notably, a central frequency variation of less than 2% is observed for both TE and TM incidence up to 80 degrees off normal.

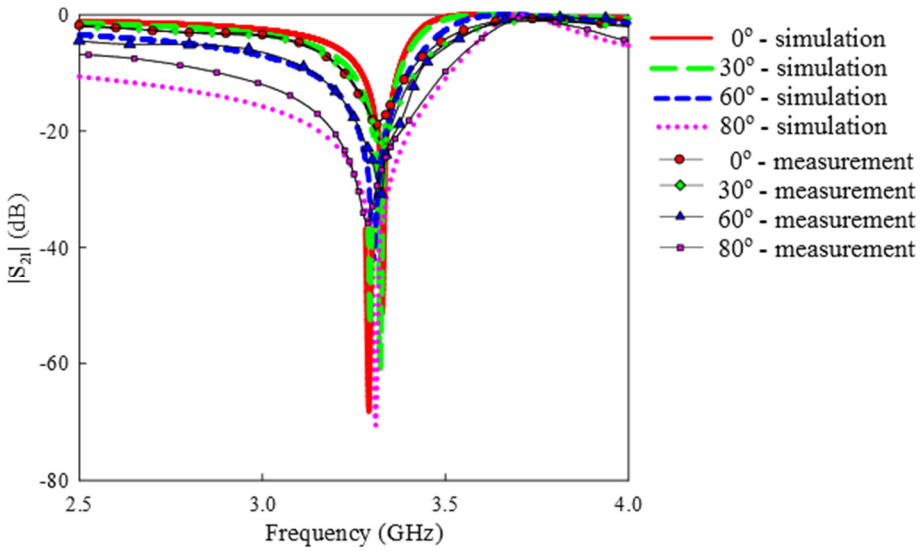

(a) TE Incidence

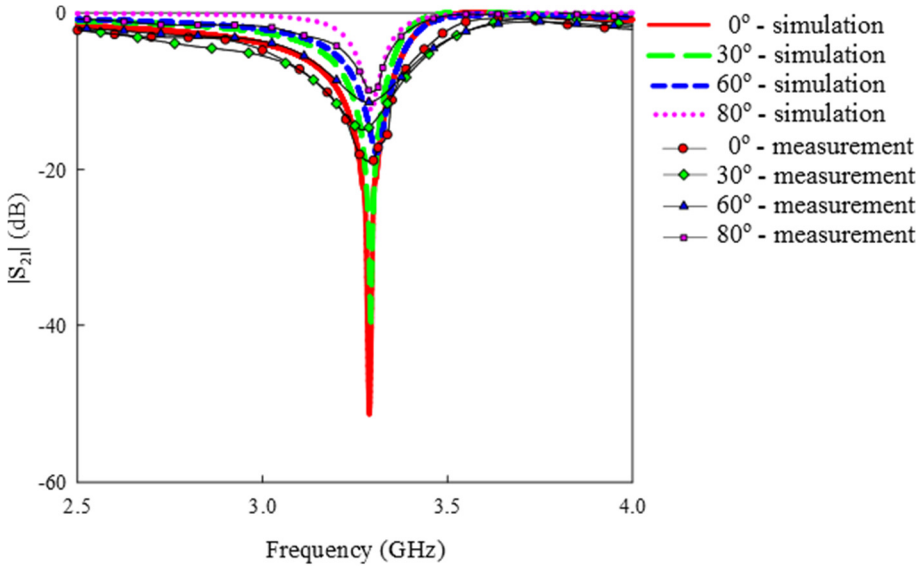

(b) TM Incidence

Figure 5.12: Measured vs simulated transmission coefficients of the micro-wire resonator FSS as a function of incident angle. (a) TE Incidence, (b) TM Incidence.

Table 5.2: Simulation and measurement data for TE incident angles.

Degree	Simulation			Measurement		
	Frequency (GHz)	$\|S_{21}\|$ (dB)	Frequency deviation (%)	Frequency (GHz)	$\|S_{21}\|$ (dB)	Frequency deviation (%)
0	3.33	-51.33	0.00	3.31	-18.84	0.00
30	3.32	-61.25	0.30	3.30	-21.98	0.30
60	3.31	-41.97	0.60	3.28	-30.76	0.91
80	3.31	-70.56	0.60	3.27	-35.85	1.20
82	3.31	-62.66	0.60			
84	3.30	-57.67	0.90			
86	3.29	-60.57	1.20			
88	3.28	-75.71	1.50			

Table 5.3: Simulation and measurement data for TM incident angles.

Degree	Simulation			Measurement		
	Frequency (GHz)	$\|S_{21}\|$ (dB)	Frequency deviation (%)	Frequency (GHz)	$\|S_{21}\|$ (dB)	Frequency deviation (%)
0	3.33	-51.33	0.00	3.31	-18.84	0.00
30	3.32	-40.33	0.30	3.30	-14.64	0.30
60	3.31	-17.88	0.60	3.27	-11.41	1.21
80	3.29	-12.18	1.20	3.25	-9.90	1.81
82	3.28	-4.00	1.50			
84	3.27	-3.92	1.80			
86	3.25	-3.90	2.40			
88	3.24	-3.80	2.70			

5.3 Miniature Wire Resonator with Enhanced Transmission using sub wavelength aperture

The micro-wire resonator is proposed as an alternative solution to enhance electromagnetic transmission through a sub-wavelength aperture. Inserting a miniaturized metal resonator structure in a sub-wavelength aperture couples electromagnetic energy through to the other side of the aperture plane, enhancing the transmission efficiency. Figure 5.12 illustrates how the resonators are incorporated within the aperture. The wire resonators are placed in plane with the aperture on a large metal surface with a unit cell dimension of 26.24 mm × 26.24 mm. The sub-wavelength aperture is 4.65 mm × 4.65 mm with resonator maximum dimension d = 3.61 mm, wire diameter, wt = 0.45 mm. The thickness of the substrate, t_s = 25 µm and deposited copper thickness, h = 18 µm.

The simulated transmission results of a sub-wavelength aperture with 2, 3 and 4 layers of wire resonators are plotted in Figure 5.14. The simulation shows a band pass characteristic with high selectivity and low insertion loss, essentially reaching 0 dB (100% transmission). As the number of layers are increased, the resonance shifted to lower frequency, reaching 2.3 GHz ($0.028\lambda_0$), 1.9 GHz ($0.023\lambda_0$) and 1.75 GHz ($0.021\lambda_0$) for 2, 3 and 4 layers respectively. These results provide further support for the hypothesis that by utilizing deep sub-wavelength resonators, complete transmission can be achieved from the array of subwavelength apertures.

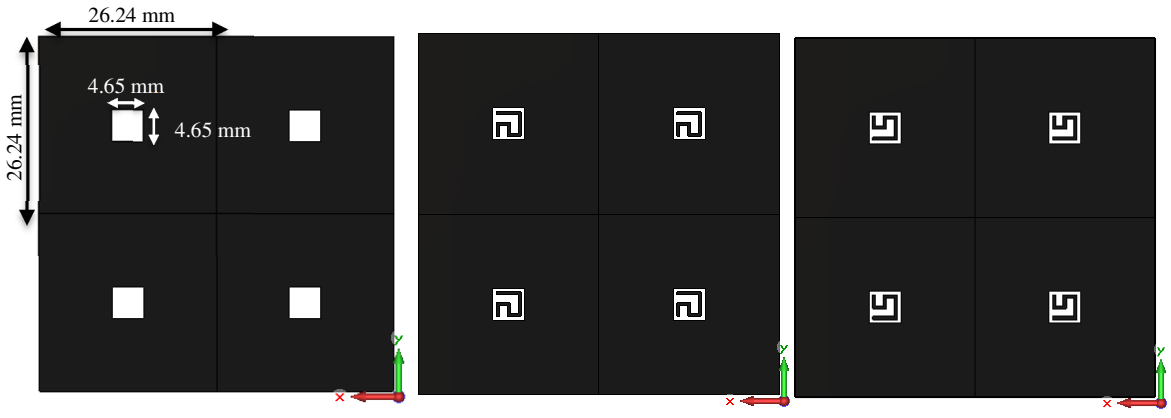

(a) (b) (c)

Figure 5.13: Proposed miniaturized wire resonator in a subwavelength aperture. (a) square hole array only, (b) wire resonator inserted (front view), (c) wire resonator inserted (rear view).

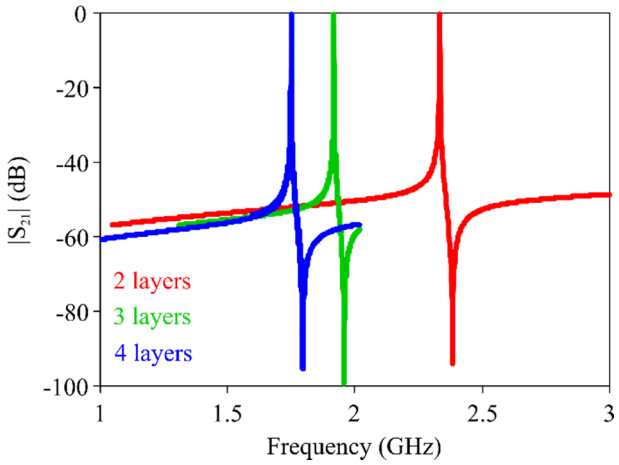

Figure 5.14: Simulated transmission response of the design as in arrays with 2, 3 and 4 layers.

5.3.1 Experimental Validation

To validate the characteristics of the proposed subwavelength aperture, prototypes were fabricated on two sides of an Ultralam 3850 substrate with $\varepsilon_r = 2.9$. The total dimension of the proposed design is 109.22 mm x 54.61 mm which equates to the size of a waveguide flange for WR-430. The behavior of the planar resonators was tested as single element in a WR-430 waveguide. This measurement method is chosen as a very large prototype panel is required using free space measurement techniques due to the low frequency, and inadequate laboratory space was available. In practice FSSs have finite dimensions, and in order to observe the desired frequency response the finite surface must include a large number of constituting elements. Therefore, an alternative waveguide measurement technique was chosen to test it as single elements resonator. A single element of the miniaturized wire resonators as shown in Figure 5.15 was designed for this purpose. Detailed explanation regarding waveguide transmission/reflection measurement setup that was used in this measurement is available in [121].

The simulated and measured transmission response of the miniaturized wire resonator is presented in Figure 5.16. A blank aperture (without a resonator) is also measured for comparison which essentially exhibits no transmission. However once the miniaturized wire resonator is added into the aperture, a sharp resonance at approximately 1.94 GHz appears. A relatively good agreement exists between the measured results and the results obtained from the CST EM simulations. The fabricated FSS demonstrates a 0.43 dB measured loss

at the center frequency of operation at 1.94 GHz ($0.023\lambda_0$), and only 0.05% shifted from simulation result. The measurement of transmission at resonance is problematic due the very high quality factor. A large number of frequency points (168 points) were required over a very narrow band (1.939 to 1.943 GHz) in order to record the transmission peak. Even given this small frequency step, it is possible that the peak is actually closer to 100% transmission than what has been experimentally observed. The resonators were detuned primarily due to fabrication tolerances; consequently the centre frequency is slightly shifted from the simulation. Frequencies away from resonance are effectively blocked, with transmission down around -40 dB. Nevertheless, these results confirm that the addition of miniaturized wire resonator can achieve close to 100% transmission through a subwavelength ($0.023\lambda_0$) aperture.

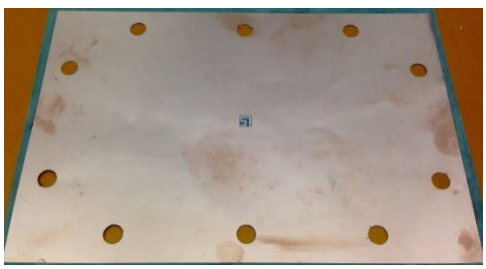

(a)

(b)

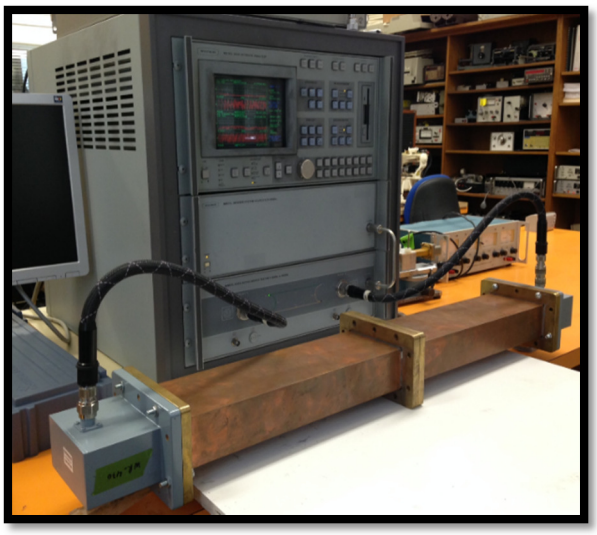

(c)

Figure 5.15: Photograph of miniaturized wire resonator with measurement setup. (a) front side, (b) rear side, (c) WR-430 Waveguide measurement setup.

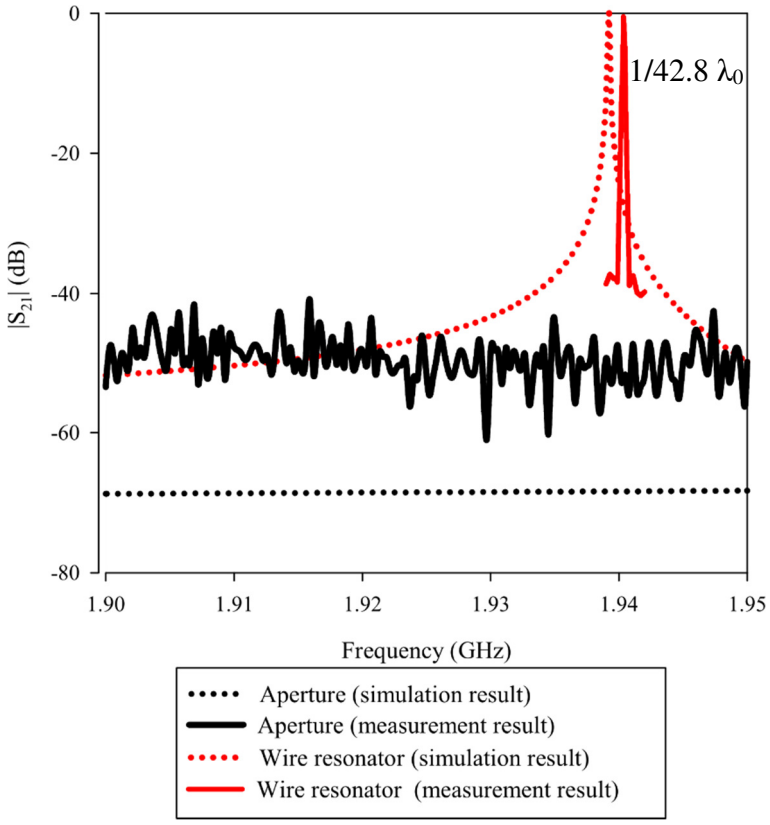

Figure 5.16: Comparison measured and simulated transmission coefficients of a fabricated prototype of the proposed miniature wire resonator as in single element measured in WR-430 waveguide.

5.3.2 Complementary Design

A complementary version of the miniaturized wire resonator cut into metallic sheets on either of an Ultralam 3850 substrate with similar dimensions to Figure 5.12 can also exhibit subwavelength transmission. Figure 5.16 shows the layout of a proposed design and the simulations results with different numbers of layers. The advantage of the complementary design is a smaller size is achieved due to an external aperture wall not being required. The resonant frequency of the complimentary structure (seen in Figure 5.16(a) and (b)) is 9% lower than the design shown in Figure 5.12. The complementary design shows a band-pass characteristic with high selectivity and it is further minaturized as more layers are added. As the number of layers is increased the frequency shifted to lower, from 2.1 GHz (0.025λ0), to 1.85 GHz (0.022λ0) and 1.72 GHz (0.02λ0) for 2, 3 and 4 layers respectively.

The proposed complementary design is fabricated using an Ultralam 3850 substrate as a single element. A similar measurement was conducted as in the previous section, where

WR-430 waveguide is used. Since the planar resonators was tested as single element in a waveguide, the resonant frequency shifted to lower frequency (1.92 GHz) compared to the 2 layer proposed design that was simulated as infinite array (2.1 GHz).

The fabricated resonator is shown in Figure 5.18, and the measured and simulated results are shown in Figure 5.19. The measured transmission loss of 0.5 dB is marginally higher than the simulated value of 0.3 dB. As before, the observed value from finite resolution measurement may not be the actual value of the transmission loss due to the high quality factor resonance. The proposed complementary resonator exhibits a narrow band filter response operating at 1.92 GHz with a fractional bandwidth of 0.04%. Once again, frequencies away from resonance are effectively blocked, with transmission down around -40 dB. The very minor frequency discrepancy between measured and simulated results is attributed to the fabrication tolerances.

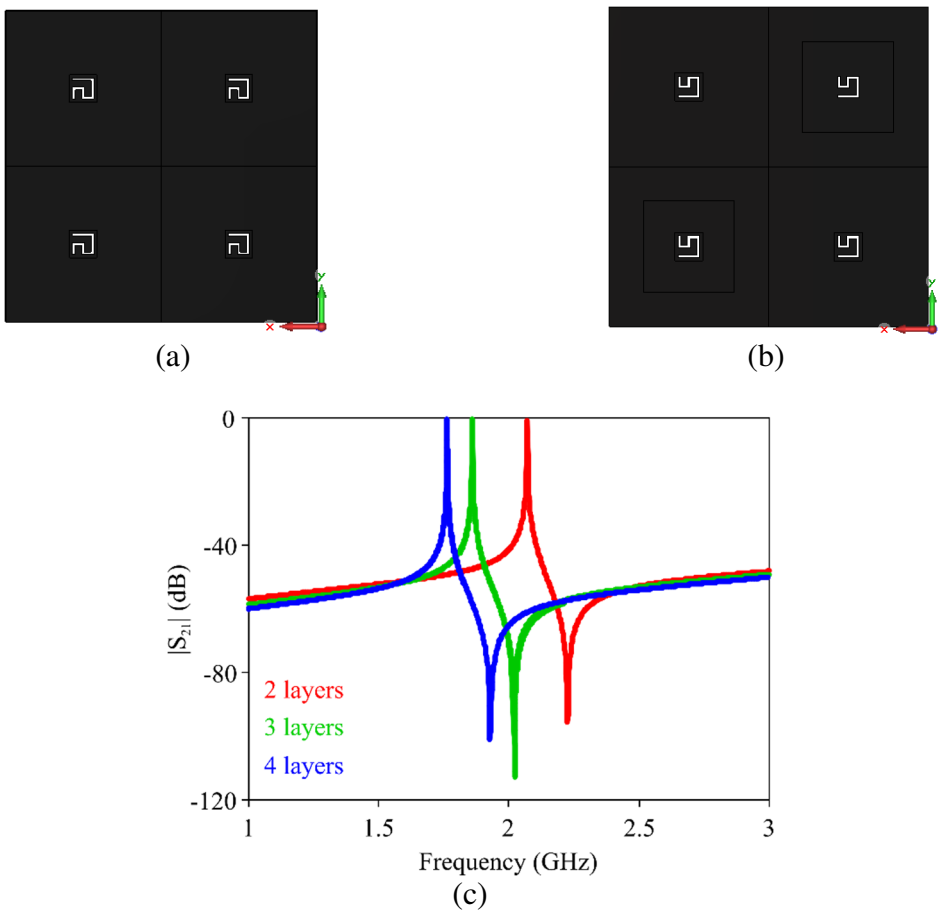

Figure 5.17: Proposed miniaturized complementary subwavelength aperture. (a) front view (b) rear view (c) Simulated transmission response with 2, 3 and 4 layers.

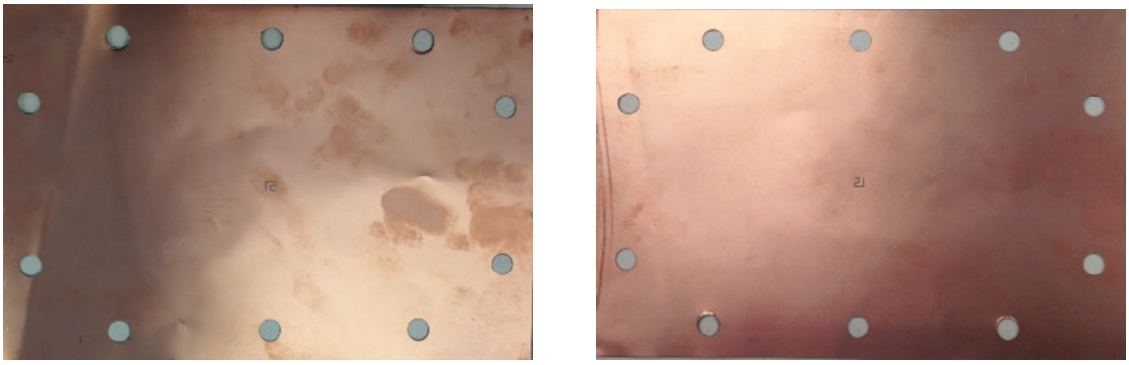

(a) (b)

Figure 5.18: Photograph of the single element miniaturized complementary subwavelength aperture. (a) front view, (b) rear view.

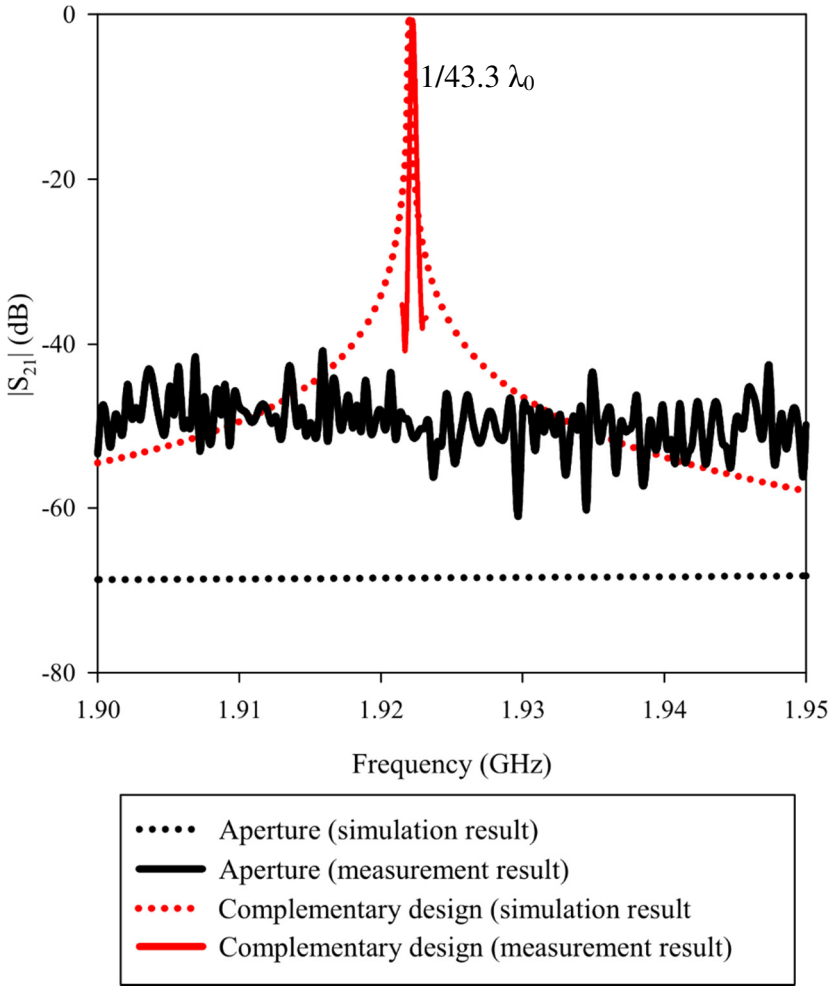

Figure 5.19: Comparison between the simulated and measured $|S_{21}|$ of the miniaturized complementary subwavelength aperture using WR-430 waveguide.

5.4 Summary

A miniature FSS with angular stability has been demonstrated in this chapter which consists of a printed micro-wire frequency selective unit cell structure that realizes a 0.067 x 0.067λ_0 resonance. The miniaturization of the unit cell reduced the sensitivity of the FSS to variation in incidence angles. The simulated results showed that the miniature FSS produced a stable angular response up to 80 degrees for TE and TM incidences. The micro-wire resonator FSS was fabricated on a Rogers RT/duroid 5880 substrate with a thickness of 0.127 mm and measured using free space measurement. A good agreement between theory, simulations, and measurement results was observed. In addition, experimental characterization of the fabricated prototype demonstrates a stable frequency response with central frequency variation of less than 2% for both TE and TM incidence up to 80 degrees off normal. The observed performance has a good agreement with the simulated results, which confirms the new FSS structure has excellent miniaturization performance.

Also presented is a method of obtaining essentially complete transmission through periodically arranged sub wavelength apertures by inserting micro-wire resonators. The micro-wire resonator approach has shown approximately 100% transmission at 1.94 GHz through an aperture that is 0.023 λ_0 square in size. The response of the micro-wire resonator in a subwavelength aperture is extremely high Q, presenting a -10 dB transmission bandwidth of 0.007%. A much smaller resonator can be achieved by using a complementary design of the wire resonator, and the resonant frequency shifted 9% lower than the previous design. It was demonstrated that the complimentary subwavelength apertures achieved excellent agreement between simulated and measured results, exhibiting transmission at 1.92 GHz with a fractional bandwidth of 0.04%.

CHAPTER 6

THESIS SUMMARY

6.1 Introduction

A summary of the developments in this area of research is provided in this chapter. Starting with Chapter 2 where it is presents a development history of the FSS, its applications and reviewing available design techniques. Chapter 3 discuss development of 3-D cylindrical FSSs unit element, followed by a new tuning technique using spring resonator. Chapter 4 focuses on examining techniques which can be used to stabilize the FSS angular response, which is 3-D Tapered FSS. Furthermore, a novel 3-D Frequency Selective Surface (FSS) with horn shaped resonators is also been studied in this chapter which exhibits a very wide stop band with stable angular response. Miniature FSS with high Q factor which enables significant reduction of the unit cell size was presented in Chapter 5. The mechanisms underlying the distinctive properties of the wire resonators were examined including formulations for the EC model and transmission passing through a sub wavelength aperture in planar.

6.2 Chapter 1,2

Background: The development history of the FSS and its common applications are addressed. As a foundation for the subsequent investigations presented in this thesis, the characteristic of FSS is examined.

Aim of the research: Objectives of this chapter include identifying the key factors, limitations which govern the FSS performance, reviewing available techniques for theoretical FSS analyses and conclude the review with a statement of hypothesis and research question that will be addressed in each technical chapter, Chapter 3, 4 and 5.

Methodology: Survey of important articles, journals article, conferences papers and text books were reviewed.

Results: A comprehensive study of the previous methods in design of frequency selective surface revealed that there are some problems and disadvantages of the current FSS. Nevertheless, 3-D FSS has demonstrated superior performance than current FSS. With this background, design of the new frequency selective surface was started with the goal of producing new microwave, Frequency Selective Surface for communication systems that can provide improved functionality and performance.

Future Work: This concludes the extent of the current research for this dissertation. However, there are several extensions possible for future research possibilities. While most of the work in this dissertation considers only planar FSS were considered here, non-planar, three dimensional periodic structures can be constructed. Also, the work presented here considered FSSs illuminated with only a plane wave which is TE and TM incidence wave. Another extension of this research could include studying the effect of varying in the degree of illumination coherence.

Original Contribution: While extensive research has been conducted on FSSs and summarized in table form, no extensive analysis on 3-D Frequency Selective Surface exists. This extensive knowledge base is necessary in order to construct a 3-D FSS design methodology.

6.3 3-D Cylindrical FSS: Chapter 3

Background: 3-D FSSs has been reported in literature review to offer greater flexibility and providing an extra degree of freedom in the design when compared to a conventional 2-D FSS where the design limitations are relatively well known. A new type of 3-D frequency selective surface based on a cylindrical unit element has proven it. The FSS was made 3D by extending ring into a cylindrical element of a certain length. This extends the potential functionality of the structure and adding extra degrees of freedom in the design. By varying the length of the 3D cylindrical FSS, the frequency response is adjusted, and a closer band response operation can be obtained through inserting a dielectric filling inside the cylindrical unit cell structure of the 3-D FSS. A similar response can be achived by extrapolating the height of planar dual ring unit cell. Two bands can be designed from the structure of dual

cylindrical 3-D FSS to produce a very close band response without using any additional active lumped components.

It is known that 3-D FSSs have displayed the ability to set resonant frequency and shift operational filter states with a change in the height of a cylindrical resonator. Therefore a novel 3-D spring FSS structure is presented that can tuned by mechanically altering the height of the spring shaped unit cell resonator. Whereas, conventional FSSs require additional bias circuitry to tune the operating frequency or to change its characteristics. This new structure can also achieve functional switching between band-stop and band-pass operation without the need for active device integration.

Aim of the research: To investigate and prove the hypothesis of the 3-D FSS functionality of the structure and extra degrees of freedom in the design can dramatically improve the limitations of conventional FSS.

Methodology: 2-D circular ring resonator element provided the basis for this investigation and it was made 3-D by introducing some height. A parametric analysis of the 3-D FSS elements is undertaken using CST electromagnetic software. The simulated FSS properties were validated through an equivalent circuit model as well as measurement of a fabricated prototype.

Results: 3-D FSSs have displayed greater flexibility and design control compared to 2-D designs, with the ability to set resonant frequency and shift operational filter states with a change in the length of resonator. It is also has a capability to produce very close band response without using any additional lumped components. 3-D Spring FSS has shown to achieve functional switching between band-stop and band-pass operation without use of additional DC bias networks. Very good agreement in frequency performance was observed between equivalent circuit calculations, numerical modeling, and experimental testing for the 3-D cylindrical FSS and 3-D Spring FSS.

Future Work: It is suggested to embed lumped reactive components between the cylinders of the Dual Cylindrical 3-D FSS. The aim of this future work is to transform the conventional passive FSSs into active ones in addition to close band response. Furthermore, to make full use of 3D design space in FSS, a promising research direction is to investigate the shape of a sphere and cubic.

Original Contribution: Cylindrical 3-D FSS has shown it has tremendous potential in solving problem faced by 2-D FSS and it offers the potential functionality of the structure beyond 2-D analogue where never been done by recent publish 3-D FSS. (*see publication*: J1, J2, C1, C2, C3)

6.4 3-D Tapered FSS: Chapter 4

Background: A symmetrical 3-D Tapered FSS with a resonant frequency independent of incident angle and polarization was presented. Unlike traditional FSS design techniques using multiple layers or additional dielectric layers to achieve enhanced angular responses, or to improve the transmission bandwidth. 3-D Tapered FSS is modification from 3-D Square FSS, where the structure is modified by tapering the square cross section of the resonator element. This feature enables the FSS to utilize higher frequency cavity resonances that have very low sensitivity to the incidence angle. Furthermore, an improved bandwidth response can be obtained as well without using additional dielectric material. 3-D FSS with horn shaped resonator is a modification from a 3-D Tapered FSS consisting of square cylinder unit elements.

Aim of the research: To investigate and develop 3-D FSS that produce stable frequency response as well as wideband response with angular stability up to more than 80° for both TE and TM incidence.

Methodology: Angular stability of 2-D square ring element is studied followed by its 3-D structure which is 3-D cylindrical Square FSS. Angular stability of 3-D cylindrical square FSS is improved by tapering the cross-sectional size of the cylindrical element, called 3-D Tapered FSS. As the angular response is achieved, 3-D Horn FSS is develop to improve the bandwidth performance.

The 3-D Tapered FSS and 3-D Horn Shape FSS were modelled using CST MWS. The influence of various key parameters on both FSS characteristics has been investigated using CST simulation software tool. Parametric analysis is done at angle of incidence of 0, 20, 40, 60 and 80, respectively for both TE and TM excitation. The effect of the structure on the electric field distribution were investigated and compare with 3-D square FSS. Finally, the validity of the proposed concept was experimentally demonstrated by fabricating 3-D

Tapered FSS using 3-D printing technology and measuring its frequency response using free space measurements.

Results: 3D Tapered FSS is shown to have significantly improved resonant frequency stability characteristics from 0 to 80° for both TE and TM incidence. The validity of the proposed concept was verified experimentally. The measurement results correspond very well with the simulation results, demonstrate that the 3D Tapered FSS structure can achieve frequency performance independent of incident angle and polarization.

The bandwidth properties of the FSS can be strongly enhanced by enlarging the aperture of the square resonator. The simulations results carried out by the CST simulation tools showed that the proposed approach is a good candidate of designing 3-D and wideband absorbing structures with angular stability is remained nearly unchanged.

Future Work: Modification of square resonator has shown to improve the bandwidth as well as angular response. Nevertheless, other elements shape also need to be studied as well. The 3-D Tapered FSS is structured out of Acrylonitrile Butadiene Styrene (ABS) hence a redesign of the 3-D tapered FSS was required. Alternatively, the structure could be printed using the Stinted Laser Melting (SLM) method with metal thus redesign shall not require.

Original Contribution: A new theoretical formula and design approach of designing 3-D FSS with angular stability is presented. It is shows that 3-D tapered FSS has a similar cavity mode for all incidence angle, therefore reinforce the finding of stable center frequency for TE and TM incidence. The tapered design in 3-D FSS introduces an additional design parameter that controls the scattered field, enabling a relatively stable cavity mode at the same frequency for the incident angles. Furthermore, a simple and fast approach to design a 3-D wideband FSS is presented and discussed. (*see publication*: J3, C4, C5)

6.5 Miniturize FSS: Chapter 5

Background: Recently, many approaches have been proposed to obtain FSS unit cell dimensions much smaller than a wavelength as an increasing demand for low frequency applications and reducing the angular dependence of the frequency selective properties. Here, a new type of miniaturized FSS with angular stability is describe. It is a printed micro-

wire frequency selective unit cell structure which could lower the resonant frequency effectively, with high Q, has less sensitivity towards incident angle and provide negative permittivity and permeability. The micro-wire structure resembles a 2-layer compressed version of the 3D dipoles without vertical conducting elements. With the proposed new method, miniaturization to a greater extend can be achieved.

Aim of the research: To develop and study a new type of miniature resonator that is independent towards incident angle and as alternative solution to enhance the light passing through a subwavelength aperture.

Methodology: Miniaturization of the FSS unit cell is achieved by coupling two meandered wire resonators separated by single thin substrate layer. The capacitance due to the small separation between the meandered wire elements results in a lowering of the resonant frequency**.** To enhance transmission efficiency, the wire resonator is placed in planar in the aperture hole regions on a large metal area. The configuration and performance of the subwavelength transmission structure are described and validated numerically using CST Microwave Studio software. The micro-wire resonator FSS was fabricated on a thin substrate and measurement results is compared with the simulations.

Results: A miniature FSS has been demonstrated to be angular stability up to 80^{o} as for TE and TM incidences. The angular response is even better as more layers is added as well as miniaturization amount increases. A good agreement between theory, simulations, and measurement results was observed.

While, the micro-wire resonator has shown approximately 100% transmission at 1.94 GHz through an aperture that is $0.023\ \lambda_0$ square in size. The response of the micro-wire resonator in an aperture is extremely high Q, presenting a -10 dB transmission bandwidth of 0.007%. A much smaller resonator can be achieved by complementary design of wire resonator as the resonance frequency shifted 9% lower than the previous design. The study is finalized by demonstrating transmission enhancement from an array of subwavelength apertures and relatively good agreement between the simulated and measured results have been achieved.

Future Work: 3-D Meandered wire resonator is proposed for future work as it is will utilization of three-dimensional space, the unit cell size of the FSS can be further reduced. A feature of interest in design of FSS's is the ability to tune the frequency response of the

surface by manipulating the FSS layers' reactive characteristics by incorporating tuning elements into the layers. Study the performance of miniature FSS under bending conditions.

Original Contribution: A novel subwavelength transmission structure is presented that utilizes a micro-wire resonator structure, which could lower the resonant frequency effectively, with high Q, has less sensitivity towards incident angle and provide negative permittivity and permeability. With the proposed new method, miniaturization to a greater extend can be achieved compares to the conventional method of realizing multilayer resonator. It is also can be fabricated via the standard planar substrate based fabrication techniques and much lower frequency is attained by adding more layers to the structures. (*see publication*: J4, J5, C6).

References

[1]. Ranga, Y., et al. "Oblique incidence performance of UWB frequency selective surfaces for reflector applications". in *Antennas and Propagation (APSURSI), 2011 IEEE International Symposium on*. 2011. IEEE.

[2]. d'Elia, U., et al., "A PHYSICAL OPTICS APPROACH TO THE ANALYSIS OF LARGE FREQUENCY SELECTIVE RADOMES". *Progress In Electromagnetics Research*, 2013. 138.

[3]. Chin, J.Y., M. Lu, and T.J. Cui, "Metamaterial polarizers by electric-field-coupled resonators". *Applied Physics Letters*, 2008. 93(25): p. 251903-251903-3.

[4]. Cooper, J.R., S. Kim, and M.M. Tentzeris, "A Novel Polarization-Independent, Free-Space, Microwave Beam Splitter Utilizing an Inkjet-Printed, 2-D Array Frequency Selective Surface". *Antennas and Wireless Propagation Letters, IEEE*, 2012. 11: p. 686-688.

[5]. Li, L., et al., "Frequency selective reflectarray using crossed-dipole elements with square loops for wireless communication applications". *Antennas and Propagation, IEEE Transactions on*, 2011. 59(1): p. 89-99.

[6]. Matson, I.L., "Antenna feed system simultaneously operable at two frequencies utilizing polarization independent frequency selective intermediate reflector", 1966, Google Patents.

[7]. Fallahi, A., et al., "Thin Wideband Radar Absorbers". *Antennas and Propagation, IEEE Transactions on*, 2010. 58(12): p. 4051-4058.

[8]. Wang, W.-T., et al., "RCS reduction of array antenna by using bandstop FSS reflector". *Journal of Electromagnetic Waves and Applications*, 2009. 23(11-12): p. 1505-1514.

[9]. Sarabandi, K. and N. Behdad, "A Frequency Selective Surface With Miniaturized Elements". *Antennas and Propagation, IEEE Transactions on*, 2007. 55(5): p. 1239-1245.

[10]. Hosseini, M., A. Pirhadi, and M. Hakkak. "Design of an AMC with Little Sensitivity to Angle of Incidence Using an Optimized Jerusalem Cross FSS". in *Antenna Technology Small Antennas and Novel Metamaterials, 2006 IEEE International Workshop on*. 2006.

[11]. Barbagallo, S., A. Monorchio, and G. Manara, "Small periodicity FSS screens with enhanced bandwidth performance". *Electronics Letters*, 2006. 42(7): p. 382-384.

[12]. Samsul Haimi, D. and M. Esa. "Miniaturized Low Pass Filter Using Modified Unifolded Single Hairpin-Line Resonator for Microwave Communication Systems". in *RF and Microwave Conference, 2006. RFM 2006. International*. 2006.

[13]. Ma, T., et al., "A FSS WITH STABLE PERFORMANCE UNDER LARGE INCIDENT ANGLES". *Progress In Electromagnetics Research Letters*, 2013. 41.

[14]. Zhou, H., et al., "Ultra-wideband frequency selective surface". *Electronics Letters*, 2012. 48(1): p. 11-13.

[15]. Zhou, H., et al., "Filter-antenna consisting of conical FSS radome and monopole antenna". *Antennas and Propagation, IEEE Transactions on*, 2012. 60(6): p. 3040-3045.

[16]. Zhang, T., et al. "A novel double-layer semi-circle fractal multi-band frequency selective surface". in *Antennas Propagation and EM Theory (ISAPE), 2010 9th International Symposium on*. 2010. IEEE.
[17]. Sakran, F., et al., "Absorbing frequency-selective-surface for the mm-wave range". *Antennas and Propagation, IEEE Transactions on*, 2008. 56(8): p. 2649-2655.
[18]. Qing, A. and C.K. Lee. "Analysis of gridded square frequency selective surfaces". in *Microwave Conference, 2000 Asia-Pacific*. 2000. IEEE.
[19]. Gomes D'Assunao Junior, A., et al. "Analysis of quasi-square open ring frequency selective surface using the Wave Concept Iterative Procedure". in *Microwave and Optoelectronics Conference (IMOC), 2009 SBMO/IEEE MTT-S International*. 2009.
[20]. Jha, K.R., G. Singh, and R. Jyoti, "A simple synthesis technique of single-square-loop frequency selective surface". *Progress In Electromagnetics Research B*, 2012. 45: p. 165-185.
[21]. Zheng, S., Y. Yin, and X. Ren. "Interdigitated hexagon loop unit cells for wideband miniaturized frequency selective surfaces". in *Antennas Propagation and EM Theory (ISAPE), 2010 9th International Symposium on*. 2010. IEEE.
[22]. Zhanbo, L., S. Rong, and Y. Xuequan. "A novel wideband frequency selective surface composite structure". in *Microwave Conference Proceedings (CJMW), 2011 China-Japan Joint*. 2011.
[23]. Brito, D.B., et al. "A Minkowski fractal Frequency Selective Surface with high angular stability". in *Microwave & Optoelectronics Conference (IMOC), 2013 SBMO/IEEE MTT-S International*. 2013.
[24]. Ribeiro da Silva, M., et al., "Stable and compact multiband frequency selective surfaces with Peano pre-fractal configurations". *Microwaves, Antennas & Propagation, IET*, 2013. 7(7): p. 543-551.
[25]. Yongjiu, L., et al. "A novel subwavelength fractal frequency selective surface based on antenna-filter-antenna". in *Cross Strait Quad-Regional Radio Science and Wireless Technology Conference (CSQRWC), 2013*. 2013.
[26]. Anuradha, A., et al. "Design of customized fractal FSS". in *Antennas and Propagation Society International Symposium (APSURSI), 2012 IEEE*. 2012.
[27]. Bao-Qin, L., et al., "Design and Simulation of a Miniature Thick-Screen Frequency Selective Surface Radome". *Antennas and Wireless Propagation Letters, IEEE*, 2009. 8: p. 1065-1068.
[28]. Ranga, Y., et al., "Multioctave frequency selective surface reflector for ultrawideband antennas". *Antennas and Wireless Propagation Letters, IEEE*, 2011. 10: p. 219-222.
[29]. Ranga, Y., et al. "Multilayer frequency-selective-surface reflector for constant gain over ultra wideband". in *Antennas and Propagation (EUCAP), Proceedings of the 5th European Conference on*. 2011.
[30]. Taylor, P., et al., "Angular independent frequency selective surfaces for interference control in indoor wireless environments". *Electronics letters*, 2012. 48(2): p. 61-62.
[31]. Sung, G.-H., et al., "A frequency-selective wall for interference reduction in wireless indoor environments". *Antennas and Propagation Magazine, IEEE*, 2006. 48(5): p. 29-37.
[32]. Costa, F. and A. Monorchio, "A Frequency Selective Radome With Wideband Absorbing Properties". *Antennas and Propagation, IEEE Transactions on*, 2012. 60(6): p. 2740-2747.
[33]. Corporation, K. *Research & Development: R & D*. 2001; Available from: http://www.kajima.co.jp/ir/annual/2002/research-development.html.

[34]. (CELANE), M.U.F.o.S. *Frequency Selective Surfaces for Energy-Saving Glass Panels*. Available from: http://research.science.mq.edu.au/celane/projects/#FSS.
[35]. wallpapersus. *aircrafts, jet fighter, missiles, digital artwork*. Available from: http://wallpapersus.com/aircrafts-jet-fighter-missiles-digital-art-artwork/.
[36]. Munk, B.A., "Frequency selective surfaces: theory and design". 2005: Wiley-Interscience.
[37]. Wu, T., "Frequency selective surface and grid array". Vol. 40. 1995: Wiley-Interscience.
[38]. Ranga, Y., et al. "Design and analysis of frequency-selective surfaces for ultrawideband applications". in *EUROCON - International Conference on Computer as a Tool (EUROCON), 2011 IEEE*. 2011.
[39]. Winkler, S.A., et al., "Polarization Rotating Frequency Selective Surface Based on Substrate Integrated Waveguide Technology". *Antennas and Propagation, IEEE Transactions on*, 2010. 58(4): p. 1202-1213.
[40]. Lv, M.-Y., M.-J. Huang, and Z. Wu. "Study on the dual-band characteristic of combined element based frequency selective surfaces". in *Antenna Technology, 2009. iWAT 2009. IEEE International Workshop on*. 2009. IEEE.
[41]. Delihacıoglu, K., "Frequency Selective Surfaces with Multiple Strip Group Elements". 2012.
[42]. Min-Jie, H., et al., "A New Type of Combined Element Multiband Frequency Selective Surface". *Antennas and Propagation, IEEE Transactions on*, 2009. 57(6): p. 1798-1803.
[43]. x and S. imen, "Novel closely spaced planar dual-band frequency-selective surface". *Microwaves, Antennas & Propagation, IET*, 2013. 7(11): p. 894-899.
[44]. Monni, S., et al., "Frequency-Selective Surface to Prevent Interference Between Radar and SATCOM Antennas". *Antennas and Wireless Propagation Letters, IEEE*, 2009. 8: p. 220-223.
[45]. Barkeshli, S., et al. "On the analysis and design of the frequency selective surface for the N-Star satellite Ku/S-shaped reflector". in *Antennas and Propagation Society International Symposium, 1995. AP-S. Digest*. 1995. IEEE.
[46]. H.M.R Nurul, P.J.S., A.A.H Azremi, N.A Saidatul, S.R Norra, M.I Ibrahim, R.B Ahmad, "A Dual Band Planar Monopole Antenna with Inverted-M Parasitic Plane", in *Asia-Pacific Conference on Applied Electromagnetics 2007 (APACE 2007)*2007, IEEE APS/MTT/EMC Malaysia Chapter, UTeM, UTM, UiTM, UTHM and UNISEL: Melaka, Malaysia.
[47]. Xu, R.-r., et al., "Dual-band capacitive loaded frequency selective surfaces with close band spacing". *Microwave and Wireless Components Letters, IEEE*, 2008. 18(12): p. 782-784.
[48]. Zong, Z.-y., et al. "Miniaturized dualband loaded frequency selective surfaces with close band spacing". in *Microwave Conference, 2008. APMC 2008. Asia-Pacific*. 2008. IEEE.
[49]. Al-Joumayly, M.A. and N. Behdad, "Low-profile, highly-selective, dual-band frequency selective surfaces with closely spaced bands of operation". *Antennas and Propagation, IEEE Transactions on*, 2010. 58(12): p. 4042-4050.
[50]. Niroo-Jazi, M. and T.A. Denidni. "Reconfigurable dual-band frequency selective surfaces using a new hybrid element". in *Antennas and Propagation (APSURSI), 2011 IEEE International Symposium on*. 2011. IEEE.
[51]. Munir, A., V. Fusco, and O. Malyuskin. "Tunable frequency selective surfaces characterisation". in *Microwave Conference, 2008. EuMC 2008. 38th European*. 2008. IEEE.

[52]. Mohammad Amjadi, S. and M. Soleimani, "Design of band-pass waveguide filter using frequency selective surfaces loaded with surface mount capacitors based on split-field update FDTD method". *Progress In Electromagnetics Research B*, 2008. 3: p. 271-281.
[53]. Mias, C., "Varactor-tunable frequency selective surface with resistive-lumped-element biasing grids". *Microwave and Wireless Components Letters, IEEE*, 2005. 15(9): p. 570-572.
[54]. Ucar, M.H., A. Sondas, and Y.E. Erdemli, "Switchable split-ring frequency selective surfaces". *Progress In Electromagnetics Research B*, 2008. 6: p. 65-79.
[55]. Bao-Qin, L., et al., "Varactor-tunable frequency selective surface with an embedded bias network". *Chinese Physics B*, 2013. 22(9): p. 094103.
[56]. Martinez-Lopez, R., et al., "AN ACTIVE RING SLOT WITH RF MEMS SWITCHABLE RADIAL STUBS FOR RECONFIGURABLE FREQUENCY SELECTIVE SURFACE APPLICATIONS". *Progress In Electromagnetics Research*, 2012. 128.
[57]. Schoenlinner, B., L.C. Kempel, and G.M. Rebeiz. "Switchable RF MEMS Ka-band frequency-selective surface". in *Microwave Symposium Digest, 2004 IEEE MTT-S International*. 2004. IEEE.
[58]. Coutts, G., R. Mansour, and S. Chaudhuri. "A MEMS-tunable frequency-selective surface monolithically integrated on a flexible substrate". in *Microwave Symposium, 2007. IEEE/MTT-S International*. 2007. IEEE.
[59]. Bossard, J.A., et al., "A novel design methodology for reconfigurable frequency selective surfaces using genetic algorithms". *Antennas and Propagation, IEEE Transactions on*, 2005. 53(4): p. 1390-1400.
[60]. Zendejas, J.M., et al., "Magnetic MEMS reconfigurable frequency-selective surfaces". *Microelectromechanical Systems, Journal of*, 2006. 15(3): p. 613-623.
[61]. Wenxun, Z. and S. Hongxin, "Analysis of mechanically tunable frequency selective surfaces". *Systems Engineering and Electronics, Journal of*, 1997. 8(4): p. 7-16.
[62]. Khodasevych, I., W.S. Rowe, and A. Mitchell, "Reconfigurable fishnet metamaterial using pneumatic actuation". *Progress In Electromagnetics Research B*, 2012. 38: p. 57-70.
[63]. Lynch, J.J. and J.S. Colburn, "Modeling polarization mode coupling in frequency-selective surfaces". *Microwave Theory and Techniques, IEEE Transactions on*, 2004. 52(4): p. 1328-1338.
[64]. Bayatpur, F. and K. Sarabandi, "Miniaturized FSS and patch antenna array coupling for angle-independent, high-order spatial filtering". *Microwave and Wireless Components Letters, IEEE*, 2010. 20(2): p. 79-81.
[65]. Zhou, H., et al., "A triband second-order frequency selective surface". *Antennas and Wireless Propagation Letters, IEEE*, 2011. 10: p. 507-509.
[66]. Guo Qing, L., et al., "Design and Experimental Verification of Compact Frequency-Selective Surface With Quasi-Elliptic Bandpass Response". *Microwave Theory and Techniques, IEEE Transactions on*, 2007. 55(12): p. 2481-2487.
[67]. Lin, L. and A. Roberts, "Angle-robust resonances in cross-shaped aperture arrays". *Applied Physics Letters*, 2010. 97(6): p. 061109-061109-3.
[68]. Hosseini, M., A. Pirhadi, and M. Hakkak, "A novel AMC with little sensitivity to the angle of incidence using 2-layer jerusalem cross FSS". *Progress In Electromagnetics Research*, 2006. 64: p. 43-51.
[69]. Yan, M., et al., "A novel miniaturized frequency selective surface with stable resonance". 2014.

[70]. Baida, F.I., "Enhanced transmission through subwavelength metallic coaxial apertures by excitation of the TEM mode". *Applied Physics B*, 2007. 89(2-3): p. 145-149.
[71]. Van Labeke, D., et al., "An angle-independent Frequency Selective Surface in the optical range". *Optics express*, 2006. 14(25): p. 11945-11951.
[72]. Wanlu, L., et al. "Novel Frequency Selective Surfaces with compact structure and ultra-wideband response". in *Electromagnetic Compatibility (APEMC), 2012 Asia-Pacific Symposium on*. 2012.
[73]. Gianvittorio, J.P., et al., "Self-similar prefractal frequency selective surfaces for multiband and dual-polarized applications". *Antennas and Propagation, IEEE Transactions on*, 2003. 51(11): p. 3088-3096.
[74]. Xue, J.-Y., et al., "A new miniaturized fractal frequency selective surface with excellent angular stability". *Progress In Electromagnetics Research Letters*, 2010. 13: p. 131-138.
[75]. Ma, Y., et al., "Miniaturized and dual-band metamaterial absorber with fractal Sierpinski structure". *JOSA B*, 2014. 31(2): p. 325-331.
[76]. Zabri, S.N., R. Cahill, and A. Schuchinsky, "Polarisation independent split ring frequency selective surface". *Electronics Letters*, 2013. 49(4): p. 245-246.
[77]. Baena, J., et al., "Isotropic frequency selective surfaces made of cubic resonators". *Applied Physics Letters*, 2007. 91(19): p. 191105-191105-3.
[78]. Yuandan, D. and T. Itoh, "Substrate Integrated Waveguide Loaded by Complementary Split-Ring Resonators for Miniaturized Diplexer Design". *Microwave and Wireless Components Letters, IEEE*, 2011. 21(1): p. 10-12.
[79]. Wei, X.-B., et al., "Miniaturized Bandpass Filter with Mixed Electric and Magnetic Coupling Using Hexagonal Stepped Impedance Resonators". *Electromagnetics*, 2013. 33(7): p. 550-559.
[80]. Abdel-Rahman, A.B., et al. "Small size third order coupled resonator band-pass filter using capacitor loaded slots". in *Antennas and Propagation (MECAP), 2010 IEEE Middle East Conference on*. 2010.
[81]. Nishiyama, E., T. Itoh, and M. Aikawa. "Varactor loaded tunable miniature resonator". in *Microwave Conference, 2009. APMC 2009. Asia Pacific*. 2009.
[82]. Hsu, H.-T. and C.-Y. Chiang. "Miniaturization of hairpin resonator filters with improved harmonic suppression by using lumped capacitors". in *Microwave Symposium Digest (IMS), 2013 IEEE MTT-S International*. 2013.
[83]. Excell, P.S. and Z.M. Hejazi, "Electrically small resonator using thick-film high-T/sub c/ superconducting wire helix". *Applied Superconductivity, IEEE Transactions on*, 1999. 9(4): p. 4654-4660.
[84]. Jian-Kang, X., J. Wu-Sheng, and H. Hui-Fen. "Miniature microstrip isosceles triangular resonator filter". in *Microwave and Millimeter Wave Technology, 2008. ICMMT 2008. International Conference on*. 2008.
[85]. Sheta, A.F., et al. "Miniature microstrip stepped impedance resonator bandpass filters and diplexers for mobile communications". in *Microwave Symposium Digest, 1996., IEEE MTT-S International*. 1996.
[86]. Min-Da, C. and C. Shih-Yuan. "An electrically small planar antenna using complementary split-ring resonators". in *Antennas and Propagation (ISAP), 2012 International Symposium on*. 2012.
[87]. Li, W., X. Ye, and H. Ma. "Design of microstrip triplexer with new miniature resonator". in *Millimeter Waves (GSMM), 2012 5th Global Symposium on*. 2012. IEEE.

[88]. Ban-Leong, O. and W. Ying, "Novel miniaturized open-square-loop resonator with inner split rings loading". *Microwave Theory and Techniques, IEEE Transactions on*, 2006. 54(7): p. 3098-3103.
[89]. Hong, J.-S. and M.J. Lancaster, "Microstrip bandpass filter using degenerate modes of a novel meander loop resonator". *Microwave and Guided Wave Letters, IEEE*, 1995. 5(11): p. 371-372.
[90]. Hong, J.-S. and M.J. Lancaster, "Cross-coupled microstrip hairpin-resonator filters". *Microwave Theory and Techniques, IEEE Transactions on*, 1998. 46(1): p. 118-122.
[91]. Jun, S. and K. Chang, "Compact Microstrip Bandpass Filter Using Miniaturized Hairpin Resonator". *Progress In Electromagnetics Research Letters*, 2013. 37: p. 65-71.
[92]. Azadegan, R. and K. Sarabandi, "Miniature high-Q double-spiral slot-line resonator filters". *Microwave Theory and Techniques, IEEE Transactions on*, 2004. 52(5): p. 1548-1557.
[93]. Alici, K.B., et al., "Optimization and tunability of deep subwavelength resonators for metamaterial applications: complete enhanced transmission through a subwavelength aperture". *Optics express*, 2009. 17(8): p. 5933-5943.
[94]. Bo, L. and S. Zhongxiang, "Three-Dimensional Bandpass Frequency-Selective Structures With Multiple Transmission Zeros". *Microwave Theory and Techniques, IEEE Transactions on*, 2013. 61(10): p. 3578-3589.
[95]. Rashid, A.K. and Z. Shen. "Three-dimensional monolithic frequency selective structure with dielectric loading". in *Microwave Conference Proceedings (APMC), 2010 Asia-Pacific*. 2010. IEEE.
[96]. Mittra, R. and C. Pelletti. "Three-dimensional FSS elements with wide frequency and angular responses". in *Antennas and Propagation Society International Symposium (APSURSI), 2012 IEEE*. 2012. IEEE.
[97]. Lee, I. and I. Hong, "3D frequency selective surface for stable angle of incidence". *Electronics Letters*, 2014. 50(6): p. 423-424.
[98]. Lu, Z.-H., P.-G. Liu, and X.-J. Huang, "A Novel Three-Dimensional Frequency Selective Structure". *Antennas and Wireless Propagation Letters, IEEE*, 2012. 11: p. 588-591.
[99]. Azemi, S.N. and W.S. Rowe. "Development and analysis of 3d frequency selective surfaces". in *Microwave Conference Proceedings (APMC), 2011 Asia-Pacific*. 2011. IEEE.
[100]. Azemi, S.N., K. Ghorbani, and W.S. Rowe, "3D Frequency Selective Surfaces". *Progress In Electromagnetics Research C*, 2012. 29: p. 191-203.
[101]. Azemi, S.N., K. Ghorbani, and W.S. Rowe. "3D Frequency Selective Surfaces with close band spacing". in *Microwave Conference Proceedings (APMC), 2012 Asia-Pacific*. 2012. IEEE.
[102]. Azemi, S.N., K. Ghorbani, and W.S. Rowe, "A Reconfigurable FSS Using a Spring Resonator Element". *Antennas and Wireless Propagation Letters, IEEE*, 2013. 12: p. 781-784.
[103]. Huang, J., T.-K. Wu, and S.-W. Lee, "Tri-band frequency selective surface with circular ring elements". *Antennas and Propagation, IEEE Transactions on*, 1994. 42(2): p. 166-175.
[104]. Hong, J.-S.G. and M.J. Lancaster, "Microstrip filters for RF/microwave applications". Vol. 167. 2004: Wiley-interscience.
[105]. Karmel, P.R., G.D. Colef, and R.L. Camisa, "Introduction to electromagnetic and microwave engineering". Vol. 53. 1998: Wiley-Interscience.

[106]. Wang, J., et al., "Wide-angle polarization-independent planar left-handed metamaterials based on dielectric resonators". *Progress In Electromagnetics Research B*, 2009. 12: p. 243-258.
[107]. Chang, K., "RF and microwave wireless systems". Vol. 161. 2004: Wiley-Interscience.
[108]. Kartikeyan, M., et al., "A study of radially thick helix: equivalent circuit approach". *Electron Devices, IEEE Transactions on*, 1992. 39(8): p. 1961-1965.
[109]. Paik, S., "Design formulas for helix dispersion shaping". *Electron Devices, IEEE Transactions on*, 1969. 16(12): p. 1010-1014.
[110]. Shaker, J. and L. Shafai, "Reduced angular sensitivity frequency selective surface". *Electronics Letters*, 1993. 29(18): p. 1655-1657.
[111]. Parker, E. and A. El Sheikh. "Convoluted array elements and reduced size unit cells for frequency-selective surfaces". in *Microwaves, Antennas and Propagation, IEE Proceedings H*. 1991. IET.
[112]. Widenberg, B., S. Poulsen, and A. Karlsson, "Scattering from thick frequency selective screens". *Journal of electromagnetic waves and applications*, 2000. 14(9): p. 1303-1328.
[113]. Weitsch, Y. and T. Eibert. "A left-handed/right-handed leaky-wave antenna derived from slotted rectangular hollow waveguide". in *Microwave Conference, 2007. European*. 2007. IEEE.
[114]. Li-Hua, Y., et al. "A miniaturized frequency selective surface based on convoluted ring slot". in *Environmental Electromagnetics (CEEM), 2012 6th Asia-Pacific Conference on*. 2012.
[115]. Deng, F. and X. Wu. "A novel miniaturized Frequency Selective Surface". in *Antennas, Propagation & EM Theory (ISAPE), 2012 10th International Symposium on*. 2012.
[116]. Yang, Y., X.-H. Wang, and H. Zhou, "Dual-band frequency selective surface with miniaturized element in low frequencies". *Progress In Electromagnetics Research Letters*, 2012. 33: p. 167-175.
[117]. Galehdar, A., D.V. Thiel, and S.G. O'Keefe, "Design methods for 3D RFID antennas located on a conducting ground plane". *Antennas and Propagation, IEEE Transactions on*, 2009. 57(2): p. 339-346.
[118]. Wadell, B.C., "Transmission line design handbook". 1991.
[119]. Tang, W.-X., et al. "A meander line resonator to realize negative index materials". in *Antennas and Propagation Society International Symposium, 2008. AP-S 2008. IEEE*. 2008. IEEE.
[120]. Schurig, D., J. Mock, and D. Smith, "Electric-field-coupled resonators for negative permittivity metamaterials". *Applied Physics Letters*, 2006. 88(4): p. 041109-041109-3.
[121]. Baum, T., L. Thompson, and K. Ghorbani, "Complex dielectric measurements of forest fire ash at X-band frequencies". *Geoscience and Remote Sensing Letters, IEEE*, 2011. 8(5): p. 859-863.